Sex differences in intestinal carbohydrate metabolism promote food intake and sperm maturation

Bruno Hudry[1,2,*], Eva de Goeij[1], Alessandro Mineo[1], Pedro Gaspar[1], Dafni Hadjieconomou[1], Chris Studd[1], Joao B. Mokochinski[1], Holger B. Kramer[1], Pierre-Yves Plaçais[3], Thomas Preat[3], Irene Miguel-Aliaga[1,*,$]

[1] MRC London Institute of Medical Sciences, Imperial College London, Hammersmith Campus, Du Cane Road, London W12 0NN, UK
[2] Université Côte d'Azur, CNRS, INSERM, iBV, France
[3] Genes and Dynamics of Memory Systems, Brain Plasticity Unit, CNRS, ESPCI Paris, PSL Research University, 10 rue Vauquelin, 75005 Paris, France

* Correspondence: i.miguel-aliaga@imperial.ac.uk (I.M-A.)
Bruno.Hudry@unice.fr (B.H.)

[$] Lead contact

Keywords: intestine, gonad, testes, gender differences, carbohydrate metabolism, sperm, citrate, organ plasticity, *Drosophila*

SUMMARY

Physiology and metabolism are often sexually dimorphic, but the underlying mechanisms remain incompletely understood. Here, we use the intestine of *Drosophila melanogaster* to investigate how gut-derived signals contribute to sex differences in whole-body physiology. We find that carbohydrate handling is male-biased in a specific portion of the intestine. In contrast to known sexual dimorphisms in invertebrates, the sex differences in intestinal carbohydrate metabolism are extrinsically controlled by the adjacent male gonad, which activates JAK-STAT signalling in enterocytes within this intestinal portion. Sex reversal experiments establish roles for this male-biased intestinal metabolic state in controlling food intake and sperm production through gut-derived citrate. Our work uncovers a male gonad-gut axis coupling diet and sperm production, and reveals that metabolic communication across organs is physiologically significant. The instructive role of citrate in inter-organ communication may be significant in more biological contexts than previously recognised.

INTRODUCTION

Males and females differ in their physiology and disease susceptibility (Link and Reue, 2017; Ober et al., 2008) yet the sex of cells/animals has often been neglected in research, or with a single sex (male) preferentially used (Wald and Wu, 2010). This may have prevented identification of sex differences that could inform clinical studies and therapies. Pressure to consider both sexes in basic and clinical research is revealing that sex differences are extensive, yet relatively underexplored (Clayton and Collins, 2014; Mauvais-Jarvis et al., 2017; Nielsen et al., 2017; Wizemann and Pardue, 2001).

Sex chromosome sensing in *Drosophila melanogaster* activates a splicing cascade that results in expression of the RNA-binding protein Tra^{F} only in females (Boggs et al., 1987), leading to sex-specific splicing of the transcription factors Doublesex (Dsx) and Fruitless (Fru) (Baker and Ridge, 1980; Ryner et al., 1996) in a subset of cells, which sculpt sexually dimorphic anatomical features, reproductive systems and behaviour (Auer and Benton, 2016; Camara et al., 2008; Christiansen et al., 2002; Clough and Oliver, 2012; Dickson, 2008; Villella and Hall, 2008). Although superficially distinct from mammalian mechanisms involving gonadal release of sex hormones, *Drosophila* and mammalian sex differentiation may share effectors such as the Dmrt/Dsx family of transcription factors (Arnold, 2017; Bellott et al., 2017; Kopp, 2012; Zarkower, 2002). Furthermore, mouse models have revealed a cell-intrinsic contribution of sex chromosome complement to sex differences in body size and adiposity in mammals (Chen et al., 2012; Chen et al., 2013; Link et al., 2017; Zore et al., 2018), and studies in flies have hinted at cell-extrinsic contributions to sex-biased phenotypes (Rideout et al., 2015; Sawala and Gould, 2017; Sieber and Spradling, 2015). Thus, sex differentiation in both insects and mammals appears to be a complex process integrating intrinsic and extrinsic inputs (Ainsworth, 2015; Arnold, 2017).

Like its mammalian counterpart, the adult *Drosophila* digestive tract is a plastic and functionally regionalised organ (Miguel-Aliaga et al., 2018; O'Brien et al., 2011), harbouring microbiota and cell types akin to those found in humans, including self-renewing epithelial progenitors, digestive/absorptive enterocytes (ECs) and hormone-secreting enteroendocrine cells (Micchelli and Perrimon, 2006; Miguel-Aliaga et al., 2018; O'Brien et al., 2011; Ohlstein and Spradling, 2006). We recently revealed sex differences in intestinal stem cell proliferation, which are adult-reversible and intrinsic to the stem cells (Hudry et al., 2016). During the course of these experiments, we also

observed intestinal sex differences in metabolic gene expression (Hudry et al., 2016), suggesting that sex-biased intestinal metabolism might contribute to sex differences in whole-body physiology.

The intestine communicates with other organs, and peptide hormones are well established mediators (Ameku et al., 2018; Droujinine and Perrimon, 2016; Gribble and Reimann, 2016; Karsenty and Olson, 2016; Scopelliti et al., 2018; Song et al., 2017). However, intermediate products of intracellular, housekeeping metabolic pathways are detected in the circulation, and recent work is revealing that both healthy tissues and tumours can use (and sometimes require) such exogenous, circulating metabolites (Boroughs and DeBerardinis, 2015; Hui et al., 2017; Mills et al., 2018). Consequently, there is considerable interest in exploring the instructive potential of metabolites in the context of inter-organ signalling (de Castro Fonseca et al., 2016; Yang et al., 2018).

In this manuscript, we uncover bidirectional communication between the male gonad and an adjacent intestinal region. This communication affects both gut and testes function, and is mediated by cytokine signalling and the metabolite citrate.

RESULTS

Male-biased and region-specific gene expression in the intestine

Adult virgin male and female flies show male-biased expression of genes with putative functions in carbohydrate transport and utilisation (Figure S1A, Table S1 and Hudry et al., 2016), including digestive enzymes (Figure S1B). This sexual dimorphism is predominantly confined to the midgut (Figure S1A, Table S1 and Leader et al., 2018). We validated male-biased expression for a subset of genes coding for carbohydrate handling (breakdown, transport or utilisation) proteins using reverse transcription-quantitative polymerase chain reaction (RT-qPCR); we selected genes with midgut-specific expression so that RT-qPCR profiling could be performed on RNA from whole, adult flies (Figure S1C). To analyse this sexual dimorphism we engineering protein or transcriptional reporters by tagging endogenous proteins representative of various sugar-handling processes with GFP (see STAR Methods), including: Phosphoglucose isomerase (Pgi), Maltase-A3 (Mal-A3), and Amylase proximal (Amy-p). Immunohistochemical analyses of these protein reporters, a transcriptional reporter for Maltase-A7 (Mal-A7, see STAR Methods) and publicly available protein/transcriptional reporters for other enzymes (Maltase A1 (Mal-A1), Trehalase (Treh), Hexokinase A (Hex-A) and lactate dehydrogenase (Ldh)) confirmed the sexual dimorphism at the protein level, and revealed that it was predominantly confined to the intestinal epithelium (Figure 1A-1I). The epithelial cell types contributing to this expression differed depending on whether the protein is involved in sugar breakdown, transport or utilisation, but invariably included the digestive/absorptive ECs (with one exception, Mal-A3, expressed exclusively in enteroendocrine cells, Figure 1D).

We observed that sexually dimorphic expression was spatially restricted to the posterior R4 region of the adult midgut (Buchon et al., 2013), even when the transcripts/proteins were expressed in other intestinal portions (see Figures 1A and S1D for Mal-A1, *Mal-A7* and Pgi, quantification in Figures 1B, 1C and 1I for Mal-A1, Amy-p and *Mal-A7*, respectively). Sexual dimorphism in the R4 region was not restricted to carbohydrate metabolism genes; it also included oxidative stress response genes such as *Glutathione S transferase D1* (*GstD1*) (Figure S1E) and genes with female-biased expression such as Yolk protein 1 (Yp1) (Figure S1F).

Thus, the proteins handling sugars in the adult gut are male-biased, and this intestinal sexual dimorphism is spatially confined to the posterior R4 midgut region.

Sex differences in sugar gene expression are independent of gut cell sex

To explore how male biased intestinal sugar gene expression arises we used RNAseq transcriptional analysis, which revealed up-regulation of sugar genes in "masculinised" female flies lacking the female sex determinant *tra* (Figure 2A and Table S1). We confirmed their expression is controlled by Tra^F and its binding partner Transformer 2 (Tra2) (Amrein et al., 1988; Fujihara et al., 1978; Goralski et al., 1989) by assessing the effect of whole-body *tra*/*tra2* mutation (masculinisation) or tra^F mis-expression (feminisation) on the subset of gut-specific, male-biased sugar genes (Figure 2A-C). We generated a *tra* allele (tra^{FRT}) that allows whole-body or cell type-specific *tra* deletion, and a $tra^{F\ K\text{-}IN}$ knock-in allele that constitutively feminises males. This allele fully rescues *tra* null mutant females (unlike *UAS-*tra^F), including their fertility (see STAR Methods and Figures S2A-D). Both genetic manipulations abrogated the sex bias in sugar gene expression; *tra*/*tra-2* mutation did so by up-regulating the expression of the sugar genes in female (masculinised) flies (Figures 2A-2C, S2I), whereas ectopic tra^F reduced their expression in male (feminised) flies to levels comparable to those detected in female guts (Figure 2B).

We expected that Tra^F would control sex differences in intestinal sugar genes intrinsically from the intestinal epithelium itself, like the sex differences in intestinal stem cell proliferation (Hudry et al., 2016). However, the sex-biased intestinal sugar gene expression is *tra2*-dependent, unlike intestinal stem cell proliferation, suggesting that a different mechanism is involved. To investigate this mechanism, we removed Tra^F/Tra2 function in specific cell types/tissues using *tra/tra2* knockdown (KD) lines and the *tra* allele that allows its cell type-specific deletion (Figures S2E-S2I). Both *tra*/*tra2* downregulation and *tra* mutation failed to affect male bias in intestinal sugar gene expression when confined to the intestinal epithelium (Figures 2D, 2E and S3A-S3D). Attempts to rescue the "masculinisation" of intestinal sugar gene expression in *tra* mutant females by re-instating tra^F expression in the intestinal epithelium were also unsuccessful (Figure 2F). Similarly, whilst forced expression of tra^F in all fly tissues "feminised" intestinal sugar gene expression in genotypically male flies (Figure S2I), we failed to observe such "feminisation" when mis-expression was confined to the different intestinal epithelial cell types (Figures S3A-S3D).

Thus, two distinct *tra*-dependent mechanisms impart sex differences to the intestinal epithelium; the intrinsic (and *tra2*-independent) sexual identity of adult intestinal progenitors controls their female-biased proliferation (Hudry et al., 2016), whereas a gut-extrinsic, *tra2* dependent mechanism controls the male bias in intestinal sugar gene expression.

The male gonad extrinsically controls region-specific intestinal sugar gene expression

To analyse the extrinsic factors influencing intestinal sugar gene expression, we "feminised" or "masculinised" specific cell types or tissues by confining *tra*/*tra-2* KD or tra^F mis-expression using tissue-specific driver lines. Targeting visceral muscles (Figure S4A), neurons (Figure S4B), glia (Figure S4C), fat body (with liver/adipose tissue-like functions, Figure S4D), immune cells (haemocytes, Figure S4E), or secretory glands such as the *corpora cardiaca* and *corpus allatum* (Figures S4F and S4G, respectively) all failed to affect male bias in intestinal sugar gene expression, suggesting that these tissues were unlikely to be the source of a sex-biased signal.

Given our previous findings ruled out the intestinal epithelium as a source of an extrinsic factor(s), we examined the spatial restriction of the intestinal sexual dimorphism in sugar gene expression in

more detail - in particular, its three-dimensional arrangement inside the male body cavity. Immunohistochemical analysis of the internal organs in their intact arrangement (see STAR Methods) revealed close proximity between the gut region with male-biased sugar gene expression and the apical tip of the testes (Figure 3A, 3B).

We hypothesised that gonadal sex may control intestinal sugar gene expression, and generated a series of flies in which we uncoupled gonadal from somatic sex. Masculinisation of female gonads in otherwise female flies resulted in male-like intestinal sugar gene expression. This was the case in *snf* mutant female flies, or in female flies with germline-specific *Sxl* or *snf* knockdowns, which result in de-repression of testis genes in the "female" gonad (Casper and Van Doren, 2009; Chau et al., 2009, 2012; Shapiro-Kulnane et al., 2015) (Figures 3C, 3D). Comparison of two *tra* mutations with different effects on the gonad pointed to a requirement for the male somatic gonad rather than the germline itself. tra^{KO} mutant "females," which have masculinised somatic tissues and pseudo-testis that develop as testis but lack male germ cells, (Yang et al., 2012) had high, male-like intestinal sugar gene expression (Figures 2B, 3C). By contrast, low, female-like intestinal sugar gene expression was observed in *tra* mutants generated by ubiquitous excision of the excisable *tra* allele (Figure 3E). Like tra^{KO} mutants, these mutant "female" flies have masculinised tissues but, unlike tra^{KO} mutants, they develop ovaries (Figures 3C, S4I, S4J). These two mutants indicate that intestinal sugar gene expression is dependent of the sex of the gonad rather than the sex of the rest of the body. We observed female-like intestinal sugar gene expression in feminised tra^{F} knock-in "males" in which all tissues are feminised but have atrophic gonads , also consistent with a male gonad requirement (rather than, for example, a repressive signal emanating from the female gonad) (Evans and Cline, 2007; Yang et al., 2012) (Figures 2B, 3C).

To demonstrate a contribution of the male somatic gonad more directly, we used *shutoff* (esg^{SHOF}) mutant males flies lacking a functional testis (Kiger et al., 2001; Tulina and Matunis, 2001; Voog et al., 2014) (Figure 3C). Absence of a male gonad in these otherwise male flies resulted in low, "feminised" intestinal sugar gene expression (Figures 3F, S4H). To confirm the involvement of the male somatic gonad (as opposed to the male germline) we used *zero population growth* (*zpg*) mutants, which lack the male germline but have an intact somatic hub (Gilboa et al., 2003; Smendziuk et al., 2015; Tazuke et al., 2002). Unlike esg^{SHOF} males, these males still displayed a male-like pattern of intestinal sugar gene expression (Figures 3C and 3F).

Overall, these experiments indicate that gonadal sex controls sex differences in intestinal sugar gene expression, and point to a signal derived from the male somatic gonad as the molecular mediator.

The male gonad promotes intestinal sugar gene expression by activating JAK-STAT

We hypothesised that the male gonad activates a signalling pathway in gut cells in a sexually dimorphic manner, leading to male-biased expression of sugar genes. To identify this pathway, we conducted a genetic screen by knocking down signal transduction components in ECs, including major hormonal pathways (e.g. juvenile hormone, ecdysone) (Droujinine and Perrimon, 2016), pathways with a sexually dimorphic signature in our transcriptional analysis (FGF signalling, peptidergic signalling by Allatostatin A, Bursicon, Tachykinin) (Hudry et al., 2016), and/or pathways that modulate carbohydrate metabolism (e.g. insulin, Mondo/Mlx, Dawdle) (Chng et al., 2014; Mattila and Hietakangas, 2017). RNAi was used to KD expression in ECs (Figure S5A) – or amorphic mutants were used when available (Figures S5B-S5D). Only interference with the JAK-STAT signalling

pathway (Hombria and Brown, 2002) reduced male bias in intestinal sugar gene expression (Figure 4A).

Consistent with male-biased activation of the JAK-STAT pathways in ECs, a Stat signalling reporter (*Stat92E-GFP*, Bach et al., 2007) displayed broader epithelial expression in the R4 midgut region of males compared to females (Figures 4C, 4D), especially in the gut portion in closest proximity to the testis hub (Figure 4E). A candidate ligand that could activate the JAK-STAT pathway in ECs was the cytokine Unpaired 1 (Upd1) (Rajan and Perrimon, 2012; Sainz et al., 2015). Upd1 is produced by the testis hub and promotes self-renewal of male somatic cyst stem cells and germ stem cell adhesion (Greenspan et al., 2015; Kiger et al., 2001; Leatherman and Dinardo, 2010; Tulina and Matunis, 2001). Downregulation of *upd1* from testis somatic cells reduced intestinal sugar expression in male guts (Figure 4B), although to a lesser extent than interfering with JAK-STAT receptor or downstream signalling from ECs, suggesting incomplete ligand downregulation and/or partial ligand redundancy.

Masculinisation of intestinal sugar gene expression has been observed in mutant females with "masculinised" tumorous ovaries, such as *snf* or *nos>Sxl-RNAi* females in which the transformed ovaries ectopically activate JAK/STAT ligands and pathway components (Figure 3C) (Shapiro-Kulnane et al., 2015). To further test whether ectopic JAK-STAT signalling affects inter-organ sex differences in females we: (1) ectopically expressed Upd1 from a wild-type female gonad using *nos-Gal4, Cas9VPR*; and (2) ectopically activated the JAK-STAT pathway in female ECs, by expressing a constitutively active Hop (*UAS-hop^{Tum}*) or the JAK-STAT ligand Upd3 from *mex1-Gal4*. In both cases, intestinal sugar gene expression was upregulated in female guts (Figures 4A, 4B).

To explore how JAK-STAT signalling conferred male identity on ECs, as well as its range of action, we induced flip-out clones (Harrison and Perrimon, 1993) in adult flies in which we either downregulated the JAK-STAT receptor *dome* in males, or ectopically activated JAK-STAT signalling in females. Clones with reduced JAK-STAT signalling in males downregulated the Amy-p reporter in R4 (Figure 4G), whereas ectopic JAK-STAT signalling was sufficient to induce Amy-p expression in ECs within the clone in the same gut region of females, from which Amy-p is normally absent (Figure 4H). Other gut regions were refractory to JAK-STAT signalling manipulations. We were unable to downregulate endogenous Amy-p in male R2 ECs by downregulating *dome* (Figure 4G), or to ectopically activate it in ECs that do not normally express it outside R4, in either males or females (Figure 4H). Thus, there is a sex-independent restriction in the competence of the migdut to respond to the testis-derived masculinising signal.

More broadly, we have uncovered inter-organ communication between the male gonad and the gut; the male gonad promotes spatially restricted JAK-STAT signalling in a subset of ECs, leading to male-biased intestinal sugar gene expression in a specific midgut portion.

Male-biased carbohydrate handling promotes food intake through secreted citrate

In mice, the intestine can make glucose *de novo*, which is secreted into the portal vein and can affect hunger and satiety (Soty et al., 2017). We hypothesised that sex differences in intestinal JAK-STAT signalling and sugar handling might similarly affect feeding in flies, perhaps through secretion of a metabolite. To test this idea, we characterised a *Gal4* driver line, *R2R4-Gal4*, expressed exclusively in ECs of the R2 and R4 regions (Figures 4C, 4F, S6A, see STAR Methods). We used this line to investigate the physiological consequences of abrogating (*Stat92E* downregulation or expression of a dominant-negative *dome*, *UAS-dome$^{\Delta CYT}$*) or exacerbating (*upd3* overexpression) JAK-STAT signalling in ECs of the midgut R4 region. We also reduced the male bias in JAK-STAT signalling independently

from the male gonad in two ways: by depleting the testis from hub cells in *esg*^{shof} males (Voog et al., 2014), and by downregulating endogenous *upd1* from the hub using *fas3-Gal4* (expressed in the hub cells of the testis, (Demarco et al., 2014; Wolfstetter and Holz, 2012)). Using flyPAD to monitor feeding behaviour in freely behaving flies (Itskov et al., 2014), we observed that reduced JAK-STAT signalling in male ECs resulted in reduced food intake, whereas its up-regulation above endogenous levels increased it (Figure 4I). Thus, the JAK-STAT signalling status of male ECs in this sexually dimorphic region controls food intake.

We hypothesised that male-biased JAK-STAT signalling in ECs would result in the male-biased production and/or secretion of a metabolite. To test this idea, we used genetically encoded FRET-based metabolic sensors expressed specifically in the ECs of R2 and R4, together with a glucose sensor (*UAS-FLII12Pglu-700μδ6*, (Takanaga et al., 2008; Volkenhoff et al., 2018)) and a lactate sensor (a *UAS*-based version of the laconic sensor (San Martin et al., 2013), see STAR Methods). The glucose sensor revealed higher glucose levels in male relative to female ECs of the R4 (but not the R2) region (Figure 5A), given the R4-specific male-biased up-regulation of digestive enzymes and sugar transporters.

To monitor lactate levels, we used our validated lactate reporter (Figure S6D) to show that, like glucose, lactate levels were sexually dimorphic in R4 and not in R2. However, lactate levels were lower in male than in female ECs (Figure 5B), suggesting that lactate or an intermediate metabolite "downstream" of glucose was exported out of the EC, or was metabolically diverted.

To test this idea, we used food intake as a behavioural readout for a genetic screen in which we knocked out male-biased intestinal sugar genes, reasoning that KD of any enzymes mediating conversions "upstream" of this metabolite or those involved in its transport out of the EC would reduce food intake, whereas KD of "downstream" enzymes would have no effect (or increase food intake if their normal function was to divert the use of this metabolite to other intracellular pathways). R2/R4-specific KD of genes for enzymes involved in sugar digestion, absorption and glycolysis (alone or in combination, see STAR Methods) all reduced food intake (Figures 6A, 6B, S6C, S6E), suggesting that the key metabolite was the glycolytic end-product pyruvate or a downstream metabolite.

Interference with the enzymes mediating pyruvate to lactate conversion or its subsequent transport, or with the pyruvate dehydrogenase complex mediating its decarboxylation into acetyl-CoA for mitochondrial oxidation (See STAR Methods; (Seegmiller et al., 2002), all failed to affect food intake (Figures 6C, 6D, S6C, S6H, S6I), arguing against anaerobic glycolysis and the oxidative entry into the tricarboxylic acid (TCA) cycle being the source of the male-biased production and/or secretion of a metabolite. Consistent with this idea, immunostaining analysis revealed higher levels of phosphorylated PDH (i.e. inactive, (Korotchkina and Patel, 2001; Linn et al., 1969)) in the R4 region of male flies (Figure 6E), and KD of genes coding for TCA cycle enzymes did not affect food intake (Figures 6C and 6D, S6G).

A third way in which pyruvate is utilised involves the anaplerotic pyruvate carboxylase (PCB)-mediated pathway leading to citrate production through the pyruvate/citrate cycle (Iacobazzi and Infantino, 2014; Jensen et al., 2008), and involves PCB-mediated production of oxaloacetate (OAA), which is then converted to citrate by citrate synthase (Knockdown (Kdn) in *Drosophila*, (Fergestad et al., 2006). Genetic manipulations predicted to interfere with this route of citrate production reduced food intake. These included *Mitochondrial pyruvate carrier 1* (*Mpc1*, (Bricker et al., 2012)) KD, expected to reduce pyruvate import into the mitochondria, and kdn/*PCB* (Camporeale et al., 2007) KD, reducing its subsequent conversions (Figures 6F, 6G). Similarly, modulating the amount of

pyruvate available for citrate production by forcing or inhibiting its conversion to Ac-CoA also affected food intake in both directions. KD of the PDH inhibitory kinase Pdk (Katsube et al., 1997), predicted to increase Ac-CoA production and thereby reduce pyruvate available for citrate production, reduced food intake (Figures S6C and S6F). By contrast, KD of the PDH-activating Pdp phosphatase (Chen et al., 2006), predicted to have the opposite effects on Ac-CoA production and pyruvate availability, increased food intake (Figures S6C and S6F). These findings suggest citrate is the key secreted metabolite downstream of JAK-STAT signalling and the intestinal sugar genes in mediating systemic effects on food intake.

We tested this further by downregulating *ATP citrate lyase* (*ATCPL*, (Ryerse et al., 1997) which converts citrate to OAA. We predicted that this would increase citrate levels available for export and, consistent with this idea, we observed increased food intake (Figures 6F, 6G). Conversely, downregulation of the *I'm not dead yet* (*Indy*) transporter (Rogina et al., 2000), known to transport citrate (Inoue et al., 2002a; Knauf et al., 2002), reduced food intake (Figures 6F and 6G). Adult-confined *Indy* KD further confirmed a role for citrate in promoting food intake in adult males (Figure S6J). To confirm that citrate is the key secreted metabolite downstream of JAK-STAT signalling, we generated a genetically encoded nanosensor for real-time *in vivo* quantification of citrate levels (CIT8, (Ewald et al., 2011), see Methods) and validated its function and specificity (Ewald et al., 2011) (Figure 5C, see Methods). Using the sensor we found that citrate levels were sexually dimorphic in R4; male ECs have 2.5 times more citrate than female ECs (Figure 5C). Monitoring citrate levels following *Indy* KD revealed increased citrate levels in male R4 ECs (Figure 5C), confirming that Indy normally transports citrate out of these cells.

Finally, we conducted a series of additional controls to validate our findings. We showed that the R2 region did not contribution to these phenotypes (Figure S7A), and that possible developmental effects of downregulating intestinal JAK-STAT signalling or the sugar genes on body or gut size did not underlie the differences in food intake (Figures S6B and S7B). We also ruled out that the food intake phenotypes resulted from effects of JAK-STAT signalling/intestinal sugar gene expression on intestinal stem cell proliferation. Most manipulations that abrogated the male bias in intestinal sugar gene expression and reduced food intake (e.g. testis hub loss, or EC-specific *Indy* knockdown) did not affect male stem cell proliferation (Figure S7C). In the few instances where stem cell proliferation was increased (following over-activation of JAK-STAT signalling in ECs by ectopic Upd3 expression, (Osman et al., 2012), the proliferation increase could be uncoupled from the effect on food intake by simultaneously downregulating an intestinal sugar gene (*Mal-A1*), which reduced food intake without reducing stem cell proliferation to basal levels (Figures S7D, S7E, S7F), providing further support for the model that male-biased carbohydrate metabolism is genetically "downstream" of the male bias in JAK-SAT signalling in ECs of the R4 region. Reducing citrate production in R2 and R4 in females (by downregulating *Mal-A1* or *Hex-A* enzymes) had no effect on their feeding behaviour (Figure S7G) indicating that modulation of feeding by the pyruvate/citrate cycle activity in ECs is male-specific.

Together, our data support a model whereby male-biased activation of JAK-STAT signalling in ECs of the R4 region upregulates intestinal sugar gene expression to produce cytosolic citrate, which is exported into the circulation by the citrate transporter Indy to promote food intake.

Intestinal citrate efflux is required for testis germline maturation

To investigate possible roles of male-specific intestinal citrate efflux, we quantified citrate levels in both haemolymph and whole flies, using LC-MS and CE-MS (see Methods), observing high levels of circulating citrate in male flies (100.5 ± 54.3µM, Figure S7H), but neither this circulating citrate nor whole-body citrate levels were significantly reduced by preventing intestinal citrate efflux (by R2R4-driven *Indy* KD, Figures 7A, S7H, Table S2). CE-MS analysis of haemolymph revealed no large-scale effects on other circulating metabolites following intestinal *Indy* KD (Table S2). We hypothesised that the testis may utilise gut-derived citrate. To test this idea, we downregulated the *Indy* citrate efflux transporter specifically in R4 intestinal ECs using *R2R4-Gal4*, and assessed the consequences in the testis. Immunohistochemical analysis indicated that downregulation of intestinal citrate efflux had little effect on the testes tissue architecture and DNA replication (assayed with phospho-Histone 3 (pH3), (Tan et al., 2017; Tapia et al., 2006)) (Figure 7B). However, pH3 quantification revealed that, whilst there were no obvious differences in mitoses in the tip region where spermatogonia are generated from stem cells (Greenspan et al., 2015), pH3 numbers were substantially reduced in the region in which spermatids are produced from spermatogonia, consistent with a delay in gamete maturation (Figure 7B), confirmed by $Comr^{GFP}$ labelling of primary spermatocyte nuclei (Jiang and White-Cooper, 2003) which revealed a reduction in spermatocyte number following intestinal *Indy* KD (Figure 7C).

We hypothesised that impaired intestinal citrate efflux may contribute to delayed gamete maturation through metabolic changes in the testis. To explore this idea, we reduced citrate import in testes by testis-specific *Indy* KD in testes early-stage somatic cells (Figure S7N) and saw no effect on mitotic spermatogonia (Figures S7I, S7J) but reduced numbers of primary spermatocytes (Figure 7D), elongating spermatids (Figure 7E) and individualising spermatids (Figure 7F), mirroring the phenotype obtained by reducing intestinal citrate efflux. Confining *Indy* KD to late-stage somatic cells (Figure S7N) also reduced the numbers of individualising spermatids (Figure 7G) without affecting mitotic spermatogonia (Figure S7K). These genetic experiments also uncoupled the roles of gut-derived citrate in sustaining sperm production from its role in stimulating appetite; reducing testis citrate import (by means of *tj*-driven *Indy* KD) impaired spermatogenesis without affecting food intake (Figures 7D-7F, 7J). Reduced food intake was, conversely, apparent when *Indy* was selectively downregulated in neurons (Figure S7O).

To more directly test whether gut-to-testis citrate transfer sustains spermatogenesis, we analysed adult testes using gas chromatography-mass spectrometry (GC-MS), comparing adult testes from control male flies to those from male flies in which the Indy citrate efflux transporter had been specifically downregulated in intestinal ECs of the R2/R4 regions. We observed a trend towards reduced citrate levels in testes samples following intestinal knockdown, consistent with reduced exogenous supply of citrate to the testis (Figure 7H, Table S2). Impaired intestinal citrate efflux also resulted in a significant accumulation of 2-hydroxyglutarate (2HG) in testes (Figure 7H, Table S2). 2HG is an oncometabolite (Chowdhury et al., 2011; Figueroa et al., 2010; Losman and Kaelin, 2013; Lu et al., 2012; Xu et al., 2011), but is also produced by healthy tissues, where it can accumulate when cytosolic citrate is low (Li et al., 2017; Li et al., 2018; Nota et al., 2013; Palmieri, 2013; Ye et al., 2018).

We monitored citrate levels in different testis cell types by expressing our citrate sensor in both gut and testis cells, whilst simultaneously preventing male-specific intestinal citrate production in R2 and R4 ECs using $Mal\text{-}A1^{RNAi}$ (we chose *Mal-A1* because its expression is highly specific to the midgut and entirely absent from testes) ((Leader et al., 2018) and data not shown). Reduced gut-derived citrate production resulted in a significant reduction in citrate intracellular levels selectively in testis late-stage somatic cells (Figure 7I) but not in germline stem cells (Figure S7L) or early-stage somatic cells

(Figure S7M) (for testis cell type-specific reporter expression, see Figures 3B and S7N). Together, these results indicate that intestinal citrate is locally transferred via the Indy transporter from the R4 midgut region to the adjacent testis, where it sustains maturation of male gametes.

DISCUSSION

Sex differences in intestinal carbohydrate metabolism

Regional differences in gene expression are observed along animal gastrointestinal tracts, suggestive of functional specialisations (Bates et al., 2002; Haber et al., 2017). We now provide evidence for region- and cell type-specific carbohydrate metabolism. Intestinal carbohydrate metabolism also differs between the sexes, illustrating how sex differences can be confined to specific organ portions; even when digestive enzymes are more broadly expressed along the midgut, their male upregulation is posterior midgut (R4)-specific. We suggest that specific gut portions may be physiologically "sexualised" to subserve reproductive needs – in this case spermatogenesis. The posterior midgut might be more broadly sexually dimorphic than other intestinal regions; redox/oxidative stress response proteins are male biased and Yolk protein 1 is female biased in this same region ((Hudry et al., 2016) and Figure 1). In female flies, posterior midgut ECs adjust their lipid metabolism after mating to maximise reproductive output (Reiff et al., 2015). It will be of interest to explore whether this requires their female identity; if it does, is female identity the "ground state" in the absence of a male gonad, or does it result from an ovary signal? Comparative studies could also explore contributions of intestinal sex differences to reproductive success in animals other than *Drosophila*, and whether the evolution of a placenta (an organ purpose-built for reproduction) replaced or reinforced such intestinal contributions in female mammals.

Gonadal control of intestinal sexual identity

The male gonad controls sex differences in intestinal carbohydrate metabolism through male-biased cytokine signalling activity. *Drosophila* Upd belong to the type I family of cytokines, like mammalian interleukins and leptin. In both humans and rodents, leptin expression is sexually dimorphic (Couillard et al., 1997; Gui et al., 2004; Havel et al., 1996; Landt et al., 1998; Montague et al., 1997; Rosenbaum et al., 1996; Saad et al., 1997). Males and females also differ in their interleukin repertoire, which contributes to sex differences in immunity and autoimmune disease (Russi et al., 2018; Voigt et al., 2016; Xiong et al., 2015). A possible contribution of cytokines such as leptin to sex differences in organ physiology deserves further investigation, particularly in light of its known reproductive and gastrointestinal roles (Sainz et al., 2015; Smith et al., 2002).

The gonadal regulation of intestinal sugar metabolism contrasts with the intrinsic, sex chromosome-dependent control of sex differences in gut stem cell proliferation (Hudry et al., 2016). This illustrates the complexity of an organ's "sexual identity"; two lineage-related cells within an epithelium (stem cells and their EC progeny) acquire sex-specific functions (proliferation and carbohydrate metabolism) through two distinct mechanisms. Sexual identity is reversible in both cases and needs to be actively maintained in adults, raising the question of whether adult plasticity in sexual identity may be adaptive. Environmental factors could modulate the expression or penetrance of sex determinants – possibly tissue-specifically. There is some evidence in support of this idea – male flies that lack Fru^M are defective in courtship, but learn to court when housed in groups with wild-type flies in a Dsx^M-dependent manner (Pan and Baker, 2014). Early-life exposure

to nutrient scarcity also affects neuronal wiring selectively of male *C. elegans* (Bayer and Hobert, 2018). In light of these and our findings, it will be of interest to explore how plastic sex differences in physiology are and why.

Inter-organ metabolic communication

Gut-gonad communication is bidirectional; the male gonad communicates with a specific gut portion, which responds by secreting citrate. Gut-derived citrate in turn promotes food intake and maturation of male gametes. How might it do so? Import of exogenous citrate may help sustain the high TCA cycle requirements of developing sperm (Bajpai et al., 1998; Boussouar and Benahmed, 2004). Sertoli cells are highly glycolytic and have been proposed to act as a paracrine source of lactate for developing gametes (Boussouar and Benahmed, 2004; Oliveira et al., 2015). It is therefore conceivable that citrate acts as another exogenous carbon source. Consistent with this idea, the mitochondrial citrate carrier is present and active in human sperm (Cappello et al., 2012), and boar sperm can metabolise exogenous citrate through the Krebs cycle *in vitro* (Medrano et al., 2006). Alternatively, import of gut-derived citrate may sustain membrane formation through its conversion to acetyl-CoA by ATCPL, then used for fatty acid synthesis; both spermatid elongation and individualization require extensive membrane biosynthesis and remodelling (Laurinyecz et al., 2016; Szafer-Glusman et al., 2008). Citrate could also support epigenetic changes relevant to male gamete maturation through its conversion to acetyl-CoA, used as a donor for histone acetyl transferase-mediated histone acetylation (Su et al., 2016).

The effects of gut-derived citrate on sperm production can be uncoupled from its orexigenic actions. Preventing citrate import into neurons reduces food intake, suggesting that its promotion of feeding may result from its actions in the nervous system. Given that preventing gut-derived citrate efflux does not impact circulating citrate, it is tempting to speculate that local gut and/or testis-innervating neurons may be the citrate sensors. This effect of citrate on food intake is male-specific – reducing gut-derived citrate efflux does not reduce feeding in females. Our ongoing work is revealing that, in females, gonad to gut communication also promotes feeding, but via a different mechanism and possibly as a result of different dynamics/metabolic requirements of male and female gamete production (Hadjieconomou et al., unpublished).

More generally, our study provides evidence that citrate functions in communication between organs. In mammals, plasma levels of citrate are amongst the highest among TCA cycle intermediates (Costello and Franklin, 1991a, 2016b; Hui et al., 2017; Mycielska et al., 2009). Organ-specific differences in citrate production and consumption have been reported (Jang et al., 2019), but little is known about its roles and regulation by diet, age or sex. Bone – an organ that controls male fertility through an endocrine hormone – produces unusually high amounts of citrate (Costello et al., 2012; Dickens, 1941; Oury et al., 2011). In the context of male gametes, the prostate should also be considered as a potentially relevant citrate source; it secretes large amounts of citrate into the seminal fluid that developing sperm will come into contact with (Costello and Franklin, 1991a; Mycielska et al., 2009). The roles of prostate citrate have been investigated in the context of the metabolic rewiring of prostate tumours (Costello and Franklin, 1991b, 2016a). Less is known about its roles in the context of sperm production, partly because surgical interventions such as prostatectomy impair other aspects of testis physiology. Contributions of exogenous citrate to sperm-mediated transgenerational effects also deserve further investigation in light of citrate's epigenetic effects. It will also be of interest to characterise the transporters for citrate import into the germline to control spermatogenesis, and/or into neurons to control food intake; *CG7309* and

Indy-2 genes code for putative citrate transporters and have testis-specific expression (Leader et al., 2018). In mammals, the Indy homologue NaCT is specifically expressed in testis, liver and brain (Inoue et al., 2002b), and NaCT knockout mice are protected from diet- and age-induced adiposity and insulin-resistance (Birkenfeld et al., 2011).

The physical proximity between the male gonad and the gut portion to which it signals raises the possibility that the relative positioning of internal organs is physiologically significant. Although this particular association is not conserved in adult humans, testis development is a complex process from a three-dimensional perspective, which in all placental mammals involves descent of testes from a position near the kidneys (Sharma et al., 2018), perhaps providing opportunities for inter-organ communication. More generally, a spectrum of conditions (so-called heterotaxy syndromes) resulting from the abnormal arrangement of internal organs including the gastrointestinal tract can lead to serious disease manifestations. Subtler, likely undiagnosed defects in intestinal positioning could result in milder gastrointestinal symptoms and/or contribute to differences in whole-body physiology across individuals.

ACKNOWLEDGEMENTS

We thank Marc Amoyel, Erika Bach, Halyna Shcherbata and Guy Tanentzapf for providing reagents and advice, and Utpal Banerjee, James Castelli-Gair Hombria, Leanne Jones, Masayasu Kojima, Ronald Kühnlein, Paul Schedl and Stefanie Schirmeier for sharing reagents. We are grateful to Marcos Gonzalez-Gaitan for advice, and Louise Fets, Susumu Hirabayashi and Santiago Vernia for providing comments on an earlier version of this manuscript. This work was funded by an ERC Advanced Grant to IM-A (ERCAdG 787470 “IntraGutSex”), an EMBO Advanced Fellowship to BH, an EMBO LTF 63-2017 to AM, an ERC Advanced Grant to TP (ERCAdG 741550 “EnergyMemo”) and MRC intramural funding. BH is currently sponsored by the CNRS and supported by an ATIP-Avenir CNRS grant and by the Université Côte d'Azur Académie 4 IDEX JEDI.

AUTHOR CONTRIBUTIONS

B.H. conducted most experiments. E.dG. conducted most of the flyPAD assays. A.M., P.G., D.H. and C.S conducted some of flyPAD assays, haemolymph extractions and/or testis dissections for metabolomics. J.B.M. and H.K. conducted metabolomics experiments. P-Y.P. generated and validated the lactate sensor and, together with T.P., provided advice on the metabolic sensors. B.H. and I.M-A. analysed data and co-wrote the manuscript, with the other authors providing editorial comments.

DECLARATION OF INTERESTS

The authors declare no competing interests.

MAIN FIGURE LEGENDS

Figure 1. Expression of the carbohydrate metabolism pathway is male-biased in a specific portion of the adult intestine.
(**A**) Expression pattern of Mal-A1^{GFP} protein in whole midguts of adult *Drosophila* (DNA labelled with DAPI, blue (throughout figures); Mal-A1^{GFP}, green). (**B**, **C**) Quantifications of Mal-A1^{GFP} (**B**) and Amy-p^{GFP} (**C**) protein levels in R2 (left) and R4 (right) regions of adult male (M) and female (F) midguts. Representative images shown (DAPI, blue; protein, green/GFP). For plots (including subsequent panels), expression levels set at 100% for control males, expression in females displayed as a percentage of male expression. (**D** to **H**) Representative images (DAPI, blue; protein, green/GFP) and quantifications of Mal-A3^{GFP} in enteroendocrine cells (**D**), Treh^{GFP} (**E**), Hex-A^{GFP} (**F**), Pgi^{GFP} (**G**) Ldh^{GFP} (**H**) expression in R4 region of adult male and female midguts. (**I**) Representative images (DAPI, blue; *Mal-A7>mCD8GFP,* green) and quantifications of *Mal-A7-Gal4* expression levels in R4 region of adult male and female midguts. Data combined from at least two independent experiments. n = midgut number per genotype, except panel D where n = cell number. Scale bars, 50µm in all images except for (A) 200 µm, and (B), (C), (I) 10 µm. Asterisks highlighting significant comparisons across sexes displayed in grey boxes at bottom of graphs. In this and subsequent figures, data shown in boxplots with all data points shown, p-values from Mann-Whitney-Wilcoxon test (non-significant (ns): $p>0.05$; *: $0.05>p>0.01$; **: $0.01>p>0.001$; ***: $p<0.001$). See Supplemental Information for a list of full genotypes. See also Figure S1.

Figure 2. Sex differences in intestinal sugar gene expression are independent of the gut cell sex.
(**A**) Heat maps displaying normalised expression abundance for sugar genes with *transformer* (*tra*)-dependent sexually dimorphic expression in adult midgut of females, males, and whole-body *tra* null mutant "females" (Table S1 = genes and expression abundance). (**B**, **C**) RT-qPCR expression data for a subset of sugar genes with midgut-specific expression (Leader et al., 2018), (gene names at bottom of graphs) in male (M) and female (F) control flies, flies with whole-body *tra* knockout (*tra^{KO}*) or flies with whole-body *tra^{F}* knock-in gain-of-function (*tra$^{F\ K\text{-}IN}$*) (B) and flies harbouring a whole-body *tra2* null mutation (C). In these and subsequent panels, expression abundance for each gene was arbitrarily set at 100% for control males, and the percentage of that expression is displayed for the other sex and genotypes. (**D**, **E, F**) RT-qPCR expression data for the same set of sugar genes in flies in which *tra* was downregulated (D, *esg, mex1>tra^{RNAi}*), knocked out (E, *esg, mex1>flp,tra^{F}*) or re-introduced in a *tra* whole-body mutant (*tra^{KO},esg, mex1>tra^{F}*) in intestinal stem cells and ECs relative to controls. In all panels, n = number of fly groups analysed per genotype (each group = 20 flies). Asterisks highlighting significant comparisons across sexes are displayed in grey boxes at bottom of graphs. See Supplemental Information for a list of full genotypes. See also Figures S2, S3, Table S1.

Figure 3. Male gonad is adjacent to midgut R4 region and extrinsically controls region-specific intestinal sugar gene expression.
(**A**) Immunostaining of abdominal internal organs in their intact three-dimensional organization (DAPI, blue; *Mal-A7-Gal4>UAS-GFP,* green; muscles, Phalloidin/red). R4 intestinal region (white arrow and inset) is adjacent to apical tip of testes (scale bar, 200µm, or 50µm in inset). R2, hollow arrow. (**B**) Quantification of intestine-testes proximity in intact male abdomens. A representative image shown. Apical tips of testes highlighted with white asterisks and visualised with GFP/green (*nanos>UAS-StingerGFP*); muscles with Phalloidin/red. (**C**) For each boxed genotype, panel summarises sex chromosome complement (XY or XX), sexual phenotype of the soma (whole fly

images), presence/state of gonads (representative images below each description) and intestinal sugar gene expression. Genotypes, left to right: female-sterile *snf*^{148} female flies, (confocal image shows wild-type ovariole, left, with egg chambers spanning the fourteen stages of oogenesis; *snf* mutant ovariole, right, lacking differentiating egg chambers); whole-body *tra* knockout (*tra*^{KO}) "masculinised" females; *Actin5C-Gal4*-driven *tra* knockout (*Act5C>flp,tra*^{FRT}) females; whole-body *transformer*^{F} (*tra*$^{F\ K\text{-}IN}$) knock-in gain-of-function feminised males; sterile *esg*^{SHOF} male flies (hub cells labelled with Fasciclin 3 (Fas3) in red; DAPI, blue); and sterile *zpg*$^{z\text{-}2533/z\text{-}5352}$ male flies (intact hub cells, labelled with Fasciclin 3 (Fas3) in red, DAPI, blue) (Smendziuk et al., 2015). (**D**) RT-qPCR expression analysis of midgut-specific sugar genes in males (M) and females (F) with germline-specific *snf* mutation (*snf*^{148}), KD (*nos>snf*^{RNAi}) or germline-specific *Sxl* KD (*nos>Sxl*^{RNAi}) relative to relevant controls. (**E**) RT-qPCR expression analysis of midgut-specific sugar genes in flies with *Act5C-Gal4* driven *tra* KD (*Act5C>flp,tra*^{FRT}) relative to controls. (**F**) RT-qPCR expression analysis of midgut-specific sugar genes in sterile male flies lacking hub and germline stem cells (*esg*^{SHOF}), and in sterile males lacking germline but with intact hub (*zpg*$^{z\text{-}2533/z\text{-}5352}$). In all panels, n = number of fly groups analysed per genotype (each group = 20 flies), except panel B where n = viscera number analysed. Asterisks highlighting significant comparisons across sexes are displayed in grey boxes at bottom of graphs; those highlighting significant comparisons within female and male datasets are displayed in red and blue boxes, respectively. See Supplemental Information for a list of full genotypes. See also Figure S4.

Figure 4. Gonadal activation of intestinal JAK/STAT signalling promotes intestinal sugar gene expression in male enterocytes of the R4 region.

(**A**) RT-qPCR expression analysis of midgut-specific sugar genes in males (M) and females (F) following EC-specific KD of JAK-STAT receptor *dome* (*mex1>dome*^{RNAi}), downstream signaling transducers *hop* (*mex1>hop*^{RNAi}), and *Stat92E* (*mex1>Stat92E*^{RNAi}), or EC-specific mis-expression of constitutively active Hop (*mex1>hop*^{Tum}), and JAK-STAT ligand *upd3 (mex1>upd3*^{OE}). (**B**) RT-qPCR expression analysis of midgut-specific sugar genes following testis-specific downregulation of *upd1* (*tj>upd1*^{RNAi} and *fas3>upd1*^{RNAi}), or ectopic expression of *upd1* from female germline (*nos>Cas9*^{VPR}*,upd1*^{OE}), compared to both relevant controls and flies of the opposite sex with an identical genetic manipulation. (**C**) Representative midgut expression of *Stat92E-GFP* and *R2R4-Gal4* reporters (DAPI, blue; reporter-driven GFP, green). (**D**) Higher magnification images of *Stat92E-GFP* expression (green) in the R4 region of male and female midguts. ECs identified by larger DAPI-positive nuclei, blue. (**E**) Immunostaining of male midgut and testes in intact three-dimensional arrangement (DNA: DAPI, blue; Stat92E-GFP: GFP, green; Actin: Phalloidin, red). (**F**) *R2R4-Gal4* reporter is expressed only in ECs (with larger, endoreplicating nuclei, DAPI, blue), not in intestinal progenitors/enteroendocrine cells (small DAPI-positive nuclei, white arrowheads) (*R2R4>mCD8GFP*: GFP, green). (**G**, **H**) Expression of Amy-p (green, Amy-p^{GFP}) following clonal KD of JAK-STAT receptor *dome (dome*^{RNAi}*)* (G) or clonal production of constitutively active Hop protein (*hop*^{Tum}) (H) (DNA: blue,DAPI; anti-beta galactosidase, red, staining LacZ-positive cells inside the clone in which *dome*^{RNAi} or *hop*^{Tum} expression has been induced). (**I**) Food intake quantifications based on FlyPAD-monitored sips per male fly following R2 and R4 EC-specific manipulations of JAK-SAT signalling (left) or interference with gonadal JAK-STAT ligand production (right). Manipulations, left to right: mis-expression of JAK-STAT ligand Upd3 *(mex1>upd3*^{OE}*)*, expression of dominant-negative JAK-STAT receptor (*mex1>dome*$^{\Delta CYT}$), R2 and R4 EC-specific *Stat92E* KD (*mex1>Stat92E*^{RNAi}), loss of testis hub cells (*esg*^{SHOF}), and hub cell-specific *upd1* KD (*fas3>upd1*^{RNAi}). For each manipulation, median number of sips was arbitrarily set at 100% for control males and the percentage of that expression displayed for other genotypes. n = number of fly groups analysed per genotype in panels A and B (each group =

20 flies), or fly numbers monitored using FlyPAD in panel (I). Asterisks highlighting significant comparisons across sexes are displayed in grey boxes, those highlighting significant comparisons within same-sex datasets are displayed in blue boxes (males) and red boxes for females. Scale bars, 50µm in all images except for (C) 200µm and (I) 10µm. See Supplemental Information for a list of full genotypes. See also Figure S5.

Figure 5. Metabolic sensors reveal sex differences in glucose, lactate, and citrate concentrations in R4 enterocytes.

(**A**) Quantification of *FLII*^{12}*Pglu-700µδ6* glucose sensor FRET signal in R2 (left graph) and R4 (right graph) ECs of dissected male (M) and female (F) midguts (quantified based on acceptor photobleaching, see Methods). In this and subsequent panels, median FRET ratio for each genotype was arbitrarily set at 100% for control males, and the percentage of that expression is displayed for the other genotypes/sexes. Representative FRET ratio images in R4 shown. (**B**) Quantification of laconic lactate sensor FRET signal in R2 (left graph) and R4 (right graph) ECs of dissected male (M) and female (F) midguts (quantified based on acceptor photobleaching, see Methods). Representative FRET ratio images in R4 shown. (**C**) Left: quantification of FRET signal of CIT8 citrate sensor in R4 ECs of control midguts and midguts with R2/R4 EC-specific KD of citrate synthase (*kdn*^{RNAi}). Quantification of FRET signal in R4 ECs expressing CIT8 or CIT0 citrate sensors from control male midguts. Middle: quantification and representative images of FRET signal in control male and female R4 ECs expressing CIT8 citrate sensor. Right: quantification of FRET signal of CIT8 citrate sensor in R4 ECs of control midguts and midguts with R2/R4 EC-specific KD of plasma membrane citrate transporter *Indy (Indy*^{RNAi}). Representative FRET ratio images in R4 shown. In all panels, n = number of midguts analysed per genotype/condition. Scale bars, 5µm in all images. Asterisks highlighting significant comparisons across sexes are displayed in grey boxes at bottom of boxplots, those highlighting significant comparisons within male datasets are displayed in blue boxes. See Supplemental Information for a list of full genotypes.

Figure 6. Male-biased intestinal carbohydrate metabolism promotes food intake through secreted citrate.

(**A**) Glycolytic pathway enzymes/metabolites. Enzymes in blue have male-biased intestinal expression; enzymes with blue asterisk are tested in panel B. Enzymes, top to bottom: Hexokinase-A (Hex-A), Phosphoglucose isomerase (Pgi), Phosphofructokinase (Pfk), Aldolase (Ald), Glyceraldehyde 3 phosphate dehydrogenase 1 (Gapdh1), Phosphoglycerate kinase (Pgk), Phosphoglyceromutase 78 (Pglym78), Enolase (Eno), Pyruvate kinase (PyK), Fructose-1,6-bisphosphatase (Fbp). Metabolites, top to bottom: glucose-6-phosphate (G6P), fructose-6-phosphate (F6P), fructose-1,6-biphoshate (F1,6BP), glyceraldehyde-3-phosphate (GA3P), 1,3 bisphosphoglycerate (1,3BPG), 3 phosphoglycerate (3PG), 2 phosphoglycerate (2PG), phosphoenolpyruvate (PEP). (**B**) Food intake quantifications based on FlyPAD-monitored sips per male fly following R2 and R4 EC-specific glycolytic enzyme KD: *Hex-A*, *Ald*, *Pgk*, *PyK,* and *fbp*. For all panels; median number of sips was arbitrarily set at 100% for control males and the percentage of that expression displayed for other genotypes. (**C**) Tricarboxylic acid (TCA) cycle enzymes/metabolites. Enzymes with blue asterisk; tested in panel D. Enzymes, top to bottom: Pyruvate dehydrogenase E1 alpha subunit (PDH), Pyruvate dehydrogenase phosphatase (Pdp), Pyruvate dehydrogenase kinase (Pdk), Aconitase (Acon), Malate dehydrogenase 2 (Mdh2). Metabolites, top to bottom: acetyl coenzyme A (Ac-CoA), citrate (CIT), isocitrate (ICT), malate (MAL), oxaloacetate (OAA). (**D**) Food intake quantifications based on FlyPAD-monitored sips per male fly following R2 and R4 EC-specific KD of TCA cycle enzymes: *PDH, Acon*, *Mdh2*. (**E**) Quantification of expression level of phospho-PDH (pPDH) protein in R4 region of adult male (M) and female (F) midguts. Representative images shown (nuclei: blue,

DAPI; pPDH, green). (**F**) Enzymes and metabolites of the pyruvate-citrate cycle. Enzymes in blue have male-biased intestinal expression; enzymes with blue asterisk are tested in panel G. Enzymes/genes, top to bottom: Mitochondrial pyruvate carrier (Mpc1), Pyruvate carboxylase (PCB), Knockdown (Kdn), ATP citrate lyase (ATPCL), *Drosophila* plasma membrane citrate efflux transporter Indy. (**G**) Food intake quantifications based on FlyPAD-monitored sips per male fly following R2 and R4 EC-specific KD of: *Mpc1*, *PCB*, *kdn*, *ATPCL, Indy*. n = fly numbers analysed per genotype/condition, except panel E where n = midguts. Scale bars, 50µm in all images. Asterisks highlighting significant comparisons across sexes displayed in grey boxes at bottom of graphs, whereas those highlighting significant comparisons within male datasets displayed in blue boxes. See Supplemental Information for a list of full genotypes. See also Figures S6 and S7.

Figure 7. Intestinal citrate efflux is required for testis germline maturation.
(**A**) CE-MS measurement of haemolymph citrate in control males and in males following R2/R4 EC-specific KD of plasma membrane Indy citrate transporter. n = 4 samples, each containing haemolymph from 120-280 flies. (**B**) Immunohistochemical analysis of testis anatomy and germline maturation based on expression of Fasciclin 3 (Fas3, labelling hub cells (white arrowhead), green), DAPI (blue) and number of pH3-positive cells (staining mitotic (arrow) and meiotic (asterisk) cells, red) in testes of control males and males with R2/R4 EC-specific *Indy* KD. (**C**) Quantification of Comr expression pattern ($Comr^{GFP}$, green) in control testes and testes following R2/R4 EC-specific *Indy* KD. Representative images shown (DNA: DAPI, blue). (**D** to **F**) Representative images (DNA: DAPI, blue; protein, green) and quantifications of $Comr^{GFP}$ (D), $Boule^{GFP}$ (E) cleaved Dcp-1 (F) expression in testes of control males and in males following testis-specific *Indy* KD (*tj-Gal4* line). (**G**) Quantification of cleaved Dcp-1 expression (green) in control testes and testes following testis-specific *Indy* KD (*eya-Gal4* line). Representative images shown (DNA: DAPI, blue). (**H**) GC-MS measurements of the testis concentration of citrate and 2-hydroxyglutarate (2HG) in control males and in males following R2/R4 EC-specific *Indy* KD. n = 4 samples, each containing 150 dissected testes. (**I**) Quantification of FRET signal in late somatic testis cells expressing CIT8 from control males or males with R2/R4 EC-specific KD of *Maltase-A1* ($Mal\text{-}A1^{RNAi}$). (**J**) Food intake quantification based on FlyPAD-monitored sips per male fly following testis-specific *Indy* KD (*tj-Gal4* line). n = testes number analysed per genotype except for panel J where n = fly number analysed. Scale bars, 200µm in all images. Asterisks highlighting significant comparisons across male datasets are displayed in a blue box. See Supplemental Table 2 for metabolites/ concentrations. See Supplemental Information for a list of full genotypes. See also Figure S7 and Table S2.

STAR METHODS

KEY RESOURCES TABLE

LEAD CONTACT AND MATERIALS AVAILABILITY

Further information and requests for resources and reagents (such as newly generated *Drosophila* stocks) should be directed to and will be fulfilled by the Lead Contact, Irene Miguel-Aliaga (i.miguel-aliaga@imperial.ac.uk).

EXPERIMENTAL MODELS AND SUBJECT DETAILS

Fly husbandry

Fly stocks were reared on a standard cornmeal/agar diet (6.65% cornmeal, 7.15% dextrose, 5% yeast, 0.66% agar supplemented with 2.2% nipagin and 3.4 mL/L propionic acid). All experimental flies were kept in incubators at 25°C, 65% humidity and on a 12 hr light/dark cycle. Flies were transferred to fresh vials every 3 days, and fly density was kept to a maximum of 15 flies per vial. 5-day old virgin flies were used unless otherwise indicated.

For metabolomics and testis immunostainings, males were aged from 10-days before dissection. For clonal analyses (flip-out clones), 3-day-old adults (raised and aged at 25°C) were heat-shocked for 12 minutes at 37°C to induce clones, and were then kept at 25°C 5 days until dissection. Flies were transferred to fresh vials every 3 days.

Fly stocks

Reporters: Mal-A1^{GFP} (VDRC: 318296), Mal-A3^{GFP} (this study), Treh^{GFP} (BDSC: 59825), Hex-A^{GFP} (VDRC: 318587), Pgi^{GFP} (this study), Amy-p^{GFP} (this study), Ldh^{GFP} (gift from U. Banerjee, YD0852, generated by Quinones-Coello et al., 2007), *Stat92E-GFP* (BDSC: 26199), *GstD1-GFP* (gift from U. Banerjee, generated by Sykiotis and Bohmann, 2008), Yp1^{GFP} (VDRC: 318746), Comr^{GFP} (VDRC: 318559), Boule^{GFP} (BDSC: 64431), bam^{GFP} (VDRC: 318001).

Gal4 drivers: *R2R4-Gal4* (this study, enhancer VT004416: a 2541 base pair fragment from the flanking non-coding or intronic region of *LManVI* fused upstream of a *Drosophila* synthetic core promoter (DSCP) followed by sequence encoding a *Gal4* driver, (Kvon et al., 2014)), *esg-Gal4^{NP7397}* (gift from J. de Navascués), *mex1-Gal4* (Phillips and Thomas, 2006), *Mal-A7-Gal4* (this study, see below for details), *nos-Gal4* (BDSC: 4937), *Act5C-Gal4* (BDSC: 4414), *tj-Gal4* (DGGR: 104055), *Act5C-FRT-y-FRT-GAL4* (BDSC: 4410), *Fas3-Gal4* (DGGR: 103948), *da-Gal4* (BDSC: 55851), *pros^{V1}-Gal4* (Balakireva et al., 1998), *Myo1A-Gal4* (DGGR: 112001), *vm-Gal4* (BDSC: 48547), *elav-Gal4* (BDSC: 458), *repo-Gal4* (BDSC: 7415), *Lpp-Gal4* (Brankatschk and Eaton, 2010), *Hml-Gal4* (BDSC: 30139), *Akh-Gal4* (BDSC: 25683), *Aug21-Gal4* (BDSC: 30137), *eya-Gal4* (*eyaA3-GAL4*, gift from M. Amoyel, generated by Leatherman

and Dinardo, 2008), *tubP-Gal80^{TS}* (BDSC: 7019), *R2R5-Gal4* (DGGR: 112920, generated by Buchon et al., 2013).

UAS transgenes: *UAS-StingerGFP* (BDSC: 65402), *UAS-mCD8GFP* (*UAS-IVS-mCD8GFP*, BDSC: 32186), *UAS-FLII12Pglu-700µδ6* (Volkenhoff et al., 2018), *UAS-laconic* (this study, see below for details), *UAS-Ldh* (FlyORF: F002924), *UAS-flp* (BDSC: 4539), *UAS-tra^{F}* (BDSC: 4590), *UAS-upd3-GFP* (Wang et al., 2014), *UAS-hop^{Tum}* (gift from E. Bach, generated by Harrison et al., 1995), *UAS-dCas9^{VPR}* (BDSC: 67052), *UAS-dome$^{\Delta CYT}$* (Brown et al., 2001), *UAS-dcr2* (VDRC: 60010), *UAS-InR^{DN}* (BDSC: 8252), *UAS-gRNAS Amy-p/Amy-d/Mal-A1* (this study, see below for details), *UAS-Cas9* (BDSC: 54594), *UAS-Ldh^{RNAi}* (BDSC: 33640), *UAS-tra^{RNAi}* (BDSC: 28512), *UAS-snf^{RNAi}* (BDSC: 55914), *UAS-Sxl^{RNAi}* (BDSC: 38195), *UAS-GFP* (BDSC: 35786), *attP2* control line (BDSC: 36303), *attP40* control line (36304), *GD* control line (VDRC: 60000), *KK* control line (VDRC: 60100), *UAS-dome^{RNAi}* (BDSC: 34618), *UAS-hop^{RNAi}* (VDRC: GD 40037), *UAS-Stat92E^{RNAi}* (BDSC: 31318), *UAS-upd1^{RNAi}* (BDSC: 28722), *UAS-upd1^{OE}* (BDSC: 67555), *UAS-Hex-A^{RNAi}* (VDRC: KK 104680), *UAS-Ald^{RNAi}* (BDSC: 65884), *UAS-Pgk^{RNAi}* (VDRC: KK 110081), *UAS-PyK^{RNAi}* (VDRC: GD 49533), *UAS-fbp^{RNAi}* (VDRC: KK 108554), *UAS-PDH^{RNAi}* (VDRC: GD 40410), *UAS-Acon^{RNAi}* (BDSC: 34028), *UAS-Mdh2^{RNAi}* (BDSC: 36606), *UAS-Mpc1^{RNAi}* (VDRC: KK 103829), *UAS-PCB^{RNAi}* (VDRC: KK 105936), *UAS-kdn^{RNAi}* (BDSC: 36740), *UAS-ATPCL^{RNAi}* (VDRC: GD 30282), *UAS-Indy^{RNAi}* (VDRC: GD 9982), *UAS-tra2^{RNAi}* (BDSC: 28018), *UAS-AstA-R2^{RNAi}* (BDSC: 25935), *UAS-TkR99D^{RNAi}* (BDSC: 27513), *UAS-rk^{RNAi}* (BDSC: 31958), *UAS-Put^{RNAi}* (BDSC: 35195), *UAS-InR^{RNAi}* (BDSC: 35251), *UAS-LRP1^{RNAi}* (BDSC: 44579), *UAS-babo^{RNAi}* (BDSC: 25933), *UAS-LpR1^{RNAi}* (BDSC: 50737), *UAS-mgl^{RNAi}* (BDSC: 33940), *UAS-LpR2^{RNAi}* (BDSC: 54461), *UAS-tor^{RNAi}* (BDSC: 35639), *UAS-ITP^{RNAi}* (BDSC: 25799), *UAS-Tl^{RNAi}* (BDSC: 35628), *UAS-Mlx^{RNAi}* (VDRC: KK 110630), *UAS-Mondo^{RNAi}* (VDRC: KK 109821), *UAS-Met^{RNAi}* (VDRC: KK 100638), *UAS-Npc2e^{RNAi}* (VDRC: KK 100445), *UAS-NLaz^{RNAi}* (VDRC: KK 107553), *UAS-grnd^{RNAi}* (VDRC: KK 104538), *UAS-slif^{RNAi}* (VDRC: GD 45590), *UAS-AdipoR^{RNAi}* (VDRC: GD 40936), *UAS-EcR^{RNAi}* (VDRC: GD 37058), *UAS-usp^{RNAi}* (VDRC: GD 16893), *UAS-btl^{RNAi}* (BDSC: 60013), *UAS-gce^{RNAi}* (BDSC: 61852), *UAS-Mal-A1^{RNAi}* (VDRC: KK 106220), *UAS-CG6484^{RNAi}* (VDRC: KK 109484), *UAS-Pdp^{RNAi}* (VDRC: KK 107271), *UAS-Pdk^{RNAi}* (VDRC: KK 106641), *UAS-CG13907^{RNAi}* (VDRC: KK 107339), *UAS-Mct1^{RNAi}* (VDRC: KK 106773), *UAS-Prestin^{RNAi}* (VDRC: GD 5341), *UAS-Out^{RNAi}* (VDRC: GD 51157), *UAS-CG8925^{RNAi}* (VDRC: KK 101128).

Mutants: *tra^{KO}* (BDSC: 67412), *Df(3L)$^{st-j7}$* (BDSC: 5416), *tra$^{F\ K-IN}$* (constitutive *traF* knock-in, this study, see below for details), *Df(2R)^{trix}* (BDSC: 1896), *tra2^{1}* (gift from P. Schedl, generated by Fujihara et al., 1978), *tra^{FRT}* (FRT-flanked *tra* knock-in, this study, see below for details), *snf^{148}* (BDSC: 7398), *esg^{SHOF}* (generated by (Voog et al., 2014), *zpg^{z-2533}* and *zpg^{z-5352}* (gift from Guy Tanentzapf, generated by Arkov et al., 2006), *CCHa2-R^{TAL34}* and *CCHa2-R^{KO51-2}* (generated by (Sano et al., 2015), *Akh^{AP} and* A*kh^{A}* (Galikova et al., 2015), *AkhR^{1}* (Gronke et al., 2007), and *Df(2L)^{Exel7027}* (BDSC: 7801).

METHOD DETAILS

FlyPAD assays

FlyPAD assays were performed as described in (Itskov et al., 2014). One well of the flyPAD arenas was filled with 2.4µL of food (5% yeast 7% dextrose in 1% agarose) or our standard food, and the other was left empty. For all experiments, 5 day-old fed flies were individually transferred to flyPAD arenas by mouth aspiration and allowed to feed for 1-2h at 25°C or 29^{o}C, 65% relative humidity. The total number of sips per animal over this period was acquired using the Bonsai framework (Lopes et al., 2015), and analysed in MATLAB using previously described custom-written software (Itskov et al., 2014). Non-eating flies (defined as having fewer than two activity bouts during the assay) were excluded from the analysis**.** All flyPAD experiments were performed during the day from 11:00 until 15:00. N values shown in figures indicate the number of flies tested for each genotype. Data for experimental and control genotypes (or sexes) used for comparison was always acquired in the same flyPAD assay.

Immunohistochemistry

Intact guts were fixed at room temperature for 20 min in PBS, 3.7% formaldehyde. All subsequent incubations were done in PBS, 4% horse serum, 0.2% Triton X-100 at 4°C following standard protocols. To visualise the three-dimensional arrangement of the internal organs inside the male body cavity, intact abdomens were dissected, then fixed at room temperature for 20 min in PBS, 3.7% formaldehyde prior cuticle removal.

The following primary antibodies were used: chicken anti-GFP (ab13970, Abcam) 1/10000, mouse anti-GFP (11814460001, Roche) 1/1000, chicken anti-beta Galactosidase (ab9361, Abcam) 1/200, rabbit anti-phospho-Histone H3 Ser10 (9701L, Cell Signalling Technology) 1/500, mouse anti-Fas3 (7G10, DSHB) 1/50, rabbit anti-Pyruvate dehydrogenase E1-alpha subunit (phospho S293) (ab92696, Abcam) 1/200, rabbit anti-Aconitase 2 (ab83528, Abcam) 1/200, rabbit anti-cleaved *Drosophila* Dcp-1 (Asp216) (9578S, Ozyme) 1/500, and rhodamine Phalloidin (R415, ThermoFisher scientific) 1/1000. Fluorescent secondary antibodies (FITC-, Cy3- and Cy5-conjugated) were obtained from Jackson Immunoresearch. Vectashield with DAPI (Vector Labs) was used to stain DNA.

Generation of Mal-A3^{GFP}, Pgi^{GFP} and Amy-p^{GFP} transgenic reporter lines

The following GFP-tagged clones from the fosmid library TransgeneOme Resource (Source Bioscience (Sarov et al., 2016) were ordered for *Mal-A3*, *Pgi* and *Amy-p* respectively: CBGtg9060D0780D, CBGtg9060F0441D and CBGtg9060B10205D. The clones were sequence-verified and transgenic lines were established through ΦC-31 integrase mediated transformation (Bestgene). *attP* sites used were *VK33* (BDSC: 9750) for *Mal-A3* and *Amy-p*, and *attP40* (BDSC: 36304) for *Pgi*.

Generation of *Mal-A7-Gal4* driver

To generate a knock-in *Gal4* under the control of *Mal-A7* regulatory sequences, recombination mediated cassette exchange of the following Mi (Micchelli and Perrimon) insertion was performed: *Mi{y[+mDint2]=MIC}Mal-A7[MI00819]* (BDSC:32708). The swapping strategy previously described in (Diao et al., 2015) was employed. Briefly, the

chromosome containing the MiMIC insertion (BDSC: 32708) was combined with a chromosome bearing a *Gal4* donor (BDSC: 603111). Flies with both components were then crossed to flies with both germline-expressing *Cre* and *ΦC-31* transgenes (BDSC: 60299). Offspring were then crossed to flies carrying a *UAS-GFP* reporter (BDSC: 60291) and the progeny were screened by fluorescence microscopy. Recombinants were selected to establish stable lines.

Generation of the excisable FRT-flanked *tra* knock-in allele (*tra^{FRT}*)

To generate an excisable FRT-flanked *tra* knock-in allele, the *tra* locus (3869 nucleotides (nt) containing: *tra* coding region, the 1910 nt upstream and the 967 nt downstream) was cloned using the following primer pair: 5'-AAAACGGCCGGACAGCACAACCAGTTCCGAC-3' and 5'-AAAACTCGAGATGCCCATCCCCTGCAATAC-3'. PCR was performed with Q5 high-fidelity polymerase from New England Biolabs (M0491S). The PCR product was digested with EagI and XhoI prior to cloning into the RIV FRTnMCS1FRT white vector (DGRC: 1333, generated by (Baena-Lopez et al., 2013). The construct was sequence-verified and a transgenic line was established through ΦC-31 integrase mediated transformation (Bestgene), using a recently generated amorphic allele of *tra* (Hudry et al., 2016) in which *tra* locus has been replaced by an *attP* site (BDSC: 67412). The generated allele rescue *tra* null mutant females to fertility.

Generation of the constitutive *traF* knock-in allele (*tra$^{K\text{-}IN}$*)

To generate a constitutive *traF* knock-in allele, the *traF cDNA* (fused with the 353nt nt upstream and the 310nt downstream of *tra*) was cloned using the following primer pair: 5'-AAAAGAATTCAATTTGTTTTATTTGTGCCTG-3' and 5'-AAAACTCGAGAGTTTCGTCCGCGGGTC-3'. PCR was performed with Q5 high-fidelity polymerase from New England Biolabs (M0491S). The PCR product was digested with EcoRI and XhoI prior to cloning into the RIV FRTnMCS1FRT white vector (DGRC: 1333, generated by (Baena-Lopez et al., 2013). The construct was sequence-verified and a transgenic line was established through ΦC-31 integrase mediated transformation (Bestgene), using a recently generated amorphic allele of *tra* in which *tra* locus has been replaced by an *attP* site (BDSC: 67412, generated by (Hudry et al., 2016). The generated allele behaves as constitutively feminising transgene and rescue *tra* null mutant females to fertility.

Generation of the *UAS-gRNAs* transgene for combined knockdown of digestive enzymes

To generate a UAS transgene carrying *gRNAs* targeting the *Mal-A1* (*gRNA:* AACTGCATCTATACGGAATCCGG), *Amy-p* (*gRNA*: TCTACAACATGGTGGCCTTCCGG) and *Amy-d* (*gRNA*: TCTACAACATGGTGGCCTTCCGG) genes, the three *gRNAs* were assembled from two overlapping PCR products. PCRs were performed with Q5 high-fidelity polymerase from New England Biolabs (M0491S). The final PCR product was then cloned into Bbs1 digested pCFD6 vector (Addgene: Plasmid #73915, generated by Port and Bullock, 2016). The construct was sequence-verified and a transgenic line was established through ΦC-31 integrase mediated transformation (Bestgene), using the VK05 (BDSC: 9725) *attP* site line.

Generation of *UAS* laconic sensor

The pcDNA3.1(-)Laconic plasmid (San Martin et al., 2013) was digested with BamHI and BclI. The resulting 2,254bp fragment was purified by electrophoresis and cloned into a pUAST vector previoulsy digested with BglII. Restriction enzyme analysis was used to confirm correct orientation of the insert. Transgenic fly strains were obtained by embryonic injection of the resulting
UAS-Laconic vector (outsourced to Rainbow Transgenic Flies Inc, CA, USA). The expression efficiency of the recovered transformant lines was assessed by crossing them to a mushroom body *GAL4* driver. The line used in this study was the one found to have the highest expression and harbours an insertion into chromosome II.

Generation of *UAS* citrate sensors

Three different nanosensors for citrate were generated by gene synthesis (GenScript): CIT96, CIT8 and CIT0 (Ewald et al., 2011). CIT8 corresponds to the citrate binding domain of the *Klebsiella pneumoniae* histidine sensor kinase CitA (amino acids: 6-130), inserted between the FRET pair Venus/CFP; CIT96 carries a point mutation (K77A) decreasing the affinity for citrate and CIT0 is a control sensor which harbours a mutation (R66A) that completely abolishes citrate binding. These three sensors were cloned into the *pUASTattb* vector (PMID: 17360644) with EcoRI and NotI. The constructs were sequence-verified and transgenic lines were established through ΦC-31 integrase mediated transformation (Bestgene, attP site VK00028, DBSC: 9745).

RT-qPCR

RNAs were extracted from 20 whole flies using Trizol (Invitrogen). RNAs were cleaned using RNAeasy mini Kit (QIAGEN), and cDNAs were synthesised using the iScript cDNA synthesis kit (Bio-Rad) from 500ng of total RNAs. Quantitative PCRs were performed by mixing cDNA samples (5ng) with iTaq™ Universal SYBR® Green Supermix (Bio-Rad, #172-5124) and the relevant primers in 384-well plates. Expression abundance was calculated using a standard curve for each gene, and normalised to the expression of *Vha100-4*, which is not sexually dimorphic. For data display purposes, the average of the expression abundance was arbitrarily set at 100% for each gene for control males, and percentage of that expression is displayed for all sexes and genotypes. In graphs displaying expression of the five gut-specific sugar genes (*Amyrel*, *Mal-A1*, *Mal-A6*, *Mal-A7* and *Mal-A8*), the median of expression of these five genes taken together is also displayed for both sexes. See Table S3 for primer details such as sequences and efficiency.

RNA-seq

The RNA-seq transcriptional data of adult midguts obtained from virgin males, females and *tra* mutant females used for Figures 2A and S1A is available from GEO under accession number GSE74775. A summary of relevant data for the intestinal sugar genes is provided in Table S1.

Metabolite measurements using FRET-based metabolite sensors

All imaging experiments were performed on dissected midguts or testes expressing laconic, the glucose sensor or the citrate sensors. Adult midguts or testes of 5-day-old flies were dissected in HL3 buffer (70mM NaCl, 5mM KCl, 1.5mM $CaCl_2$, 4mM MgC_{l2}, 10mM $NaHCO_3$, 115mM sucrose, 5mM trehalose, 5mM HEPES; pH 7.1; around 350mOsm). The dissected organs were placed into an open µ-slide (chambered coverslip, ibidi #80826) and analysed using a confocal microscope. Fluorescent images were acquired using a 20x objective, and the following filter sets: excitation 405nm, emission 470-522nm (CFP channel); excitation 405nm, emission 532-627nm (FRET channel). For data analysis, regions of interest (ROI) were delimited and the average intensity of both mTFP and Venus channels over each ROI were calculated. The design of the laconic sensor is such that FRET from mTFP to Venus decreases when lactate concentration increases. To obtain a signal that positively correlates with lactate concentration, the inverse FRET ratio was calculated by dividing mTFP intensity by Venus intensity. For experiments with the FLII^{12}Pglu-700µδ6 glucose sensor or the citrate sensors, the FRET ratio (YFP/CFP) was computed to obtain a signal positively correlated to glucose or citrate concentrations. For the experiments displayed in Figure 5, FRET efficiency was measured after acceptor photobleaching. Briefly, the fluorescence intensities of the donors before and after photodestruction of the acceptors were compared. For all sensors, increased fluorescence intensity of the donors (donor dequenching) was observed after bleaching of acceptors, indicating FRET occurrence.

GC-MS metabolomics of whole, dissected testes

Metabolite profiling analysis was performed by the metabolomics core of the University of Utah (http://cihd.cores.utah.edu/metabolomics/). Samples for GC-MS analysis were processed as previously described (Li and Tennessen, 2018). For each condition, four independent samples were collected from independent mating vials. Each sample is composed of 150 dissected testes from mated male flies.

All GC-MS analysis was performed with an Agilent 5977B GC-MS with HES source and an Agilent 7693A automatic liquid sampler. Dried samples were suspended in 40µL of a 40mg/mL solution of O-methoxylamine hydrochloride (MOX) in pyridine, and incubated for 1h at 30°C. 25µL of this solution were added to auto sampler vials. 60µL of N-methyl-N-trimethylsilyltrifluoracetamide (MSTFA) were added automatically via the auto sampler and incubated for 30min at 37°C with shaking. After incubation, 1µL of the prepared sample was injected into the gas chromatograph inlet in the split mode with the inlet temperature held at 250°C. A 10:1 split ratio was used for analysis. The gas chromatograph had an initial temperature of 60°C for 1min, followed by a 10°C/min ramp to 325°C and a hold time of 2min. A 30-meter Agilent Zorbax DB-5MS with 10m Duraguard capillary column was employed for chromatographic separation. Helium was used as the carrier gas at a rate of 1mL/min. Data was collected using MassHunter software (Agilent). Metabolites were identified and their peak area was recorded using MassHunter Quant. This data was transferred to an Excel spread sheet (Microsoft, Redmond WA). Metabolite identity was established using a combination of an in-house metabolite library developed using pure purchased standards, the NIST library and the Fiehn library. Data was normalised to both the sample mass and an internal standard (d27-myristic acid). Statistical analysis was

performed using Metaboanalsyt 3.0 (http://www.metaboanalyst.ca/) (Xia and Wishart, 2016).

LC-MS metabolomics on adult haemolymph and whole fly

For haemolymph extractions, males were decapitated in groups of 15-20 and placed in a 0.5ml Eppendorf tube perforated with a 30G needle. These Eppendorf tubes were placed inside 1.5m Eppendorf tubes and were centrifuged for 15min at 1500 g at 4°C to collect their haemolymph as described in (Demontis and Perrimon, 2010). For each sample, haemolymph was pooled from a total of 120-280 mated males (final sample volume ranged from 3.5-11µL). 3 samples were used per genotype. For whole flies, 8 samples of 5 mated males each were used for each genotype. 3µL of each haemolymph sample were extracted with metabolite extraction solution (300µL, 80% methanol, 0.1% formic acid (FA)), and whole fly samples were homogenised using a TissueLyser II (Qiagen, Hilden, Germany) with a tungsten carbide bead (30Hz, 3min) in metabolite extraction solution (300µL). Isotopically labelled citric acid (1,5,6-carboxyl-$^{13}C_3$ citric acid 99% - Cambridge Isotope Laboratories, USA) was added as an internal standard in the extraction solution (150ng/mL). Following vortex mixing (30s) and sonication on an ultrasonic water bath (10min), samples were centrifuged (13,000g, 10min). Finally, the supernatants were collected, filtered using PTFE membrane (0.22µm) and transferred to autosampler vials prior to injection on the liquid chromatography system. Total protein content was determined from the pellet obtained after centrifugation (haemolymph: protein precipitate; whole fly: tissue debris) by agitation in RIPA buffer (200µL, 95°C, 1000rpm, 10min), centrifugation (13,000g, 10min) and measurement of protein content using a BCA assay kit (Pierce, Rockford, USA).

Chromatographic analyses were carried out on a Vanquish Flex Binary UHPLC system (Thermo Fisher Scientific Inc., MA, USA) coupled to a benchtop hybrid quadrupole-Orbitrap Q Exactive mass spectrometer (Thermo Fisher Scientific Inc., Bremen, Germany). Baseline separation of isocitric acid and citric acid was achieved using a C18 Accucore Thermo Scientific column (150 × 2.1mm, 2.6µm) equipped with vanguard column (30 × 2.1mm, 2.6µm), both held at a temperature of 40°C and a flow rate of 0.2mL/min. Mobile phases were water with 0.5% formic acid (v/v) (Solvent A) and 90% acetonitrile with 0.5% formic acid (v/v) (Solvent B). The gradient elution was performed with a 0-80% solvent B gradient over 5min, followed by column washing and equilibration, yielding a total run time of 13min. Ionization was performed in the negative ion mode using a heated electrospray ionization source (HESI), under the following conditions: spray voltage -3.0 KV, heater temperature 330°C, capillary temperature 320°C, S-lens RF level 50, sheath and auxiliary gas flow rate, 35 and 10 units, respectively. Mass accuracy was calibrated using a customised calibration solution prior to sample analysis. Data was acquired in profile mode using Parallel Reaction Monitoring (PRM) with information regarding all the compounds defined in the inclusion list (see Table below), at a MS2 resolution of 17,500 at m/z 200 and isolation window of m/z 2.0. Nitrogen was used as collision gas in the higher energy collision dissociation (HCD) cell with normalised collision energy (NCE) set to 10%. Automatic gain

control (AGC) was set to 2e4 and maximum injection time 50 ms. Xcalibur version 4.1 was used for data acquisition and processing.

Compound name	Mass (*m/z*)	Formula	Species	Retention time (min)	Start (min)	End (min)	NCE
Isocitric acid	191.01973	$C_6H_8O_7$	$[M-H]^-$	1.88	1.00	4.00	10
Citric acid	191.01973	$C_6H_8O_7$	$[M-H]^-$	2.35	1.00	4.00	10
Citric acid (1,5,6-carboxyl-$^{13}C_3$, 99%)	194.02979	$[^{13}C]_3C_3H_8O_7$	$[M-H]^-$	2.35	1.00	4.00	10

CE-MS metabolomics on adult haemolymph

Haemolymph was prepared as above. Each sample consisted of pooled haemolymph of a total of 120-280 mated males (final sample volume ranged from 6.4-10µL), which was diluted 1:6 in distilled water prior to metabolomics analysis. Metabolome analysis was performed in 4 samples of fly adult body fluid per genotype using CE-TOFMS by Human Metabolome Technologies, Inc (HMT). Each sample was mixed with 450µL of methanol containing internal standards (20µM) and mixed. Then, chloroform (500µL) and Milli-Q water (200µL) were added, mixed thoroughly and centrifuged (2,300g, 4°C, 5min). The water layer (400µL) was filtrated through a 5kDa cut-off filter (ULTRAFREE-MC-PLHCC, Human Metabolome Technologies, Yamagata, Japan) to remove macromolecules. The filtrate was centrifugally concentrated and resuspended in 50µL of ultrapure water immediately before the measurement. The compounds were measured in the Cation and Anion modes of CE-TOFMS based metabolome as previously described (Soga et al., 2003). All CE−MS experiments were performed using an Agilent CE Capillary Electrophoresis System equipped with an air pressure pump, an Agilent 1100 series MSD mass spectrometer and an Agilent1100 series isocratic HPLC pump, a G1603A Agilent CE−MS adapter kit and a G1607A Agilent CE−ESI−MS sprayer kit (Agilent Technologies). System control, data acquisition and MSD data evaluation were performed via a G2201AA Agilent ChemStation software for CE−MSD.

CE−MS Conditions for Cationic Metabolites. Separations were carried out on a fused silica capillary (50µm i.d. × 100cm total length) using 1M formic acid as the electrolyte. Sample was injected with a pressure injection of 50mbar for 3s (3 nL). The applied voltage was set at +30kV. The capillary temperature was maintained at 20°C using a thermostat and the sample tray was cooled below 5°C. 5 mM ammonium acetate in 50% (v/v) methanol−water was delivered as the sheath liquid at 10µL/min. ESI−MS was conducted in the positive ion mode and the capillary voltage was set at 4000V. A flow of heated dry nitrogen gas (heater temperature of 300 °C) was maintained at 10L/min. In MS with selective ion monitoring (SIM), sets of 30 protonated [M+H]+ ions were analyzed successively to cover the whole range of m/z values from 70 through 1027.

CE−MS Conditions for Anionic Metabolites. A cationic polymer coated SMILE (+) capillary was obtained from Nacalai Tesque (Kyoto, Japan) and used as the separation capillary (50µm i.d. × 100 cm total length). The electrolyte for the CE separation was 50mM ammonium acetate solution, pH 8.5. Sample was injected with a pressure injection of 50mbar for 30s (30nL). The applied voltage was set at −30 kV. ESI−MS was conducted in the negative ion mode and the capillary voltage was set at 3500 V. In MS with SIM, sets of 30 deprotonated [M−H]- ions were analysed successively to cover the whole range of m/z values from 70 through 1027. Other conditions were the same as in cationic metabolite analysis.

Peaks detected in CE-TOFMS analysis were extracted using automatic integration software (MasterHands ver. 2.17.1.11 developed at Keio University) in order to obtain peak information including m/z, migration time (MT), and peak area. Putative metabolites were then assigned from HMT's standard library and Known-Unknown peak library on the basis of m/z and MT. The tolerance was ±0.5min in MT and ±10 ppm†3 in m/z. All the metabolite concentrations were calculated by normalising the peak area of each metabolite with respect to the area of the internal standard and by using standard curves, which were obtained by single-point (100µM or 50µM) calibrations. Hierarchical cluster analysis (HCA) and principal component analysis (PCA) were performed by statistical analysis software (developed at HMT).

QUANTIFICATION AND STATISTICAL ANALYSIS

GFP and pH3 quantifications

Mitotic and meiotic indices were quantified by counting pH3-positive cells in >40 testes or >10 midguts per genotype and/or condition (e.g. male/female).

For quantification of intestinal GFP protein expression level, a midgut portion (corresponding to R2 or R4 regions) was imaged at 20x magnification. GFP level was quantified using ImageJ in areas of identical size across all genotypes. Threshold was adjusted for the GFP channel (ImageJ function: Image>Adjust>Threshold) to subtract background, then the size and the intensity mean of the area above the threshold was considered (ImageJ function: analyse particles). Data was collected from at least 10 midguts per genotype and/or sex, and is displayed as boxplots showing all data points.

For quantification of testis GFP protein expression patterns, whole testes were imaged at 20x magnification. GFP area was quantified using ImageJ. Threshold was adjusted for the GFP channel (ImageJ function: Image>Adjust>Threshold) to subtract background, then the size of the area above the threshold was considered (ImageJ function: analyse particles) and averaged by testis size. Data was collected from at least 25 testes per genotype, and is displayed as boxplots showing all data points.

Wing area measurements

Left wings of females and males were dissected, dehydrated in ethanol and mounted between slide and cover slip in Euparal mounting medium. Slides were dried on a heating block overnight (60°C). Wing areas were quantified using ImageJ by manually selecting the Cartesian coordinates of six landmarks that represent junctions of veins with the wing contour, and then measuring the number of pixels included in the resulting outline (method adapted from (Trotta et al., 2007).

Statistics and data presentation

All statistical analyses were carried out in GraphPad Prism 7.04. Comparisons between two genotypes/conditions were analysed with the Mann-Whitney-Wilcoxon rank sum test. The Mann-Whitney-Wilcoxon rank sum test does not require the assumption of normal distributions, so no methods were used to determine whether the data met such assumptions. All graphs were generated using GraphPad Prism 7.04. All confocal and bright field images belonging to the same experiment and displayed together in our figures were acquired using the exact same settings. For visualisation purposes, level and channel adjustments were applied using ImageJ to the confocal images shown in the figure panels (the same correction was applied to all images belonging to the same experiment), but all quantitative analyses were carried out on unadjusted raw images or maximum projections. In all figures, n denotes the number of midguts, wings, testes, flies or group of flies that were analysed for each genotype. Data is presented as boxplots with all data points shown, p-values from Mann-Whitney-Wilcoxon test (non-significant (ns): $p>0.05$; *: $0.05>p>0.01$; **: $0.01>p>0.001$; ***: $p<0.001$). Asterisks highlighting significant comparisons across sexes are displayed in grey boxes, whereas those highlighting significant comparisons within same-sex datasets are displayed in red boxes (for females) and blue boxes (for males).

DATA AND CODE AVAILABILITY

The accession number for gene expression reported in this paper is GEO: GSE74775.
Data in this paper are available upon request to the Lead Contact.

ADDITIONAL RESOURCES

Figure S1. Expression of the carbohydrate-handling machinery is male-biased in a specific portion of the adult intestine.

(**A**) Heat map displaying normalised expression abundance for the sugar genes with sexually dimorphic expression in the adult midgut of females and males (left, using the transcriptional data sets in (Hudry et al., 2016); and heat map displaying the normalised ratio of male over female expression of the same genes in the adult midgut, brain (CNS) and Malpighian tubules (Tub), based on FlyAtlas 2 transcriptional data (Leader et al., 2018). See Table S1 for details of genes and their expression abundance. (**B**) List of the intestinal male-biased sugar genes organised by molecular functions. The specific genes from top to bottom are: *Trehalose transporter 1-1* (*Tret1-1*), *sugar transporter 1* (*sut1*), *Amylase proximal* (*Amy-p*), *Amylase distal* (*Amy-d*), *Maltase A1* (*Mal-A1*), *Maltase A2* (*Mal-A2*), *Maltase A3* (*Mal-A4*), *Maltase A4* (*Mal-A4*), *Maltase A5* (*Mal-A5*), *Maltase A6* (*Mal-A6*), *Maltase A7* (*Mal-A7*), *Maltase A8* (*Mal-A8*), *target of brain insulin* (*tobi*), *Glucocerebrosidase 1a* (*Gba1a*),

Trehalase (Treh), *Hexokinase-A* (*Hex-A*), *Phosphoglucose isomerase* (*Pgi*), *Aldolase* (*Ald*), *Glyceraldehyde 3 phosphate dehydrogenase 1* (*Gapdh1*), *Phosphoglycerate kinase* (*Pgk*), *Phosphoglyceromutase 78* (*Pglym78*), *Enolase* (*Eno*), *Pyruvate carboxylase* (*PCB*). (**C**) RT-qPCR expression data for a subset of gut-specific sugar genes (specified at the top of the graph) in male (M) and female (F) control flies. In this and all subsequent figures, expression abundance for each gene was arbitrarily set up at 100% for control males, and percentage of that expression is displayed for the other sex and genotypes. (**D**) Expression pattern of *Maltase-A7-Gal4* reporter and Pgi^{GFP} protein in whole midguts of adult *Drosophila* (DNA: DAPI, in blue; GFP, in green). The R4 region is highlighted in green in the cartoon above depicting midgut regionalisation. (**E**) Quantification of *Glutathione S transferase D1-GFP* (*GstD1-GFP*) reporter expression levels in the R4 region of adult male (M) and female (F) midguts. Representative images are shown (DNA is labelled with DAPI in blue; *GstD1-GFP* is visualised in green with GFP). In this panel, GFP expression abundance was set up at 100% for control males, and expression in females is displayed as percentage of male expression. (**F**) Expression level of Yolk protein 1^{GFP} ($Yp1^{GFP}$) in the R4 region of adult male (M) and female (F) midguts. Representative images are shown (DNA is labelled with DAPI in blue; Yp1 is visualised in green with GFP). n denotes the number of groups of flies analysed for each genotype (each group consisting of 20 flies) in panel C, and the number of midguts in panel E. Scale bars, 50µm in all images except for (D) 200µm. Asterisks highlighting significant comparisons across sexes are displayed in grey boxes at the bottom of the graphs. In this and all subsequent figures, data is presented as boxplots with all data points shown, p-values from Mann-Whitney-Wilcoxon test (non-significant (ns): $p>0.05$; *: $0.05>p>0.01$; **: $0.01>p>0.001$; ***: $p<0.001$). See Supplemental Information for a list of full genotypes. See also Table S1. Related to Figure 1.

Figure S2. Functional validation of *transformer* (*tra*) knockout, knock-in, gain-of-function and RNAi lines.

(**A**) Sex transformations induced by whole-body *tra* knockout (tra^{KO}) and whole-body tra^{F} knock-in gain-of-function ($tra^{F\ K\text{-}IN}$). Female mutants lacking *tra* display masculinised appearance and are referred to as "pseudomales". Male expressing *tra* display a feminised appearance and are referred to as "pseudofemales". (**B**) RT-qPCR expression data for the male-specific *doublesex* (*dsx*) and *fruitless* (*fru*) transcripts in male (M) and female (F) control flies, flies with whole-body *tra* knockout (tra^{KO}) or flies with whole-body tra^{F} knock-in gain-of-function ($tra^{F\ K\text{-}IN}$) relative to controls. (**C**) Sex transformations induced by whole-body *transformer 2* (*tra2*) null mutations ($tra2^{1}/Df(2R)^{trix}$). Female mutants lacking *tra2* display masculinised pseudomale appearance. (**D**) RT-qPCR expression data for the male-specific *dsx* and *fru* transcripts in male (M) and female (F) control flies, and in flies harbouring a whole-body *tra2* null mutation relative to controls. (**E**) Sex transformations induced by whole-body *tra* knockdown ($da>tra^{RNAi}$). Females with *da-Gal4*-driven *tra* knockdown display masculinised pseudomale appearance. (**F**) RT-qPCR expression data for the female-specific *tra* transcript in male (M) and female (F) control flies and flies following whole-body *tra* knockdown ($Act5C>tra^{RNAi}$). (**G**) RT-qPCR expression data for a set of midgut-specific sugar genes (indicated at the top of the graph) in flies with whole-body *tra* knockdown ($Act5C>tra^{RNAi}$). *Act5C-Gal4*-driven *tra* knockdown masculinises the intestinal sugar gene expression of females. (**H**) Sex transformations induced by *Act5C-Gal4* driven *tra* knockout ($Act5C>flp,tra^{FRT}$). Females with *Act5C-Gal4*-driven *tra* knockout display masculinised pseudomale appearance. (**I**) RT-qPCR expression data for a set of midgut-

specific sugar genes (indicated at the top of the graph) in flies with whole-body *tra* knockout (*tra^{KO},da>*) and with whole-body *tra* knockout rescued by ubiquitous *tra^{F}* expression (*tra^{KO},da>tra^{F}*). Ubiquitous *tra^{F}* re-introduction in *tra* whole-body mutants (*tra^{KO},da>tra^{F}*) restores the feminised intestinal sugar gene expression of whole body *tra* mutant females (*tra^{KO},da>*) to wild-type female-like levels (*tra^{KO},da>* control). In all panels, n denotes the number of group of flies analysed for each genotype (each group consisting of 20 flies). Asterisks highlighting significant comparisons across sexes are displayed in grey boxes at the bottom of the graphs. See Supplemental Information for a list of full genotypes. Related to Figure 2.

Figure S3. The sex differences in intestinal sugar gene expression are independent of the genetic sex of gut cells.

(**A**) RT-qPCR expression analysis of midgut-specific sugar genes (indicated at the bottom of the graph) in male (M) and female (F) flies of different *UAS* controls. RT-qPCR expression data for the same set of sugar genes in male (M) and female (F) flies with *transformer^{F}* knockdown or mis-expression specifically in intestinal progenitors (**B**, *esg>*), enteroendocrine cells (**C**, *pros^{V1}>*) and enterocytes (**D**, *MyoIA>* or *mex1>*). None of these manipulations affected the sexual dimorphism in intestinal sugar gene expression. In all panels, n denotes the number of group of flies analysed for each genotype (each group consisting of 20 flies). Asterisks highlighting significant comparisons across sexes are displayed in grey boxes at the bottom of the graphs. See Supplemental Information for a list of full genotypes. Related to Figure 2.

Figure S4. Tissue-specific screen to identify the cell types and/or organs controlling intestinal sex differences in sugar gene expression.

(**A**-**G**) RT-qPCR expression analysis of midgut-specific sugar genes (indicated at the bottom of the graph) in male (M) and female (F) flies following *transformer^{F}* (*tra^{F}*) knockdown or mis-expression specifically in intestinal muscles (**A**, *vm>*), neurons (**B**, *elav>*), glial cells (**C**, *repo>*), fat body cells (**D**, *Lpp>*), haemocytes (**E**, *Hml>*), and secretory glands such as the *corpora cardiaca* (**F**, *Akh>*) and *corpus allatum* (**G**, *Aug21>*). None of these manipulations affected the sexual dimorphism in intestinal sugar gene expression. (**H**) RT-qPCR expression analysis of the same midgut-specific sugar genes in *esg^{SHOF}* females relative to control females (control for Figure 3E). (**I**) RT-qPCR expression data for the female-specific *tra* transcript in male (M) and female (F) dissected gonads of controls, whole-body *tra* knockout (*tra^{KO}*) and *Act5C-Gal4*-driven *tra* knockout (*Act5C>flp,tra^{FRT}*), and rest of body of *Act5C-Gal4*-driven *tra* knockout. As expected from their anatomical masculinisation (Figure 3B), *tra* excision leads to loss of *tra^{F}* expression in the body (minus gonads) of *Act5C-Gal4*-driven *tra* knockouts, but *tra^{F}* expression is retained in their ovaries. This is in contrast to *tra^{KO}* flies, in which *tra^{F}* expression is also lost in gonads. (**J**) RT-qPCR expression data for the *Chorion protein 18* and *16* transcripts, used as transcriptional readouts of ovarian differentiation (Griffin-Shea et al., 1982), in male (M) and female (F) dissected gonads of controls, whole-body *tra* knockout (*tra^{KO}*) and *Act5C-Gal4*-driven *tra* knockout (*Act5C>flp,tra^{FRT}*). As expected from their anatomical features (Figure 3B), these transcripts are absent from *tra^{KO}* masculinised females, but are retained in *Act5C-Gal4*-driven *tra* knockout females, in which *tra* expression in the female gonad (and female identity) has been spared in the gonad. In all

panels, n denotes the number of group of flies analysed for each genotype (each group containing 20 flies). Asterisks highlighting significant comparisons across sexes are displayed in grey boxes at the bottom of the graphs. See Supplemental Information for a list of full genotypes. Related to Figure 3.

Figure S5. Enterocyte-specific knockdown screen to identify the signaling pathway driving intestinal sex differences in sugar gene expression.
(**A**) RT-qPCR expression analysis of midgut-specific sugar genes (indicated at the bottom of the graph) in male (M) and female (F) flies following enterocyte-specific knockdown of signal transduction components. The specific genes targeted from top to bottom are: *Allatostatin A receptor 2* (*Asta-R2*), *Tachykinin-like receptor at 99D* (*TkR99D*), *rickets* (*rk*), *punt* (*put*), *Insulin-like receptor* (*InR*), *LDL receptor protein 1* (*LRP1*), *baboon* (*babo*), *Lipophorin receptor 1* (*LpR1*), *Megalin* (*mgl*), *Lipophorin receptor 2* (*LpR2*), *torso* (*tor*), *Ion transport peptide* (*ITP*), *Toll* (*Tl*), *bigmax* (*Mlx*), *Methoprene-tolerant* (*Met*), *Niemann-Pick type C-2e* (*Npc2e*), *Neural Lazarillo* (*Nlaz*), *grindelwald* (*grnd*), *slimfast* (*slif*), *Adiponectin receptor* (*AdipoR*), *Ecdysone receptor* (*EcR*), *ultraspiracle* (*usp*), *breathless* (*btl*), *germ cell-expressed bHLH-PAS* (*gce*). (**B**-**D**) RT-qPCR expression analysis of the same midgut-specific sugar genes in male (M) and female (F) flies with *CCHamide-2 receptor* (**B**, *CCHa2-R$^{TAL/KO}$*), *Adipokinetic hormone* (**C**, *Akh$^{AP/A}$*), and *Adipokinetic hormone receptor* (***D***, *AkhR$^{1/\Delta}$*) null mutations. None of these genetic manipulations affected the sexual dimorphism in intestinal sugar gene expression. In all panels, n denotes the number of group of flies analysed for each genotype (each group contains 20 flies). Asterisks highlighting significant comparisons across sexes are displayed in grey boxes at the bottom of the graphs. See Supplemental Information for a list of full genotypes. Related to Figure 4.

Figure S6. Sex differences in intestinal carbohydrate handling by midgut R4 enterocytes promote food intake through secreted citrate.
(**A**) The *R2R4-Gal4* reporter is exclusively expressed in a subset of larval enterocytes. It is absent from testes, brain and fat body cells (DNA: DAPI, in blue; *R2R4>StingerGFP*: GFP, in green). (**B**) Representative images (DNA labelled with DAPI in blue; R4-driven GFP (*R2R4-Gal4>UAS-mCD8GFP*) is visualised in green) and quantifications of R4 midgut region diameter and size in control males and in males following R2/R4 enterocyte-specific knockdown of the JAK-STAT receptor dome (*dome^{RNAi}*). (**C**) Male-biased enzymes and metabolic pathways in the adult *Drosophila* midgut. Enzymes with male-biased intestinal expression are displayed in blue; enzymes investigated functionally are highlighted with a blue asterisk. Grey bars are proportional to the relative expression levels of each enzyme for enzymes with redundant functions. The specific enzymes from top to bottom are: Amylase proximal (Amy-p), Amylase distal (Amy-d), Maltase A1 (Mal-A1), Maltase A6 (Mal-A6), Maltase A8 (Mal-A8), Maltase A7 (Mal-A7), Maltase A3 (Mal-A3), Maltase A4 (Mal-A4), Hexokinase-A (Hex-A), Phosphoglucose isomerase (Pgi), Phosphofructokinase (Pfk), Fructose-1,6-bisphosphatase (Fbp), Aldolase (Ald), Glyceraldehyde 3 phosphate dehydrogenase 1 (Gapdh1), Phosphoglycerate kinase (Pgk), Phosphoglyceromutase 78 (Pglym78), Enolase (Eno), Pyruvate kinase (PyK), Lactate dehydrogenase (Ldh), Monocarboxylate transporter 1 (Mct1), Outsiders (Out), Mitochondrial pyruvate carrier (Mpc1), Pyruvate dehydrogenase E1 alpha subunit (PDH), Pyruvate dehydrogenase

phosphatase (Pdp), Pyruvate dehydrogenase kinase (Pdk), Pyruvate carboxylase (PCB), Knockdown (Kdn), Aconitase (Acon), Malate dehydrogenase 2 (Mdh2), ATP citrate lyase (ATPCL), I'm not dead yet (Indy). The specific metabolites from top to bottom are: glucose-6-phosphate (G6P), fructose-6-phosphate (F6P), fructose-1,6-biphoshate (F1,6BP), glyceraldehyde-3-phosphate (GA3P), 1,3 bisphosphoglycerate (1,3BPG), 3 phosphoglycerate (3PG), 2 phosphoglycerate (2PG), phosphoenolpyruvate (PEP), acetyl coenzyme A (Ac-CoA), isocitrate (ICT), malate (MAL), and oxaloacetate (OAA). (**D**) Quantification of the FRET signal in R4 enterocytes expressing the laconic lactate sensor from control male midguts, midguts with R2/R4 enterocyte-specific lactate dehydrogenase knockdown (Ldh^{RNAi}), or R2/R4 enterocyte-specific *Ldh* misexpression (Ldh^{OE}). (**E**) Food intake quantifications based on the number of FlyPAD-monitored sips per male (M) fly following R2 and R4 enterocyte-specific knockdown of the following digestive enzymes and sugar transporter: *Amy-p/Amy-d/Mal-A1*, *Mal-A1* and *CG6484*. For each genetic manipulation in this and all subsequent panels, the median number of sips was arbitrarily set up at 100% for control males, and percentage of that expression is displayed for the other genotypes. (**F**) Food intake quantifications based on the number of FlyPAD-monitored sips per male (M) fly following R2 and R4 enterocyte-specific knockdown of the *Pdp* and *Pdk* enzymes. (**G**) Midgut expression of phospho-PDH (pPDH) following clonal knockdown of *PDH* (DNA is labelled in blue with DAPI, anti-beta galactosidase in red is used to stain LacZ-positive cells inside the clone in which PDH knockdown has been induced). Expression of Acon following clonal knockdown of *Acon* (DNA is labelled in blue with DAPI, anti-beta galactosidase in red is used to stain LacZ-positive cells inside the clone in which Acon knockdown has been induced). Expression is reduced within both *PDH* and *Acon* clones, indicative of effective knockdown. **(H)** Food intake quantifications based on the number of FlyPAD-monitored sips per male (M) fly following R2 and R4 enterocyte-specific knockdown or mis-expression of the *Drosophila* homologue of *Ldh*. (**I**) Food intake quantifications based on the number of FlyPAD-monitored sips per male (M) fly following R2 and R4 enterocyte-specific knockdown of the following monocarboxylate transporters: *Mct1, Prestin, out, CG8925* and *CG13907*. (**J**) Food intake quantifications based on the number of FlyPAD-monitored sips per male fly following R2/R4 enterocyte and adult-specific *Indy* knockdown ($R2R4TS>Indy^{RNAi}$). n denotes the number of flies analysed for each genotype/condition, except in panels (B) and (D), where n indicates the number of midguts. Scale bars, 50µm in all images. Asterisks highlighting significant comparisons within male datasets are displayed in blue boxes. See Supplemental Information for a list of full genotypes. Related to Figure 6.

Figure S7. Male-biased carbohydrate metabolism is genetically downstream of the JAK-SAT signalling in enterocytes of the R4 region and can be uncoupled from larval growth and intestinal proliferation.

(**A**) Food intake quantifications based on the number of FlyPAD-monitored sips per male (M) fly following R2 and R5 enterocyte-specific knockdown of the *Maltase-A1* (*Mal-A1*) and *CG6484* enzymes. Downregulation of intestinal sugar genes sugar genes in R2 and R5 does not affect male food intake. (**B**) Adult wing size quantifications (used as a measurement of body size, (Shingleton et al., 2009; Shingleton et al., 2017)) for male (M) flies following enterocyte-specific knockdown of the following enzymes: *CG6484*, *Aldolase* (*Ald*), *Pyruvate dehydrogenase kinase* (*Pdk*), *Pyruvate dehydrogenase phosphatase* (*Pdp*), *Pyruvate carboxylase* (*PCB*), *I'm not dead yet* (*Indy*) and $domeless^{\Delta CYT}$ ($dome^{\Delta CYT}$). Downregulation of

intestinal sugar genes sugar genes or JAK-STAT signalling in R2 and R4 does not reduced male body size. (**C**) Intestinal proliferation quantified as the number of pH3-positive cells in male midguts following enterocyte-specific knockdown of the following enzymes: *Pyruvate dehydrogenase phosphatase* (*Pdp*), *Pyruvate carboxylase* (*PCB*), *I'm not dead yet* (*Indy*) and for the *escargot*^{Shutoff} mutation. Downregulation of intestinal sugar genes sugar genes in R2 and R4 does not impact male intestinal proliferation. (**D**) Food intake quantifications based on the number of FlyPAD-monitored sips per male (M) fly following R2 and R4 enterocyte-specific mis-expression of the JAK-STAT ligand *udp3* alone or in combination with *Mal-A1* downregulation. The increased food intake resulting from *upd3* overexpression in male enterocytes can be reduced to wild-type levels by simultaneous downregulation of *Mal-A1*. (**E**) Intestinal proliferation quantified as the number of pH3-positive cells in male midguts following enterocyte-specific mis-expression of the JAK-STAT ligand *udp3* alone or in combination with *Mal-A1* downregulation. In contrast to its effect on food intake, *Mal-A1* downregulation fails to reduce the increased stem cell proliferation observed following *upd3* overexpression. (**F**) Body size assessments based on adult wing size quantifications for male flies following R2 and R4 enterocyte-specific mis-expression of the JAK-STAT ligand *udp3* alone or in combination with *Mal-A1* downregulation. Concurrent over-activation of JAK-STAT signalling in ECs (by ectopic Upd3 expression) and downregulation of the intestinal sugar gene *Mal-A1* reduces food intake without affecting body size. (**G**) Food intake quantifications based on the number of FlyPAD-monitored sips per female (F) fly following R2 and R4 enterocyte-specific knockdown of the *Maltase-A1* (*Mal-A1*) and *Hexokinase-A (Hex-A)* enzymes. Downregulation of intestinal sugar genes does not affect female food intake. (**H**) LC-MS quantifications of haemolymph (left graph) and whole-body (right graph) citrate in control males and in males following R2/R4 enterocyte-specific knockdown of the plasma membrane Indy citrate transporter. Intestinal *Indy* knockdown has no impact on circulating or whole body citrate. (**I**) Quantifications of the number of mitotic and meiotic pH3-positive germ cells in control testes and in testes following testis-specific *Indy* knockdown from the *tj-Gal4* driver line. (**J**) Expression pattern of Bam (visualised in green using the Bam^{GFP} protein reporter) in control testes and in testes following testis-specific *Indy* knockdown with the *tj-Gal4* reporter line. Representative images are shown (DNA is labelled with DAPI in blue). (**K**) Quantifications of the number of mitotic and meiotic pH3-positive germ cells in control testes and in testes following testis-specific *Indy* knockdown from the *eya-Gal4* driver line. (**L**, **M**) Quantification of the CIT8 citrate sensor's FRET signal in germline stem cells (*nos-Gal4*-positive) (L) or early-stage somatic cells (M) of testes of control males or males with R2/R4 enterocyte-specific knockdown of *Maltase-A1* (*Mal-A1*^{RNAi}). (**N**) The *tj-Gal4* and *eya-Gal4* reporters are selectively expressed in early-stage and late-stage somatic cells of the testis (respectively), and not in the germ cells (DNA: DAPI, in blue; *tj/eya>StingerGFP*: GFP, in green; hub cells: Fasciclin 3 (Fas3), in red). (**O**) Food intake quantifications based on the number of FlyPAD-monitored sips per male fly following neuronal-specific *Indy* downregulation (*nSyb>Indy*^{RNAi}). n denotes the number of flies (A, D, G and H), wings (B and F), midguts (C and E) or testes (I, K, L, M and O). Scale bars, 200µm in all images. Asterisks highlighting significant comparisons within female and male datasets are displayed in red and blue boxes respectively. See Supplemental Information for a list of full genotypes. See also Table S2. Related to Figures 5, 6 and 7.

Table S1. Sex-specific expression of intestinal sugar genes.

The first spreadsheet ("RNAseq Hudry et al") shows raw abundance values for the intestinal sugar gene transcripts from female (F), male (M) and *tra* mutant masculinised midguts. Expression data was obtained from (Hudry et al., 2016). The second spreadsheet ("FlyAtlas") features relative male/female expression abundance ratios for intestinal sugar genes in brain/CNS, midgut and Malpighian tubules. Transcript expression data was obtained from FlyAtlas 2 (Leader et al., 2018). Related to Figures 2A and S1.

Table S2. Metabolomics data.
Each individual spreadhseet show raw data for the different metabolomics experiments: targeted GC-MS quantification of multiple metabolites in testes of control versus *R2R4>Indy-RNAi* males (related to Figure 7), targeted LC-MS quantification of citrate in adult male haemolymph of control versus *R2R4>Indy-RNAi* males (related to Figure S7), targeted LC-MS quantification of citrate in the whole body of adult male controls versus *R2R4>Indy-RNAi* males (related to Figure S7), and CE-MS profiling of adult male haemolymph of control versus *R2R4>Indy-RNAi* males (related to Figure 7).

Table S3. Primers used for RT-qPCR experiments. Related to STAR Methods.

Table S4. Fly stocks used in this study. Related to STAR Methods.

REFERENCES

Ainsworth, C. (2015). Sex redefined. Nature *518*, 288-291.

Ameku, T., Yoshinari, Y., Texada, M.J., Kondo, S., Amezawa, K., Yoshizaki, G., Shimada-Niwa, Y., and Niwa, R. (2018). Midgut-derived neuropeptide F controls germline stem cell proliferation in a mating-dependent manner. PLoS Biol *16*, e2005004.

Amrein, H., Gorman, M., and Nothiger, R. (1988). The sex-determining gene tra-2 of Drosophila encodes a putative RNA binding protein. Cell *55*, 1025-1035.

Arkov, A.L., Wang, J.Y., Ramos, A., and Lehmann, R. (2006). The role of Tudor domains in germline development and polar granule architecture. Development *133*, 4053-4062.

Arnold, A.P. (2017). A general theory of sexual differentiation. J Neurosci Res *95*, 291-300.

Auer, T.O., and Benton, R. (2016). Sexual circuitry in Drosophila. Curr Opin Neurobiol *38*, 18-26.

Bach, E.A., Ekas, L.A., Ayala-Camargo, A., Flaherty, M.S., Lee, H., Perrimon, N., and Baeg, G.H. (2007). GFP reporters detect the activation of the Drosophila JAK/STAT pathway in vivo. Gene Expr Patterns *7*, 323-331.

Baena-Lopez, L.A., Alexandre, C., Mitchell, A., Pasakarnis, L., and Vincent, J.P. (2013). Accelerated homologous recombination and subsequent genome modification in Drosophila. Development *140*, 4818-4825.

Bajpai, M., Gupta, G., and Setty, B.S. (1998). Changes in carbohydrate metabolism of testicular germ cells during meiosis in the rat. Eur J Endocrinol *138*, 322-327.

Baker, B.S., and Ridge, K.A. (1980). Sex and the single cell. I. On the action of major loci affecting sex determination in Drosophila melanogaster. Genetics *94*, 383-423.

Balakireva, M., Stocker, R.F., Gendre, N., and Ferveur, J.F. (1998). Voila, a new Drosophila courtship variant that affects the nervous system: behavioral, neural, and genetic characterization. J Neurosci *18*, 4335-4343.

Bates, M.D., Erwin, C.R., Sanford, L.P., Wiginton, D., Bezerra, J.A., Schatzman, L.C., Jegga, A.G., Ley-Ebert, C., Williams, S.S., Steinbrecher, K.A*., et al.* (2002). Novel genes and functional relationships in the adult mouse gastrointestinal tract identified by microarray analysis. Gastroenterology *122*, 1467-1482.

Bayer, E.A., and Hobert, O. (2018). Past experience shapes sexually dimorphic neuronal wiring through monoaminergic signalling. Nature *561*, 117-121.

Bellott, D.W., Skaletsky, H., Cho, T.J., Brown, L., Locke, D., Chen, N., Galkina, S., Pyntikova, T., Koutseva, N., Graves, T*., et al.* (2017). Avian W and mammalian Y chromosomes convergently retained dosage-sensitive regulators. Nat Genet *49*, 387-394.

Birkenfeld, A.L., Lee, H.Y., Guebre-Egziabher, F., Alves, T.C., Jurczak, M.J., Jornayvaz, F.R., Zhang, D., Hsiao, J.J., Martin-Montalvo, A., Fischer-Rosinsky, A*., et al.* (2011). Deletion of the mammalian INDY homolog mimics aspects of dietary restriction and protects against adiposity and insulin resistance in mice. Cell Metab *14*, 184-195.

Boggs, R.T., Gregor, P., Idriss, S., Belote, J.M., and McKeown, M. (1987). Regulation of sexual differentiation in D. melanogaster via alternative splicing of RNA from the transformer gene. Cell *50*, 739-747.

Boroughs, L.K., and DeBerardinis, R.J. (2015). Metabolic pathways promoting cancer cell survival and growth. Nat Cell Biol *17*, 351-359.

Boussouar, F., and Benahmed, M. (2004). Lactate and energy metabolism in male germ cells. Trends Endocrinol Metab *15*, 345-350.

Brankatschk, M., and Eaton, S. (2010). Lipoprotein particles cross the blood-brain barrier in Drosophila. J Neurosci *30*, 10441-10447.

Bricker, D.K., Taylor, E.B., Schell, J.C., Orsak, T., Boutron, A., Chen, Y.C., Cox, J.E., Cardon, C.M., Van Vranken, J.G., Dephoure, N*., et al.* (2012). A mitochondrial pyruvate carrier required for pyruvate uptake in yeast, Drosophila, and humans. Science *337*, 96-100.

Brown, S., Hu, N., and Hombria, J.C. (2001). Identification of the first invertebrate interleukin JAK/STAT receptor, the Drosophila gene domeless. Curr Biol *11*, 1700-1705.

Buchon, N., Osman, D., David, F.P., Fang, H.Y., Boquete, J.P., Deplancke, B., and Lemaitre, B. (2013). Morphological and molecular characterization of adult midgut compartmentalization in Drosophila. Cell Rep *3*, 1725-1738.
Camara, N., Whitworth, C., and Van Doren, M. (2008). The creation of sexual dimorphism in the Drosophila soma. Curr Top Dev Biol *83*, 65-107.
Camporeale, G., Zempleni, J., and Eissenberg, J.C. (2007). Susceptibility to heat stress and aberrant gene expression patterns in holocarboxylase synthetase-deficient Drosophila melanogaster are caused by decreased biotinylation of histones, not of carboxylases. J Nutr *137*, 885-889.
Cappello, A.R., Guido, C., Santoro, A., Santoro, M., Capobianco, L., Montanaro, D., Madeo, M., Ando, S., Dolce, V., and Aquila, S. (2012). The mitochondrial citrate carrier (CIC) is present and regulates insulin secretion by human male gamete. Endocrinology *153*, 1743-1754.
Casper, A.L., and Van Doren, M. (2009). The establishment of sexual identity in the Drosophila germline. Development *136*, 3821-3830.
Chau, J., Kulnane, L.S., and Salz, H.K. (2009). Sex-lethal facilitates the transition from germline stem cell to committed daughter cell in the Drosophila ovary. Genetics *182*, 121-132.
Chau, J., Kulnane, L.S., and Salz, H.K. (2012). Sex-lethal enables germline stem cell differentiation by downregulating Nanos protein levels during Drosophila oogenesis. Proc Natl Acad Sci U S A *109*, 9465-9470.
Chen, H.B., Shen, J., Ip, Y.T., and Xu, L. (2006). Identification of phosphatases for Smad in the BMP/DPP pathway. Genes Dev *20*, 648-653.
Chen, X., McClusky, R., Chen, J., Beaven, S.W., Tontonoz, P., Arnold, A.P., and Reue, K. (2012). The number of x chromosomes causes sex differences in adiposity in mice. PLoS Genet *8*, e1002709.
Chen, X., McClusky, R., Itoh, Y., Reue, K., and Arnold, A.P. (2013). X and Y chromosome complement influence adiposity and metabolism in mice. Endocrinology *154*, 1092-1104.
Chng, W.A., Sleiman, M.S.B., Schupfer, F., and Lemaitre, B. (2014). Transforming growth factor beta/activin signaling functions as a sugar-sensing feedback loop to regulate digestive enzyme expression. Cell Rep *9*, 336-348.
Chowdhury, R., Yeoh, K.K., Tian, Y.M., Hillringhaus, L., Bagg, E.A., Rose, N.R., Leung, I.K., Li, X.S., Woon, E.C., Yang, M.*, et al.* (2011). The oncometabolite 2-hydroxyglutarate inhibits histone lysine demethylases. EMBO Rep *12*, 463-469.
Christiansen, A.E., Keisman, E.L., Ahmad, S.M., and Baker, B.S. (2002). Sex comes in from the cold: the integration of sex and pattern. Trends Genet *18*, 510-516.
Clayton, J.A., and Collins, F.S. (2014). Policy: NIH to balance sex in cell and animal studies. Nature *509*, 282-283.
Clough, E., and Oliver, B. (2012). Genomics of sex determination in Drosophila. Brief Funct Genomics *11*, 387-394.
Costello, L.C., and Franklin, R.B. (1991a). Concepts of citrate production and secretion by prostate. 1. Metabolic relationships. Prostate *18*, 25-46.
Costello, L.C., and Franklin, R.B. (1991b). Concepts of citrate production and secretion by prostate: 2. Hormonal relationships in normal and neoplastic prostate. Prostate *19*, 181-205.
Costello, L.C., and Franklin, R.B. (2016a). A comprehensive review of the role of zinc in normal prostate function and metabolism; and its implications in prostate cancer. Arch Biochem Biophys *611*, 100-112.
Costello, L.C., and Franklin, R.B. (2016b). Plasma Citrate Homeostasis: How It Is Regulated; And Its Physiological and Clinical Implications. An Important, But Neglected, Relationship in Medicine. HSOA J Hum Endocrinol *1*.
Costello, L.C., Franklin, R.B., Reynolds, M.A., and Chellaiah, M. (2012). The Important Role of Osteoblasts and Citrate Production in Bone Formation: "Osteoblast Citration" as a New Concept for an Old Relationship. Open Bone J *4*.

Couillard, C., Mauriege, P., Prud'homme, D., Nadeau, A., Tremblay, A., Bouchard, C., and Despres, J.P. (1997). Plasma leptin concentrations: gender differences and associations with metabolic risk factors for cardiovascular disease. Diabetologia *40*, 1178-1184.
de Castro Fonseca, M., Aguiar, C.J., da Rocha Franco, J.A., Gingold, R.N., and Leite, M.F. (2016). GPR91: expanding the frontiers of Krebs cycle intermediates. Cell Commun Signal *14*, 3.
Demarco, R.S., Eikenes, A.H., Haglund, K., and Jones, D.L. (2014). Investigating spermatogenesis in Drosophila melanogaster. Methods *68*, 218-227.
Demontis, F., and Perrimon, N. (2010). FOXO/4E-BP signaling in Drosophila muscles regulates organism-wide proteostasis during aging. Cell *143*, 813-825.
Diao, F., Ironfield, H., Luan, H., Diao, F., Shropshire, W.C., Ewer, J., Marr, E., Potter, C.J., Landgraf, M., and White, B.H. (2015). Plug-and-play genetic access to drosophila cell types using exchangeable exon cassettes. Cell Rep *10*, 1410-1421.
Dickens, F. (1941). The citric acid content of animal tissues, with reference to its occurrence in bone and tumour. Biochem J *35*, 1011-1023.
Dickson, B.J. (2008). Wired for sex: the neurobiology of Drosophila mating decisions. Science *322*, 904-909.
Droujinine, I.A., and Perrimon, N. (2016). Interorgan Communication Pathways in Physiology: Focus on Drosophila. Annu Rev Genet *50*, 539-570.
Evans, D.S., and Cline, T.W. (2007). Drosophila melanogaster male somatic cells feminized solely by TraF can collaborate with female germ cells to make functional eggs. Genetics *175*, 631-642.
Ewald, J.C., Reich, S., Baumann, S., Frommer, W.B., and Zamboni, N. (2011). Engineering genetically encoded nanosensors for real-time in vivo measurements of citrate concentrations. PLoS One *6*, e28245.
Fergestad, T., Bostwick, B., and Ganetzky, B. (2006). Metabolic disruption in Drosophila bang-sensitive seizure mutants. Genetics *173*, 1357-1364.
Figueroa, M.E., Abdel-Wahab, O., Lu, C., Ward, P.S., Patel, J., Shih, A., Li, Y., Bhagwat, N., Vasanthakumar, A., Fernandez, H.F*., et al.* (2010). Leukemic IDH1 and IDH2 mutations result in a hypermethylation phenotype, disrupt TET2 function, and impair hematopoietic differentiation. Cancer Cell *18*, 553-567.
Fujihara, T., Kawabe, M., and Oishi, K. (1978). A sex-transformation gene in Drosophila melanogaster. J Hered *69*, 229-236.
Galikova, M., Diesner, M., Klepsatel, P., Hehlert, P., Xu, Y., Bickmeyer, I., Predel, R., and Kuhnlein, R.P. (2015). Energy Homeostasis Control in Drosophila Adipokinetic Hormone Mutants. Genetics *201*, 665-683.
Gilboa, L., Forbes, A., Tazuke, S.I., Fuller, M.T., and Lehmann, R. (2003). Germ line stem cell differentiation in Drosophila requires gap junctions and proceeds via an intermediate state. Development *130*, 6625-6634.
Goralski, T.J., Edstrom, J.E., and Baker, B.S. (1989). The sex determination locus transformer-2 of Drosophila encodes a polypeptide with similarity to RNA binding proteins. Cell *56*, 1011-1018.
Greenspan, L.J., de Cuevas, M., and Matunis, E. (2015). Genetics of gonadal stem cell renewal. Annu Rev Cell Dev Biol *31*, 291-315.
Gribble, F.M., and Reimann, F. (2016). Enteroendocrine Cells: Chemosensors in the Intestinal Epithelium. Annu Rev Physiol *78*, 277-299.
Griffin-Shea, R., Thireos, G., and Kafatos, F.C. (1982). Organization of a cluster of four chorion genes in Drosophila and its relationship to developmental expression and amplification. Dev Biol *91*, 325-336.
Gronke, S., Muller, G., Hirsch, J., Fellert, S., Andreou, A., Haase, T., Jackle, H., and Kuhnlein, R.P. (2007). Dual lipolytic control of body fat storage and mobilization in Drosophila. PLoS Biol *5*, e137.
Gui, Y., Silha, J.V., and Murphy, L.J. (2004). Sexual dimorphism and regulation of resistin, adiponectin, and leptin expression in the mouse. Obes Res *12*, 1481-1491.

Haber, A.L., Biton, M., Rogel, N., Herbst, R.H., Shekhar, K., Smillie, C., Burgin, G., Delorey, T.M., Howitt, M.R., Katz, Y.*, et al.* (2017). A single-cell survey of the small intestinal epithelium. Nature *551*, 333-339.
Harrison, D.A., Binari, R., Nahreini, T.S., Gilman, M., and Perrimon, N. (1995). Activation of a Drosophila Janus kinase (JAK) causes hematopoietic neoplasia and developmental defects. EMBO J *14*, 2857-2865.
Harrison, D.A., and Perrimon, N. (1993). Simple and efficient generation of marked clones in Drosophila. Curr Biol *3*, 424-433.
Havel, P.J., Kasim-Karakas, S., Dubuc, G.R., Mueller, W., and Phinney, S.D. (1996). Gender differences in plasma leptin concentrations. Nat Med *2*, 949-950.
Hombria, J.C., and Brown, S. (2002). The fertile field of Drosophila Jak/STAT signalling. Curr Biol *12*, R569-575.
Hudry, B., Khadayate, S., and Miguel-Aliaga, I. (2016). The sexual identity of adult intestinal stem cells controls organ size and plasticity. Nature *530*, 344-348.
Hui, S., Ghergurovich, J.M., Morscher, R.J., Jang, C., Teng, X., Lu, W., Esparza, L.A., Reya, T., Le, Z., Yanxiang Guo, J.*, et al.* (2017). Glucose feeds the TCA cycle via circulating lactate. Nature *551*, 115-118.
Iacobazzi, V., and Infantino, V. (2014). Citrate--new functions for an old metabolite. Biol Chem *395*, 387-399.
Inoue, K., Fei, Y.J., Huang, W., Zhuang, L., Chen, Z., and Ganapathy, V. (2002a). Functional identity of Drosophila melanogaster Indy as a cation-independent, electroneutral transporter for tricarboxylic acid-cycle intermediates. Biochem J *367*, 313-319.
Inoue, K., Zhuang, L., Maddox, D.M., Smith, S.B., and Ganapathy, V. (2002b). Structure, function, and expression pattern of a novel sodium-coupled citrate transporter (NaCT) cloned from mammalian brain. J Biol Chem *277*, 39469-39476.
Itskov, P.M., Moreira, J.M., Vinnik, E., Lopes, G., Safarik, S., Dickinson, M.H., and Ribeiro, C. (2014). Automated monitoring and quantitative analysis of feeding behaviour in Drosophila. Nat Commun *5*, 4560.
Jang, C., Hui, S., Zeng, X., Cowan, A.J., Wang, L., Chen, L., Morscher, R.J., Reyes, J., Frezza, C., Hwang, H.Y.*, et al.* (2019). Metabolite Exchange between Mammalian Organs Quantified in Pigs. Cell Metab.
Jensen, M.V., Joseph, J.W., Ronnebaum, S.M., Burgess, S.C., Sherry, A.D., and Newgard, C.B. (2008). Metabolic cycling in control of glucose-stimulated insulin secretion. Am J Physiol Endocrinol Metab *295*, E1287-1297.
Jiang, J., and White-Cooper, H. (2003). Transcriptional activation in Drosophila spermatogenesis involves the mutually dependent function of aly and a novel meiotic arrest gene cookie monster. Development *130*, 563-573.
Karsenty, G., and Olson, E.N. (2016). Bone and Muscle Endocrine Functions: Unexpected Paradigms of Inter-organ Communication. Cell *164*, 1248-1256.
Katsube, T., Nomoto, S., Togashi, S., Ueda, R., Kobayashi, M., and Takahisa, M. (1997). cDNA sequence and expression of a gene encoding a pyruvate dehydrogenase kinase homolog of Drosophila melanogaster. DNA Cell Biol *16*, 335-339.
Kiger, A.A., Jones, D.L., Schulz, C., Rogers, M.B., and Fuller, M.T. (2001). Stem cell self-renewal specified by JAK-STAT activation in response to a support cell cue. Science *294*, 2542-2545.
Knauf, F., Rogina, B., Jiang, Z., Aronson, P.S., and Helfand, S.L. (2002). Functional characterization and immunolocalization of the transporter encoded by the life-extending gene Indy. Proc Natl Acad Sci U S A *99*, 14315-14319.
Kopp, A. (2012). Dmrt genes in the development and evolution of sexual dimorphism. Trends Genet *28*, 175-184.
Korotchkina, L.G., and Patel, M.S. (2001). Site specificity of four pyruvate dehydrogenase kinase isoenzymes toward the three phosphorylation sites of human pyruvate dehydrogenase. J Biol Chem *276*, 37223-37229.

Kvon, E.Z., Kazmar, T., Stampfel, G., Yanez-Cuna, J.O., Pagani, M., Schernhuber, K., Dickson, B.J., and Stark, A. (2014). Genome-scale functional characterization of Drosophila developmental enhancers in vivo. Nature *512*, 91-95.
Landt, M., Gingerich, R.L., Havel, P.J., Mueller, W.M., Schoner, B., Hale, J.E., and Heiman, M.L. (1998). Radioimmunoassay of rat leptin: sexual dimorphism reversed from humans. Clin Chem *44*, 565-570.
Laurinyecz, B., Peter, M., Vedelek, V., Kovacs, A.L., Juhasz, G., Maroy, P., Vigh, L., Balogh, G., and Sinka, R. (2016). Reduced expression of CDP-DAG synthase changes lipid composition and leads to male sterility in Drosophila. Open Biol *6*, 50169.
Leader, D.P., Krause, S.A., Pandit, A., Davies, S.A., and Dow, J.A.T. (2018). FlyAtlas 2: a new version of the Drosophila melanogaster expression atlas with RNA-Seq, miRNA-Seq and sex-specific data. Nucleic Acids Res *46*, D809-D815.
Leatherman, J.L., and Dinardo, S. (2008). Zfh-1 controls somatic stem cell self-renewal in the Drosophila testis and nonautonomously influences germline stem cell self-renewal. Cell Stem Cell *3*, 44-54.
Leatherman, J.L., and Dinardo, S. (2010). Germline self-renewal requires cyst stem cells and stat regulates niche adhesion in Drosophila testes. Nat Cell Biol *12*, 806-811.
Li, H., Chawla, G., Hurlburt, A.J., Sterrett, M.C., Zaslaver, O., Cox, J., Karty, J.A., Rosebrock, A.P., Caudy, A.A., and Tennessen, J.M. (2017). Drosophila larvae synthesize the putative oncometabolite L-2-hydroxyglutarate during normal developmental growth. Proc Natl Acad Sci U S A *114*, 1353-1358.
Li, H., Hurlburt, A.J., and Tennessen, J.M. (2018). A Drosophila model of combined D-2- and L-2-hydroxyglutaric aciduria reveals a mechanism linking mitochondrial citrate export with oncometabolite accumulation. Dis Model Mech *11*.
Li, H., and Tennessen, J.M. (2018). Preparation of Drosophila Larval Samples for Gas Chromatography-Mass Spectrometry (GC-MS)-based Metabolomics. J Vis Exp.
Link, J.C., Hasin-Brumshtein, Y., Cantor, R.M., Chen, X., Arnold, A.P., Lusis, A.J., and Reue, K. (2017). Diet, gonadal sex, and sex chromosome complement influence white adipose tissue miRNA expression. BMC Genomics *18*, 89.
Linn, T.C., Pettit, F.H., and Reed, L.J. (1969). Alpha-keto acid dehydrogenase complexes. X. Regulation of the activity of the pyruvate dehydrogenase complex from beef kidney mitochondria by phosphorylation and dephosphorylation. Proc Natl Acad Sci U S A *62*, 234-241.
Lopes, G., Bonacchi, N., Frazao, J., Neto, J.P., Atallah, B.V., Soares, S., Moreira, L., Matias, S., Itskov, P.M., Correia, P.A*., et al.* (2015). Bonsai: an event-based framework for processing and controlling data streams. Front Neuroinform *9*, 7.
Losman, J.A., and Kaelin, W.G., Jr. (2013). What a difference a hydroxyl makes: mutant IDH, (R)-2-hydroxyglutarate, and cancer. Genes Dev *27*, 836-852.
Lu, C., Ward, P.S., Kapoor, G.S., Rohle, D., Turcan, S., Abdel-Wahab, O., Edwards, C.R., Khanin, R., Figueroa, M.E., Melnick, A*., et al.* (2012). IDH mutation impairs histone demethylation and results in a block to cell differentiation. Nature *483*, 474-478.
Mattila, J., and Hietakangas, V. (2017). Regulation of Carbohydrate Energy Metabolism in Drosophila melanogaster. Genetics *207*, 1231-1253.
Mauvais-Jarvis, F., Arnold, A.P., and Reue, K. (2017). A Guide for the Design of Pre-clinical Studies on Sex Differences in Metabolism. Cell Metab *25*, 1216-1230.
Medrano, A., Fernandez-Novell, J.M., Ramio, L., Alvarez, J., Goldberg, E., Montserrat Rivera, M., Guinovart, J.J., Rigau, T., and Rodriguez-Gil, J.E. (2006). Utilization of citrate and lactate through a lactate dehydrogenase and ATP-regulated pathway in boar spermatozoa. Mol Reprod Dev *73*, 369-378.
Micchelli, C.A., and Perrimon, N. (2006). Evidence that stem cells reside in the adult Drosophila midgut epithelium. Nature *439*, 475-479.
Miguel-Aliaga, I., Jasper, H., and Lemaitre, B. (2018). Anatomy and Physiology of the Digestive Tract of Drosophila melanogaster. Genetics *210*, 357-396.

Mills, E.L., Pierce, K.A., Jedrychowski, M.P., Garrity, R., Winther, S., Vidoni, S., Yoneshiro, T., Spinelli, J.B., Lu, G.Z., Kazak, L.*, et al.* (2018). Accumulation of succinate controls activation of adipose tissue thermogenesis. Nature *560*, 102-106.
Montague, C.T., Prins, J.B., Sanders, L., Digby, J.E., and O'Rahilly, S. (1997). Depot- and sex-specific differences in human leptin mRNA expression: implications for the control of regional fat distribution. Diabetes *46*, 342-347.
Mycielska, M.E., Patel, A., Rizaner, N., Mazurek, M.P., Keun, H., Patel, A., Ganapathy, V., and Djamgoz, M.B. (2009). Citrate transport and metabolism in mammalian cells: prostate epithelial cells and prostate cancer. Bioessays *31*, 10-20.
Nielsen, M.W., Alegria, S., Borjeson, L., Etzkowitz, H., Falk-Krzesinski, H.J., Joshi, A., Leahey, E., Smith-Doerr, L., Woolley, A.W., and Schiebinger, L. (2017). Opinion: Gender diversity leads to better science. Proc Natl Acad Sci U S A *114*, 1740-1742.
Nota, B., Struys, E.A., Pop, A., Jansen, E.E., Fernandez Ojeda, M.R., Kanhai, W.A., Kranendijk, M., van Dooren, S.J., Bevova, M.R., Sistermans, E.A.*, et al.* (2013). Deficiency in SLC25A1, encoding the mitochondrial citrate carrier, causes combined D-2- and L-2-hydroxyglutaric aciduria. Am J Hum Genet *92*, 627-631.
O'Brien, L.E., Soliman, S.S., Li, X., and Bilder, D. (2011). Altered modes of stem cell division drive adaptive intestinal growth. Cell *147*, 603-614.
Ohlstein, B., and Spradling, A. (2006). The adult Drosophila posterior midgut is maintained by pluripotent stem cells. Nature *439*, 470-474.
Oliveira, P.F., Martins, A.D., Moreira, A.C., Cheng, C.Y., and Alves, M.G. (2015). The Warburg effect revisited--lesson from the Sertoli cell. Med Res Rev *35*, 126-151.
Osman, D., Buchon, N., Chakrabarti, S., Huang, Y.T., Su, W.C., Poidevin, M., Tsai, Y.C., and Lemaitre, B. (2012). Autocrine and paracrine unpaired signaling regulate intestinal stem cell maintenance and division. J Cell Sci *125*, 5944-5949.
Oury, F., Sumara, G., Sumara, O., Ferron, M., Chang, H., Smith, C.E., Hermo, L., Suarez, S., Roth, B.L., Ducy, P.*, et al.* (2011). Endocrine regulation of male fertility by the skeleton. Cell *144*, 796-809.
Palmieri, F. (2013). The mitochondrial transporter family SLC25: identification, properties and physiopathology. Mol Aspects Med *34*, 465-484.
Pan, Y., and Baker, B.S. (2014). Genetic identification and separation of innate and experience-dependent courtship behaviors in Drosophila. Cell *156*, 236-248.
Phillips, M.D., and Thomas, G.H. (2006). Brush border spectrin is required for early endosome recycling in Drosophila. J Cell Sci *119*, 1361-1370.
Port, F., and Bullock, S.L. (2016). Augmenting CRISPR applications in Drosophila with tRNA-flanked sgRNAs. Nat Methods *13*, 852-854.
Quinones-Coello, A.T., Petrella, L.N., Ayers, K., Melillo, A., Mazzalupo, S., Hudson, A.M., Wang, S., Castiblanco, C., Buszczak, M., Hoskins, R.A.*, et al.* (2007). Exploring strategies for protein trapping in Drosophila. Genetics *175*, 1089-1104.
Rajan, A., and Perrimon, N. (2012). Drosophila cytokine unpaired 2 regulates physiological homeostasis by remotely controlling insulin secretion. Cell *151*, 123-137.
Reiff, T., Jacobson, J., Cognigni, P., Antonello, Z., Ballesta, E., Tan, K.J., Yew, J.Y., Dominguez, M., and Miguel-Aliaga, I. (2015). Endocrine remodelling of the adult intestine sustains reproduction in Drosophila. Elife *4*, e06930.
Rideout, E.J., Narsaiya, M.S., and Grewal, S.S. (2015). The Sex Determination Gene transformer Regulates Male-Female Differences in Drosophila Body Size. PLoS Genet *11*, e1005683.
Rogina, B., Reenan, R.A., Nilsen, S.P., and Helfand, S.L. (2000). Extended life-span conferred by cotransporter gene mutations in Drosophila. Science *290*, 2137-2140.
Rosenbaum, M., Nicolson, M., Hirsch, J., Heymsfield, S.B., Gallagher, D., Chu, F., and Leibel, R.L. (1996). Effects of gender, body composition, and menopause on plasma concentrations of leptin. J Clin Endocrinol Metab *81*, 3424-3427.

Russi, A.E., Ebel, M.E., Yang, Y., and Brown, M.A. (2018). Male-specific IL-33 expression regulates sex-dimorphic EAE susceptibility. Proc Natl Acad Sci U S A *115*, E1520-E1529.
Ryerse, J., Swarthout, J., and Nagel, B. (1997). Cloning and molecular characterization of a partial ATP citrate lyase cDNA from Drosophila melanogaster. Drosophila Information Service *80*, 21-23.
Ryner, L.C., Goodwin, S.F., Castrillon, D.H., Anand, A., Villella, A., Baker, B.S., Hall, J.C., Taylor, B.J., and Wasserman, S.A. (1996). Control of male sexual behavior and sexual orientation in Drosophila by the fruitless gene. Cell *87*, 1079-1089.
Saad, M.F., Damani, S., Gingerich, R.L., Riad-Gabriel, M.G., Khan, A., Boyadjian, R., Jinagouda, S.D., el-Tawil, K., Rude, R.K., and Kamdar, V. (1997). Sexual dimorphism in plasma leptin concentration. J Clin Endocrinol Metab *82*, 579-584.
Sainz, N., Barrenetxe, J., Moreno-Aliaga, M.J., and Martinez, J.A. (2015). Leptin resistance and diet-induced obesity: central and peripheral actions of leptin. Metabolism *64*, 35-46.
San Martin, A., Ceballo, S., Ruminot, I., Lerchundi, R., Frommer, W.B., and Barros, L.F. (2013). A genetically encoded FRET lactate sensor and its use to detect the Warburg effect in single cancer cells. PLoS One *8*, e57712.
Sano, H., Nakamura, A., Texada, M.J., Truman, J.W., Ishimoto, H., Kamikouchi, A., Nibu, Y., Kume, K., Ida, T., and Kojima, M. (2015). The Nutrient-Responsive Hormone CCHamide-2 Controls Growth by Regulating Insulin-like Peptides in the Brain of Drosophila melanogaster. PLoS Genet *11*, e1005209.
Sarov, M., Barz, C., Jambor, H., Hein, M.Y., Schmied, C., Suchold, D., Stender, B., Janosch, S., K, J.V., Krishnan, R.T.*, et al.* (2016). A genome-wide resource for the analysis of protein localisation in Drosophila. Elife *5*, e12068.
Sawala, A., and Gould, A.P. (2017). The sex of specific neurons controls female body growth in Drosophila. PLoS Biol *15*, e2002252.
Scopelliti, A., Bauer, C., Yu, Y., Zhang, T., Kruspig, B., Murphy, D.J., Vidal, M., Maddocks, O.D.K., and Cordero, J.B. (2018). A Neuronal Relay Mediates a Nutrient Responsive Gut/Fat Body Axis Regulating Energy Homeostasis in Adult Drosophila. Cell Metab.
Seegmiller, A.C., Dobrosotskaya, I., Goldstein, J.L., Ho, Y.K., Brown, M.S., and Rawson, R.B. (2002). The SREBP pathway in Drosophila: regulation by palmitate, not sterols. Dev Cell *2*, 229-238.
Shapiro-Kulnane, L., Smolko, A.E., and Salz, H.K. (2015). Maintenance of Drosophila germline stem cell sexual identity in oogenesis and tumorigenesis. Development *142*, 1073-1082.
Sharma, V., Lehmann, T., Stuckas, H., Funke, L., and Hiller, M. (2018). Loss of RXFP2 and INSL3 genes in Afrotheria shows that testicular descent is the ancestral condition in placental mammals. PLoS Biol *16*, e2005293.
Shingleton, A.W., Estep, C.M., Driscoll, M.V., and Dworkin, I. (2009). Many ways to be small: different environmental regulators of size generate distinct scaling relationships in Drosophila melanogaster. Proc Biol Sci *276*, 2625-2633.
Shingleton, A.W., Masandika, J.R., Thorsen, L.S., Zhu, Y., and Mirth, C.K. (2017). The sex-specific effects of diet quality versus quantity on morphology in Drosophila melanogaster. R Soc Open Sci *4*, 170375.
Sieber, M.H., and Spradling, A.C. (2015). Steroid Signaling Establishes a Female Metabolic State and Regulates SREBP to Control Oocyte Lipid Accumulation. Curr Biol *25*, 993-1004.
Smendziuk, C.M., Messenberg, A., Vogl, A.W., and Tanentzapf, G. (2015). Bi-directional gap junction-mediated soma-germline communication is essential for spermatogenesis. Development *142*, 2598-2609.
Smith, G.D., Jackson, L.M., and Foster, D.L. (2002). Leptin regulation of reproductive function and fertility. Theriogenology *57*, 73-86.
Soga, T., Ohashi, Y., Ueno, Y., Naraoka, H., Tomita, M., and Nishioka, T. (2003). Quantitative metabolome analysis using capillary electrophoresis mass spectrometry. J Proteome Res *2*, 488-494.
Song, W., Cheng, D., Hong, S., Sappe, B., Hu, Y., Wei, N., Zhu, C., O'Connor, M.B., Pissios, P., and Perrimon, N. (2017). Midgut-Derived Activin Regulates Glucagon-like Action in the Fat Body and Glycemic Control. Cell Metab *25*, 386-399.

Soty, M., Gautier-Stein, A., Rajas, F., and Mithieux, G. (2017). Gut-Brain Glucose Signaling in Energy Homeostasis. Cell Metab *25*, 1231-1242.
Su, X., Wellen, K.E., and Rabinowitz, J.D. (2016). Metabolic control of methylation and acetylation. Curr Opin Chem Biol *30*, 52-60.
Sykiotis, G.P., and Bohmann, D. (2008). Keap1/Nrf2 signaling regulates oxidative stress tolerance and lifespan in Drosophila. Dev Cell *14*, 76-85.
Szafer-Glusman, E., Giansanti, M.G., Nishihama, R., Bolival, B., Pringle, J., Gatti, M., and Fuller, M.T. (2008). A role for very-long-chain fatty acids in furrow ingression during cytokinesis in Drosophila spermatocytes. Curr Biol *18*, 1426-1431.
Takanaga, H., Chaudhuri, B., and Frommer, W.B. (2008). GLUT1 and GLUT9 as major contributors to glucose influx in HepG2 cells identified by a high sensitivity intramolecular FRET glucose sensor. Biochim Biophys Acta *1778*, 1091-1099.
Tan, S.W.S., Lee, Q.Y., Wong, B.S.E., Cai, Y., and Baeg, G.H. (2017). Redox Homeostasis Plays Important Roles in the Maintenance of the Drosophila Testis Germline Stem Cells. Stem Cell Reports *9*, 342-354.
Tapia, C., Kutzner, H., Mentzel, T., Savic, S., Baumhoer, D., and Glatz, K. (2006). Two mitosis-specific antibodies, MPM-2 and phospho-histone H3 (Ser28), allow rapid and precise determination of mitotic activity. Am J Surg Pathol *30*, 83-89.
Tazuke, S.I., Schulz, C., Gilboa, L., Fogarty, M., Mahowald, A.P., Guichet, A., Ephrussi, A., Wood, C.G., Lehmann, R., and Fuller, M.T. (2002). A germline-specific gap junction protein required for survival of differentiating early germ cells. Development *129*, 2529-2539.
Trotta, V., Calboli, F.C., Ziosi, M., and Cavicchi, S. (2007). Fitness variation in response to artificial selection for reduced cell area, cell number and wing area in natural populations of Drosophila melanogaster. BMC Evol Biol *7 Suppl 2*, S10.
Tulina, N., and Matunis, E. (2001). Control of stem cell self-renewal in Drosophila spermatogenesis by JAK-STAT signaling. Science *294*, 2546-2549.
Villella, A., and Hall, J.C. (2008). Neurogenetics of courtship and mating in Drosophila. Adv Genet *62*, 67-184.
Voigt, A., Esfandiary, L., Wanchoo, A., Glenton, P., Donate, A., Craft, W.F., Craft, S.L., and Nguyen, C.Q. (2016). Sexual dimorphic function of IL-17 in salivary gland dysfunction of the C57BL/6.NOD-Aec1Aec2 model of Sjogren's syndrome. Sci Rep *6*, 38717.
Volkenhoff, A., Hirrlinger, J., Kappel, J.M., Klambt, C., and Schirmeier, S. (2018). Live imaging using a FRET glucose sensor reveals glucose delivery to all cell types in the Drosophila brain. J Insect Physiol *106*, 55-64.
Voog, J., Sandall, S.L., Hime, G.R., Resende, L.P., Loza-Coll, M., Aslanian, A., Yates, J.R., 3rd, Hunter, T., Fuller, M.T., and Jones, D.L. (2014). Escargot restricts niche cell to stem cell conversion in the Drosophila testis. Cell Rep *7*, 722-734.
Wang, L., Sexton, T.R., Venard, C., Giedt, M., Guo, Q., Chen, Q., and Harrison, D.A. (2014). Pleiotropy of the Drosophila JAK pathway cytokine Unpaired 3 in development and aging. Dev Biol *395*, 218-231.
Wizemann, T.M., and Pardue, M.L. (2001). In Exploring the Biological Contributions to Human Health: Does Sex Matter? (Washington (DC)).
Wolfstetter, G., and Holz, A. (2012). The role of LamininB2 (LanB2) during mesoderm differentiation in Drosophila. Cell Mol Life Sci *69*, 267-282.
Xia, J., and Wishart, D.S. (2016). Using MetaboAnalyst 3.0 for Comprehensive Metabolomics Data Analysis. Curr Protoc Bioinformatics *55*, 14 10 11-14 10 91.
Xiong, X., Xu, L., Wei, L., White, R.E., Ouyang, Y.B., and Giffard, R.G. (2015). IL-4 Is Required for Sex Differences in Vulnerability to Focal Ischemia in Mice. Stroke *46*, 2271-2276.
Xu, W., Yang, H., Liu, Y., Yang, Y., Wang, P., Kim, S.H., Ito, S., Yang, C., Wang, P., Xiao, M.T*., et al.* (2011). Oncometabolite 2-hydroxyglutarate is a competitive inhibitor of alpha-ketoglutarate-dependent dioxygenases. Cancer Cell *19*, 17-30.

Yang, Q., Vijayakumar, A., and Kahn, B.B. (2018). Metabolites as regulators of insulin sensitivity and metabolism. Nat Rev Mol Cell Biol *19*, 654-672.
Yang, S.Y., Baxter, E.M., and Van Doren, M. (2012). Phf7 controls male sex determination in the Drosophila germline. Dev Cell *22*, 1041-1051.
Ye, D., Guan, K.L., and Xiong, Y. (2018). Metabolism, Activity, and Targeting of D- and L-2-Hydroxyglutarates. Trends Cancer *4*, 151-165.
Zarkower, D. (2002). Invertebrates may not be so different after all. Novartis Found Symp *244*, 115-126; discussion 126-135, 203-116, 253-117.
Zore, T., Palafox, M., and Reue, K. (2018). Sex differences in obesity, lipid metabolism, and inflammation-A role for the sex chromosomes? Mol Metab *15*, 35-44.

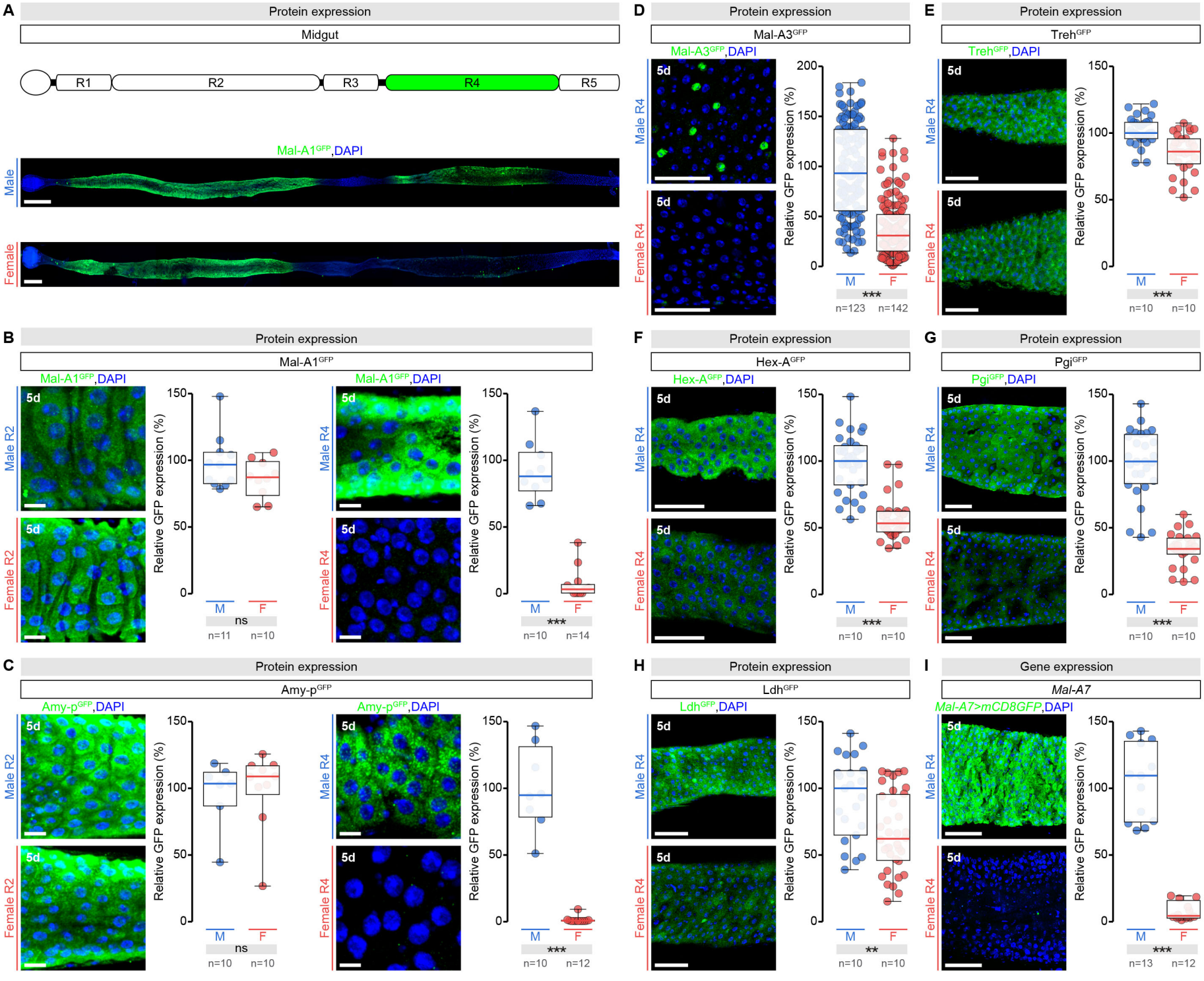
A
Protein expression
Midgut
R1
R2
R3
R4
R5
Mal-A1GFP,DAPI
Male
Female
B
Protein expression
Mal-A1GFP
Mal-A1GFP,DAPI
Male R2
Female R2
Male R4
Female R4
5d
Relative GFP expression (%)
M
F
ns
***
n=11
n=10
n=14
C
Protein expression
Amy-pGFP
Amy-pGFP,DAPI
n=12
D
Protein expression
Mal-A3GFP
Mal-A3GFP,DAPI
n=123
n=142
E
Protein expression
TrehGFP
TrehGFP,DAPI
F
Protein expression
Hex-AGFP
Hex-AGFP,DAPI
G
Protein expression
PgiGFP
PgiGFP,DAPI
H
Protein expression
LdhGFP
LdhGFP,DAPI
**
I
Gene expression
Mal-A7
Mal-A7>mCD8GFP,DAPI
n=13

Figure 1

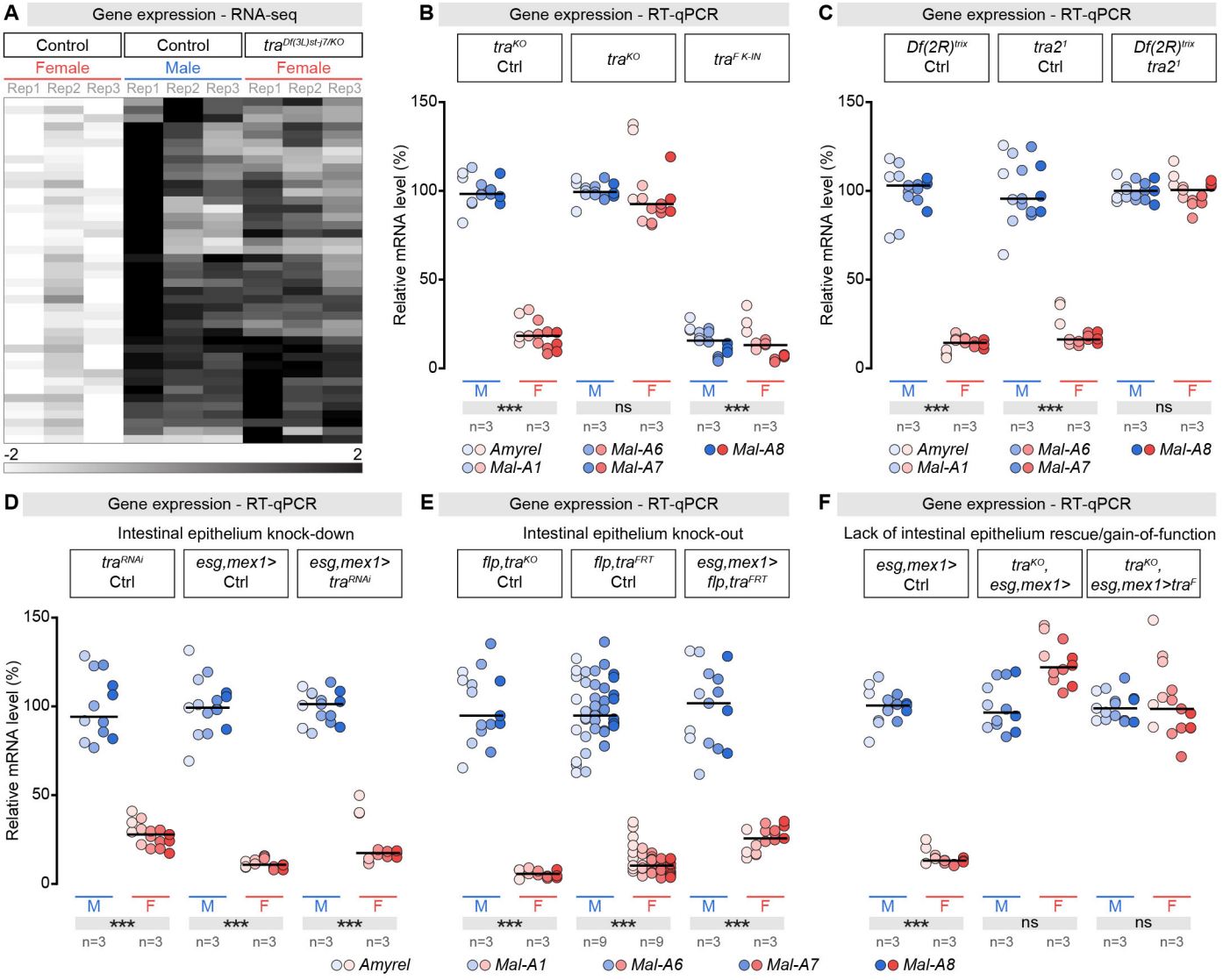
A
Gene expression - RNA-seq
Control
Control
tra^Df(3L)st-j7/KO
Female
Male
Female
Rep1 Rep2 Rep3 Rep1 Rep2 Rep3 Rep1 Rep2 Rep3
-2
2
B
Gene expression - RT-qPCR
tra^KO Ctrl
tra^KO
tra^F K-IN
Relative mRNA level (%)
150
100
50
0
M F M F M F
*** ns ***
n=3 n=3 n=3 n=3 n=3 n=3
Amyrel
Mal-A1
Mal-A6
Mal-A7
Mal-A8
C
Gene expression - RT-qPCR
Df(2R)^trix Ctrl
tra2^1 Ctrl
Df(2R)^trix tra2^1
Relative mRNA level (%)
150
100
50
0
M F M F M F
*** *** ns
n=3 n=3 n=3 n=3 n=3 n=3
Amyrel
Mal-A1
Mal-A6
Mal-A7
Mal-A8
D
Gene expression - RT-qPCR
Intestinal epithelium knock-down
tra^RNAi Ctrl
esg,mex1> Ctrl
esg,mex1> tra^RNAi
Relative mRNA level (%)
150
100
50
0
M F M F M F
*** *** ***
n=3 n=3 n=3 n=3 n=3 n=3
Amyrel
E
Gene expression - RT-qPCR
Intestinal epithelium knock-out
flp,tra^KO Ctrl
flp,tra^FRT Ctrl
esg,mex1> flp,tra^FRT
M F M F M F
*** *** ***
n=3 n=3 n=9 n=9 n=3 n=3
Mal-A1
Mal-A6
Mal-A7
F
Gene expression - RT-qPCR
Lack of intestinal epithelium rescue/gain-of-function
esg,mex1> Ctrl
tra^KO, esg,mex1>
tra^KO, esg,mex1>tra^F
M F M F M F
*** ns ns
n=3 n=3 n=3 n=3 n=3 n=3
Mal-A8

Figure 2

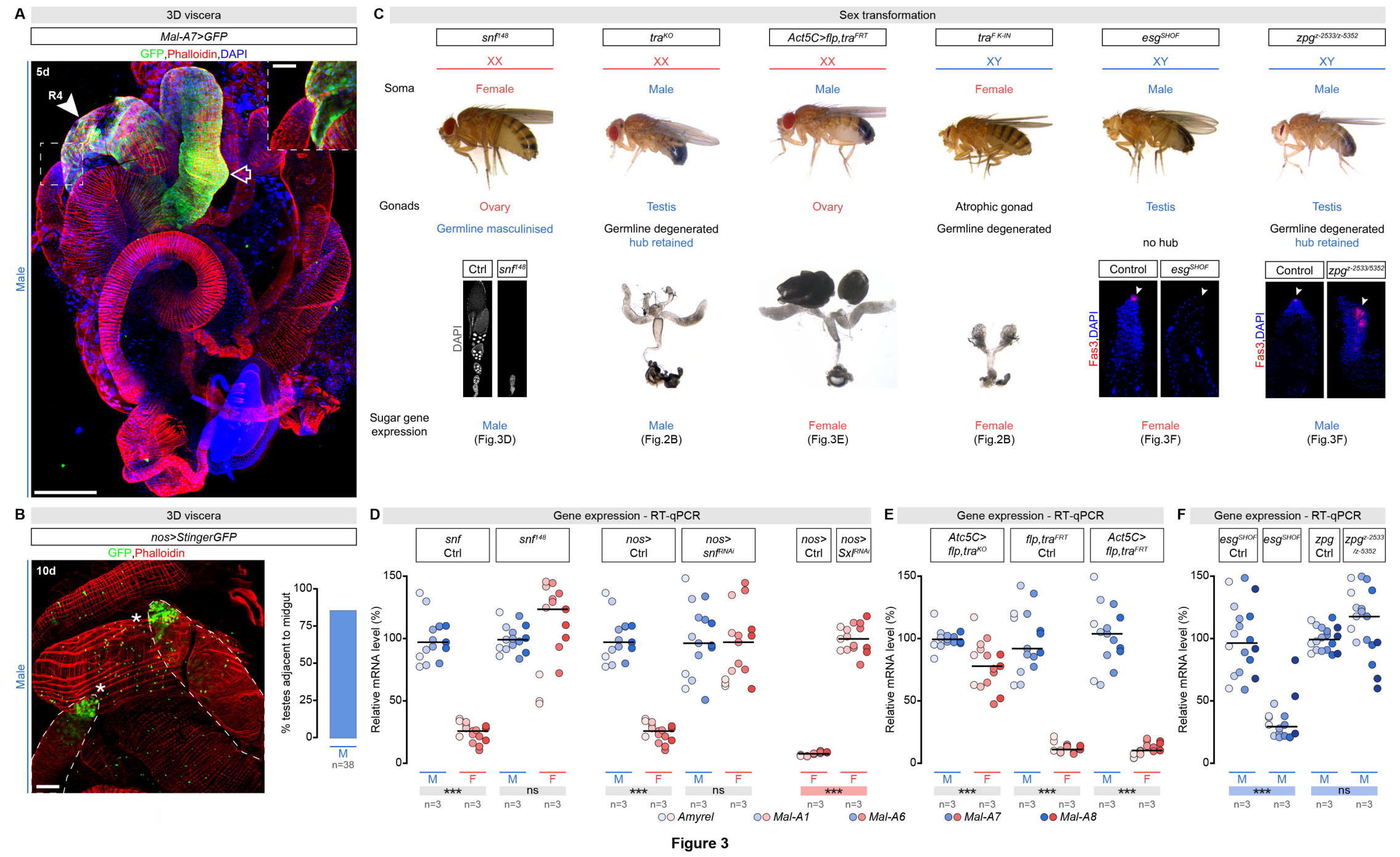
A
3D viscera
Mal-A7>GFP
GFP,Phalloidin,DAPI
5d
R4
Male
B
3D viscera
nos>StingerGFP
GFP,Phalloidin
10d
Male
% testes adjacent to midgut
100
75
50
25
0
M
n=38
C
Sex transformation
snf148
traKO
Act5C>flp,traFRT
traF K-IN
esgSHOF
zpgz-2533/z-5352
XX
XX
XX
XY
XY
XY
Soma
Female
Male
Male
Female
Male
Male
Gonads
Ovary
Testis
Ovary
Atrophic gonad
Testis
Testis
Germline masculinised
Germline degenerated
hub retained
Germline degenerated
no hub
Germline degenerated
hub retained
Ctrl
snf148
DAPI
Control
esgSHOF
Fas3,DAPI
Control
zpgz-2533/5352
Fas3,DAPI
Sugar gene expression
Male
(Fig.3D)
Male
(Fig.2B)
Female
(Fig.3E)
Female
(Fig.2B)
Female
(Fig.3F)
Male
(Fig.3F)
D
Gene expression - RT-qPCR
snf Ctrl
snf148
nos> Ctrl
nos> snfRNAi
nos> Ctrl
nos> SxlRNAi
Relative mRNA level (%)
150
100
50
0
M
F
***
ns
***
ns
***
n=3
Amyrel
Mal-A1
Mal-A6
E
Gene expression - RT-qPCR
Atc5C> flp,traKO
flp,traFRT Ctrl
Act5C> flp,traFRT
Relative mRNA level (%)
***
***
***
Mal-A7
Mal-A8
F
Gene expression - RT-qPCR
esgSHOF Ctrl
esgSHOF
zpg Ctrl
zpgz-2533 /z-5352
Relative mRNA level (%)
***
ns

Figure 3

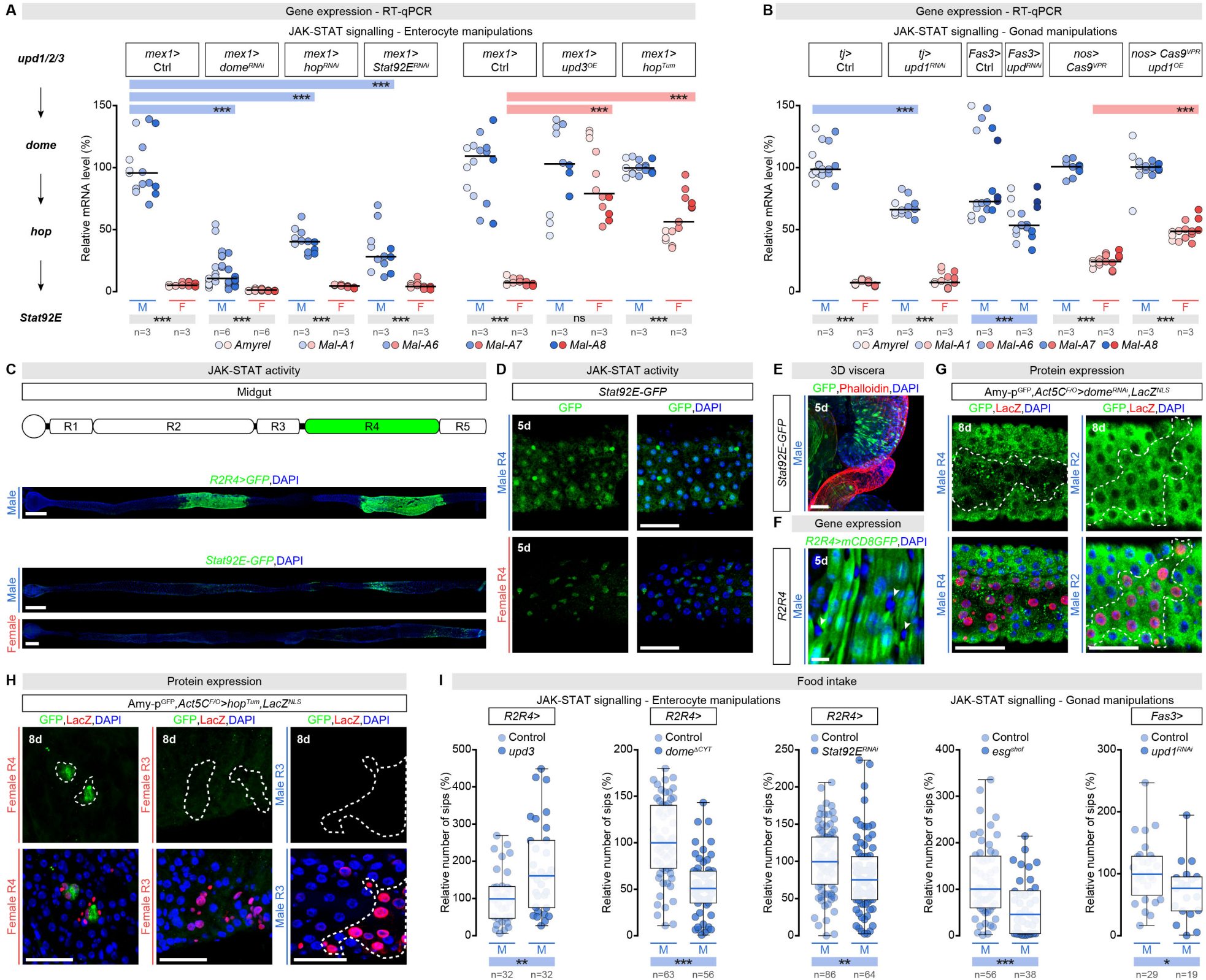
A
Gene expression - RT-qPCR
JAK-STAT signalling - Enterocyte manipulations
upd1/2/3
dome
hop
Stat92E
mex1> Ctrl
mex1> dome^RNAi
mex1> hop^RNAi
mex1> Stat92E^RNAi
mex1> Ctrl
mex1> upd3^OE
mex1> hop^Tum
Relative mRNA level (%)
Amyrel
Mal-A1
Mal-A6
Mal-A7
Mal-A8
B
Gene expression - RT-qPCR
JAK-STAT signalling - Gonad manipulations
tj> Ctrl
tj> upd1^RNAi
Fas3> Ctrl
Fas3> upd^RNAi
nos> Cas9^VPR
nos> Cas9^VPR upd1^OE
C
JAK-STAT activity
Midgut
R1
R2
R3
R4
R5
R2R4>GFP,DAPI
Stat92E-GFP,DAPI
Male
Female
D
JAK-STAT activity
Stat92E-GFP
GFP
GFP,DAPI
Male R4
Female R4
5d
E
3D viscera
GFP,Phalloidin,DAPI
Stat92E-GFP
F
Gene expression
R2R4>mCD8GFP,DAPI
R2R4
G
Protein expression
Amy-p^GFP,Act5C^F/O>dome^RNAi,LacZ^NLS
GFP,LacZ,DAPI
Male R2
8d
H
Protein expression
Amy-p^GFP,Act5C^F/O>hop^Tum,LacZ^NLS
Female R3
Male R3
I
Food intake
JAK-STAT signalling - Enterocyte manipulations
JAK-STAT signalling - Gonad manipulations
R2R4>
Fas3>
Control
upd3
dome^ΔCYT
Stat92E^RNAi
esg^shof
upd1^RNAi
Relative number of sips (%)

Figure 4

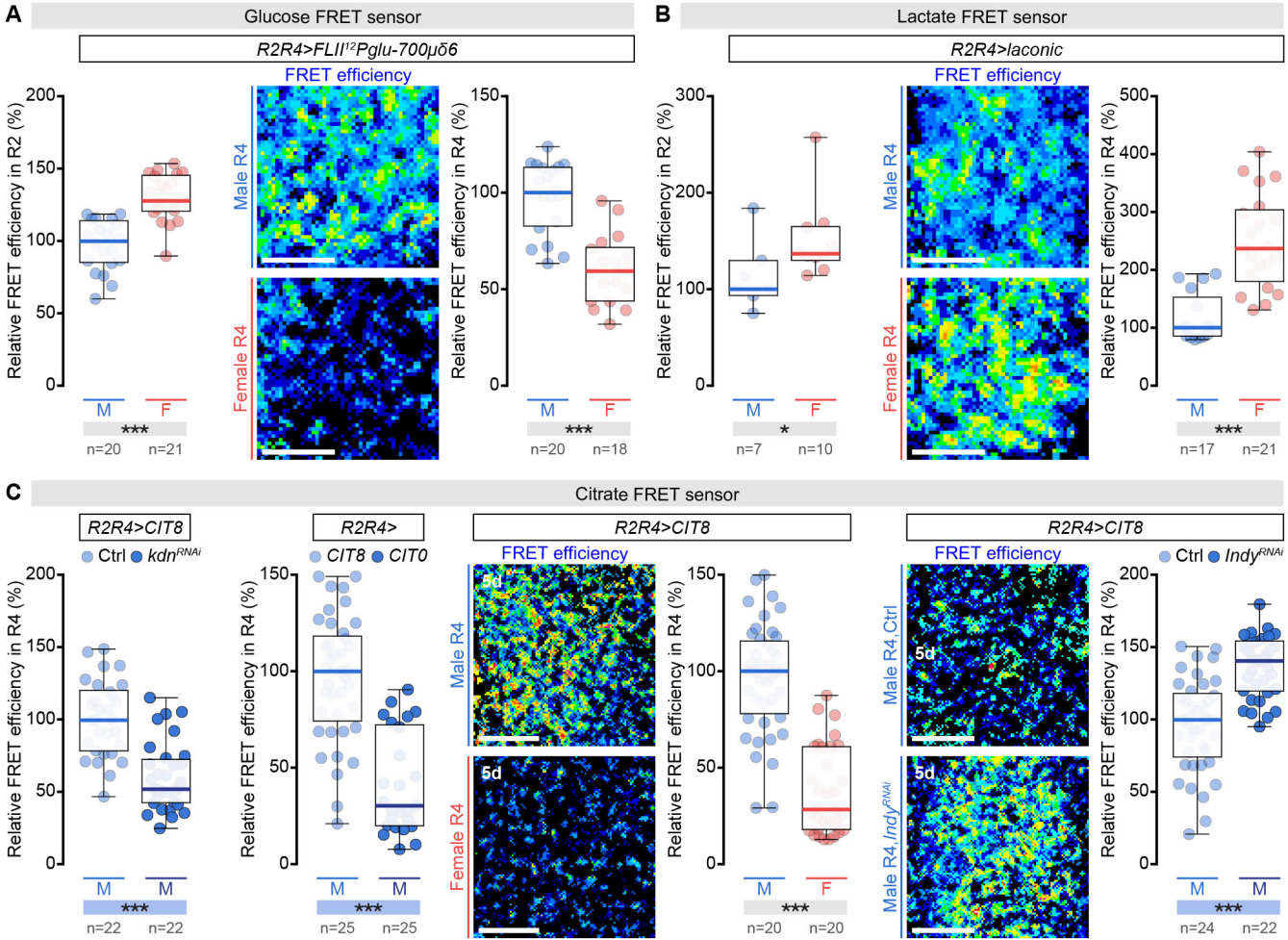
A
Glucose FRET sensor
R2R4>FLII12Pglu-700μδ6
FRET efficiency
Male R4
Female R4
Relative FRET efficiency in R2 (%)
Relative FRET efficiency in R4 (%)
M
F
***
n=20
n=21
n=20
n=18
B
Lactate FRET sensor
R2R4>laconic
FRET efficiency
Male R4
Female R4
Relative FRET efficiency in R2 (%)
Relative FRET efficiency in R4 (%)
M
F
*
***
n=7
n=10
n=17
n=21
C
Citrate FRET sensor
R2R4>CIT8
Ctrl
kdnRNAi
Relative FRET efficiency in R4 (%)
M
M
***
n=22
n=22
R2R4>
CIT8
CIT0
Relative FRET efficiency in R4 (%)
M
M
***
n=25
n=25
R2R4>CIT8
FRET efficiency
Male R4
Female R4
5d
Relative FRET efficiency in R4 (%)
M
F
***
n=20
n=20
R2R4>CIT8
FRET efficiency
Male R4;Ctrl
Male R4;IndyRNAi
5d
Ctrl
IndyRNAi
Relative FRET efficiency in R4 (%)
M
M
***
n=24
n=22

Figure 5

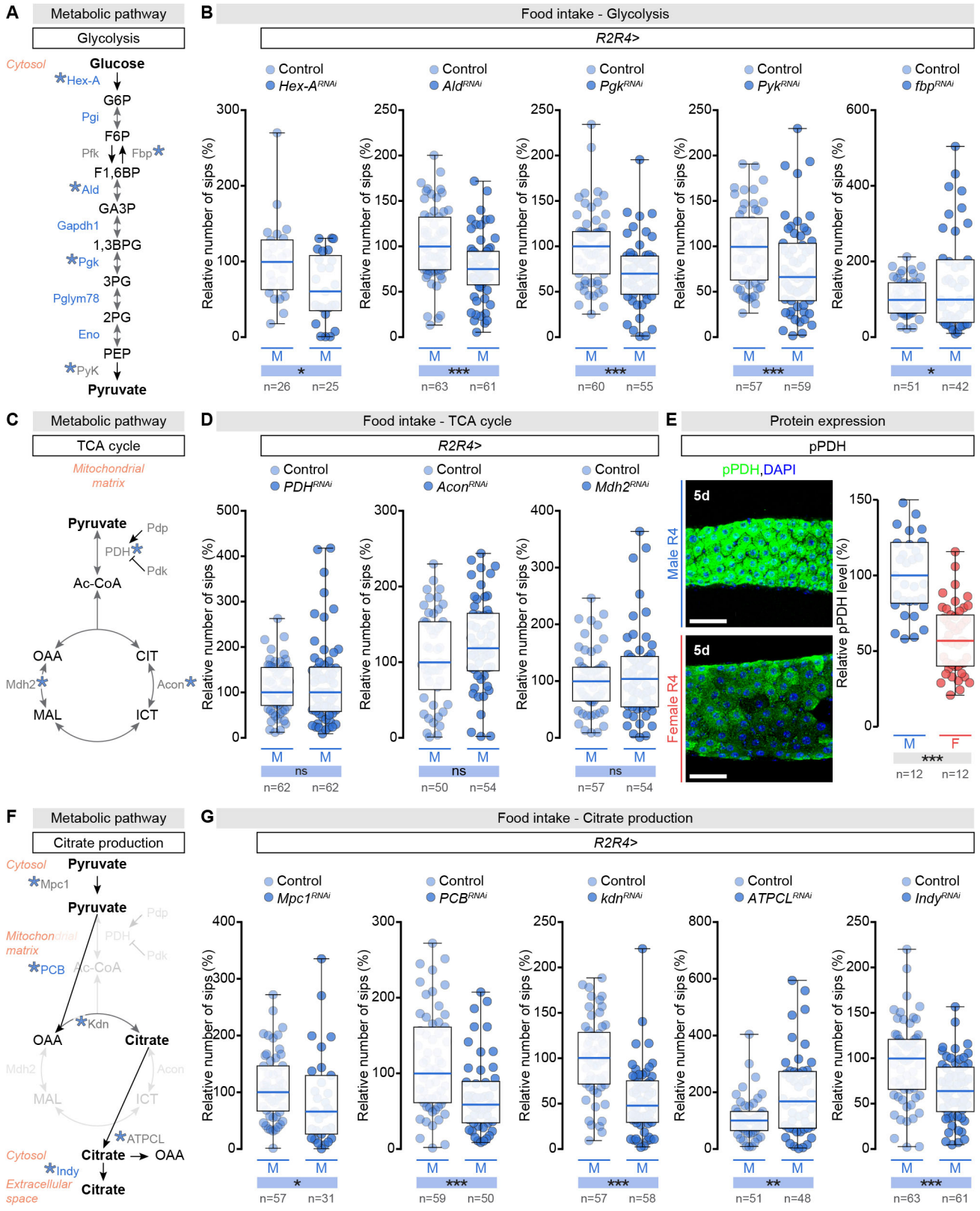
A
Metabolic pathway
Glycolysis
Cytosol
Glucose
Hex-A
G6P
Pgi
F6P
Pfk
Fbp
F1,6BP
Ald
GA3P
Gapdh1
1,3BPG
Pgk
3PG
Pglym78
2PG
Eno
PEP
PyK
Pyruvate
B
Food intake - Glycolysis
R2R4>
Control
Hex-A RNAi
Ald RNAi
Pgk RNAi
Pyk RNAi
fbp RNAi
Relative number of sips (%)
M
*
***
n=26
n=25
n=63
n=61
n=60
n=55
n=57
n=59
n=51
n=42
C
Metabolic pathway
TCA cycle
Mitochondrial matrix
Pyruvate
Pdp
PDH
Pdk
Ac-CoA
OAA
CIT
Acon
Mdh2
MAL
ICT
D
Food intake - TCA cycle
R2R4>
PDH RNAi
Acon RNAi
Mdh2 RNAi
ns
n=62
n=62
n=50
n=54
n=57
n=54
E
Protein expression
pPDH
pPDH,DAPI
5d
Male R4
Female R4
Relative pPDH level (%)
M
F
***
n=12
n=12
F
Metabolic pathway
Citrate production
Cytosol
Pyruvate
Mpc1
Pyruvate
Mitochondrial matrix
PCB
Ac-CoA
Kdn
OAA
Citrate
ATPCL
Cytosol
Citrate
OAA
Indy
Extracellular space
Citrate
G
Food intake - Citrate production
R2R4>
Mpc1 RNAi
PCB RNAi
kdn RNAi
ATPCL RNAi
Indy RNAi
**
n=57
n=31
n=59
n=50
n=57
n=58
n=51
n=48
n=63
n=61

Figure 6

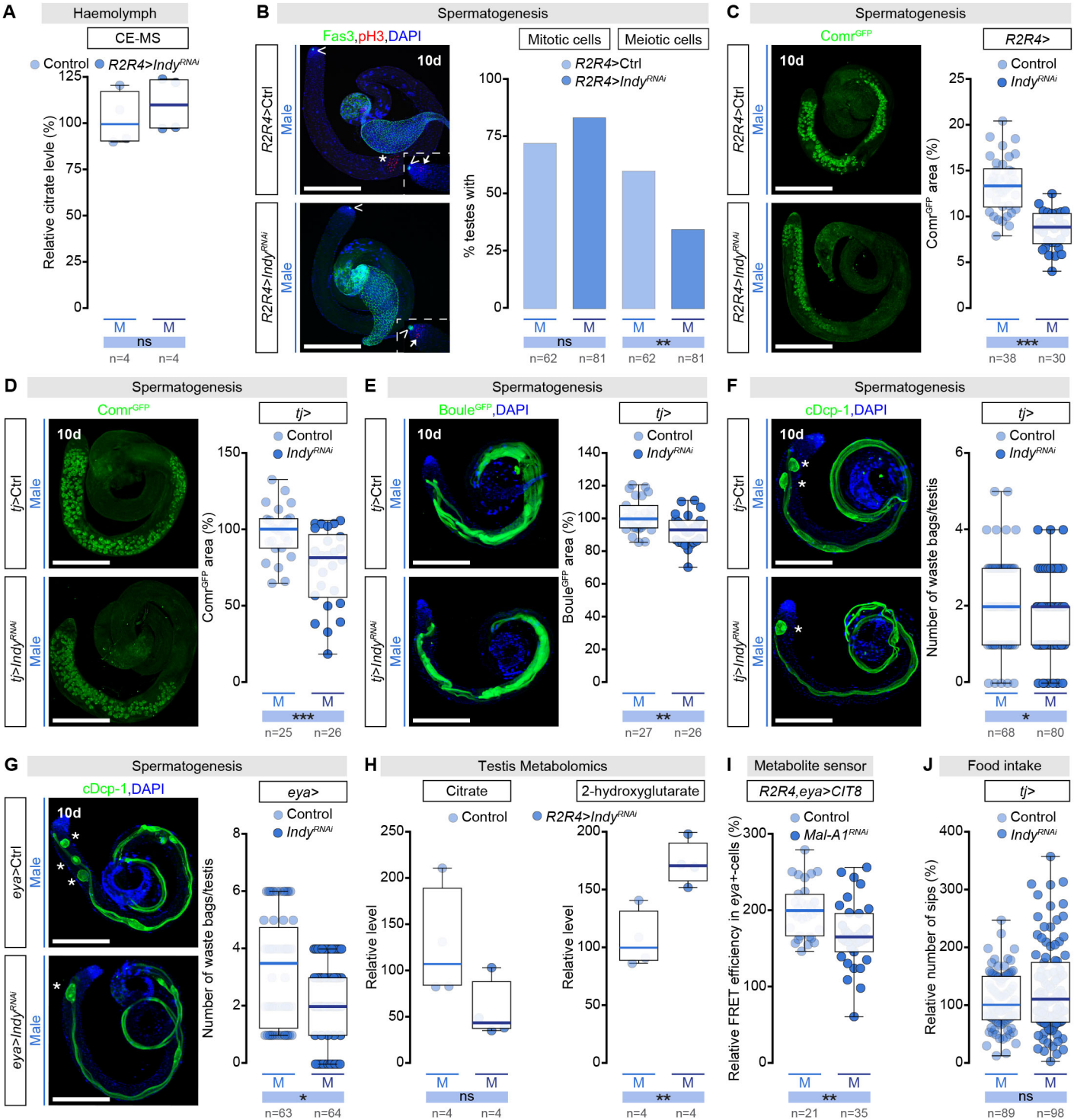
A
Haemolymph
CE-MS
Control
R2R4>Indy^RNAi
Relative citrate levle (%)
M
M
ns
n=4
n=4
B
Spermatogenesis
Fas3,pH3,DAPI
R2R4>Ctrl
R2R4>Indy^RNAi
Male
10d
Mitotic cells
Meiotic cells
% testes with
ns
**
n=62
n=81
n=62
n=81
C
Spermatogenesis
Comr^GFP
10d
Comr^GFP area (%)
***
n=38
n=30
D
Spermatogenesis
Comr^GFP
tj>Ctrl
tj>Indy^RNAi
10d
tj>
Comr^GFP area (%)
***
n=25
n=26
E
Spermatogenesis
Boule^GFP,DAPI
Boule^GFP area (%)
**
n=27
n=26
F
Spermatogenesis
cDcp-1,DAPI
Number of waste bags/testis
*
n=68
n=80
G
Spermatogenesis
cDcp-1,DAPI
eya>Ctrl
eya>Indy^RNAi
eya>
Number of waste bags/testis
*
n=63
n=64
H
Testis Metabolomics
Citrate
2-hydroxyglutarate
Relative level
ns
**
n=4
n=4
n=4
n=4
I
Metabolite sensor
R2R4,eya>CIT8
Mal-A1^RNAi
Relative FRET efficiency in eya+-cells (%)
**
n=21
n=35
J
Food intake
tj>
Relative number of sips (%)
ns
n=89
n=98

Figure 7

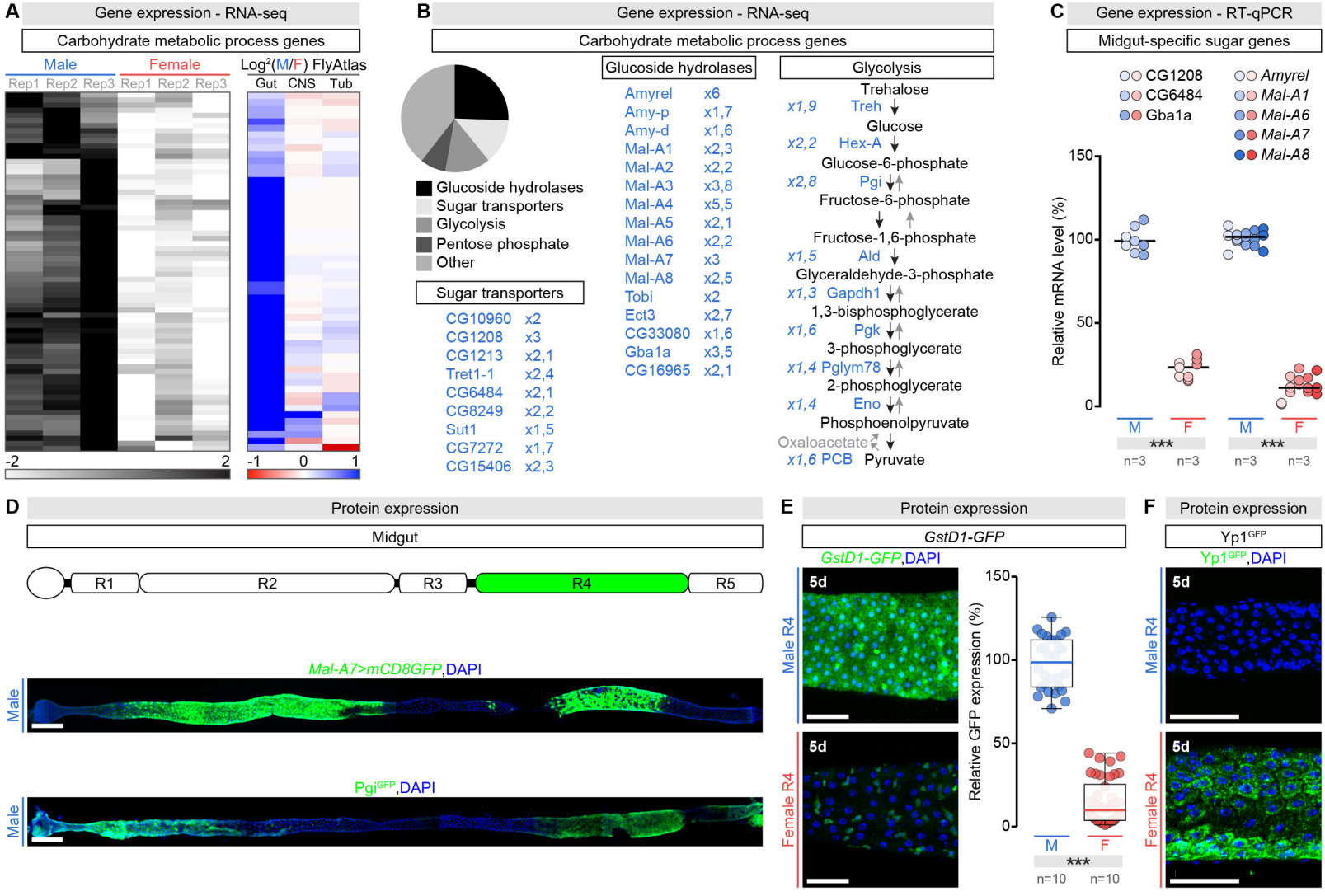
A
Gene expression - RNA-seq
Carbohydrate metabolic process genes
Male
Female
Rep1 Rep2 Rep3 Rep1 Rep2 Rep3
Log2(M/F) FlyAtlas
Gut CNS Tub
-2
2
-1 0 1
B
Gene expression - RNA-seq
Carbohydrate metabolic process genes
Glucoside hydrolases
Sugar transporters
Glycolysis
Pentose phosphate
Other
Glucoside hydrolases
Amylrel x6
Amy-p x1,7
Amy-d x1,6
Mal-A1 x2,3
Mal-A2 x2,2
Mal-A3 x3,8
Mal-A4 x5,5
Mal-A5 x2,1
Mal-A6 x2,2
Mal-A7 x3
Mal-A8 x2,5
Tobi x2
Ect3 x2,7
CG33080 x1,6
Gba1a x3,5
CG16965 x2,1
Sugar transporters
CG10960 x2
CG1208 x3
CG1213 x2,1
Tret1-1 x2,4
CG6484 x2,1
CG8249 x2,2
Sut1 x1,5
CG7272 x1,7
CG15406 x2,3
Glycolysis
Trehalose
x1,9 Treh
Glucose
x2,2 Hex-A
Glucose-6-phosphate
x2,8 Pgi
Fructose-6-phosphate
Fructose-1,6-phosphate
x1,5 Ald
Glyceraldehyde-3-phosphate
x1,3 Gapdh1
1,3-bisphosphoglycerate
x1,6 Pgk
3-phosphoglycerate
x1,4 Pglym78
2-phosphoglycerate
x1,4 Eno
Phosphoenolpyruvate
Oxaloacetate
x1,6 PCB Pyruvate
C
Gene expression - RT-qPCR
Midgut-specific sugar genes
CG1208
CG6484
Gba1a
Amyrel
Mal-A1
Mal-A6
Mal-A7
Mal-A8
Relative mRNA level (%)
150
100
50
0
M F M F
***
***
n=3 n=3 n=3 n=3
D
Protein expression
Midgut
R1 R2 R3 R4 R5
Mal-A7>mCD8GFP,DAPI
Male
PgiGFP,DAPI
Male
E
Protein expression
GstD1-GFP
GstD1-GFP,DAPI
5d
Male R4
5d
Female R4
Relative GFP expression (%)
150
100
50
0
M F
***
n=10 n=10
F
Protein expression
Yp1GFP
Yp1GFP,DAPI
5d
Male R4
5d
Female R4

Figure S1

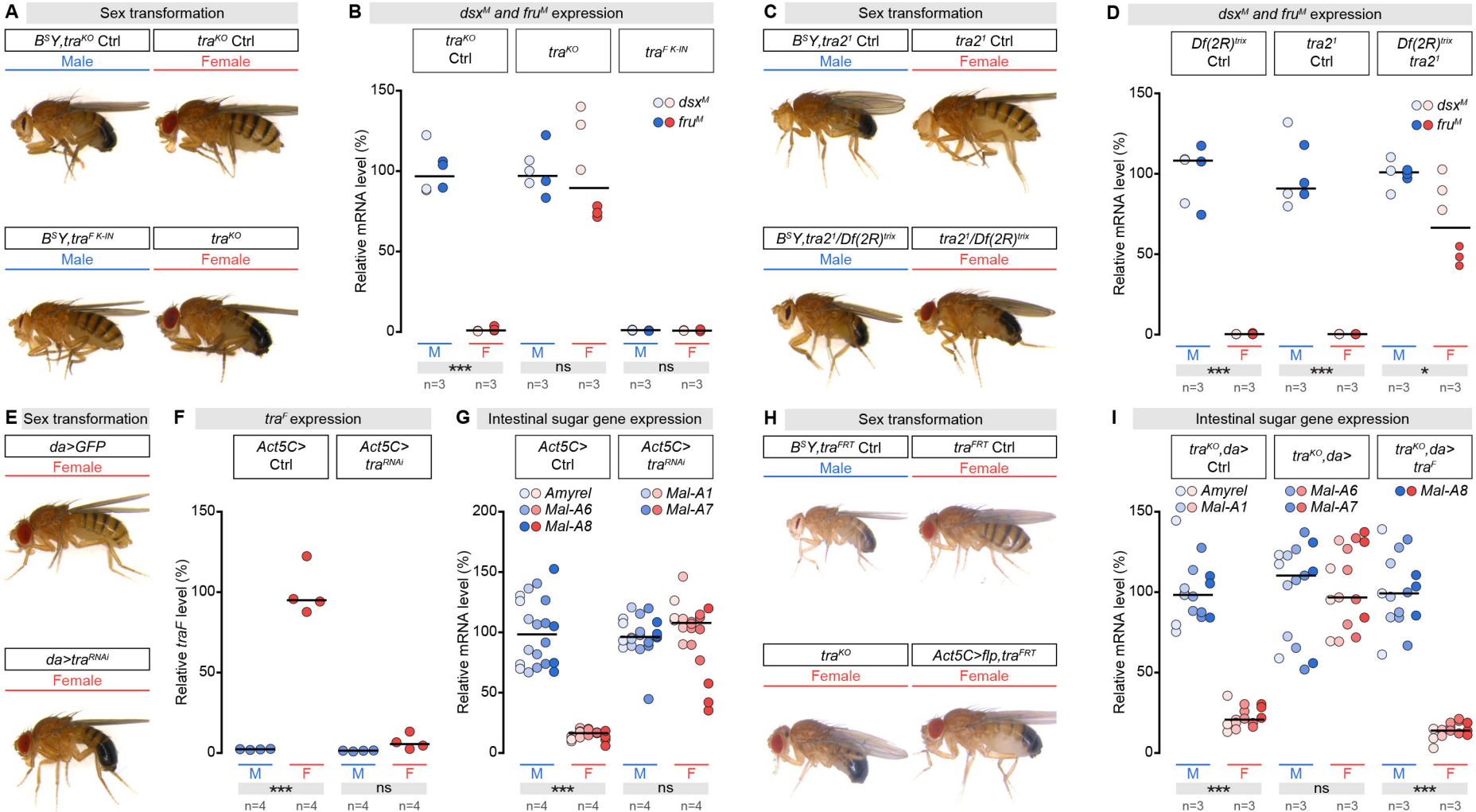
A
Sex transformation
BSY,traKO Ctrl
traKO Ctrl
Male
Female
BSY,traF K-IN
traKO
B
dsxM and fruM expression
traKO Ctrl
traKO
traF K-IN
dsxM
fruM
Relative mRNA level (%)
150
100
50
0
M
F
***
ns
n=3
C
Sex transformation
BSY,tra2¹ Ctrl
tra2¹ Ctrl
BSY,tra2¹/Df(2R)trix
tra2¹/Df(2R)trix
D
dsxM and fruM expression
Df(2R)trix Ctrl
tra2¹ Ctrl
Df(2R)trix tra2¹
*
E
Sex transformation
da>GFP
Female
da>traRNAi
F
traF expression
Act5C> Ctrl
Act5C> traRNAi
Relative traF level (%)
G
Intestinal sugar gene expression
Amyrel
Mal-A6
Mal-A8
Mal-A1
Mal-A7
Relative mRNA level (%)
200
150
100
50
0
n=4
H
Sex transformation
BSY,traFRT Ctrl
traFRT Ctrl
traKO
Act5C>flp,traFRT
I
Intestinal sugar gene expression
traKO,da> Ctrl
traKO,da>
traKO,da> traF
Mal-A8
Mal-A6
Mal-A7
Relative mRNA level (%)

Figure S2

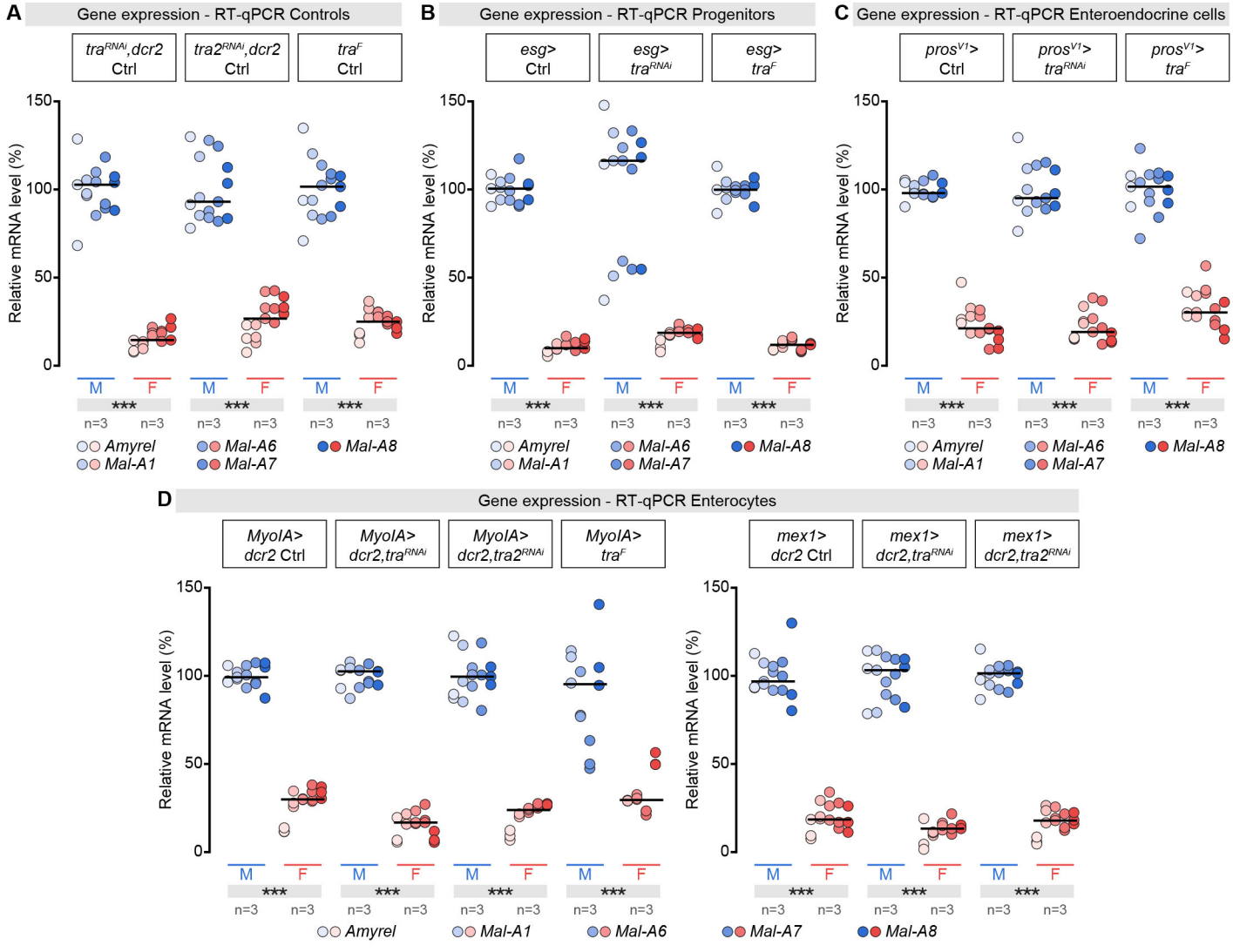
A
Gene expression - RT-qPCR Controls
tra^RNAi,dcr2 Ctrl
tra2^RNAi,dcr2 Ctrl
tra^F Ctrl
B
Gene expression - RT-qPCR Progenitors
esg> Ctrl
esg> tra^RNAi
esg> tra^F
C
Gene expression - RT-qPCR Enteroendocrine cells
pros^V1> Ctrl
pros^V1> tra^RNAi
pros^V1> tra^F
Relative mRNA level (%)
150
100
50
0
M
F
***
n=3
Amyrel
Mal-A1
Mal-A6
Mal-A7
Mal-A8
D
Gene expression - RT-qPCR Enterocytes
MyoIA> dcr2 Ctrl
MyoIA> dcr2,tra^RNAi
MyoIA> dcr2,tra2^RNAi
MyoIA> tra^F
mex1> dcr2 Ctrl
mex1> dcr2,tra^RNAi
mex1> dcr2,tra2^RNAi

Figure S3

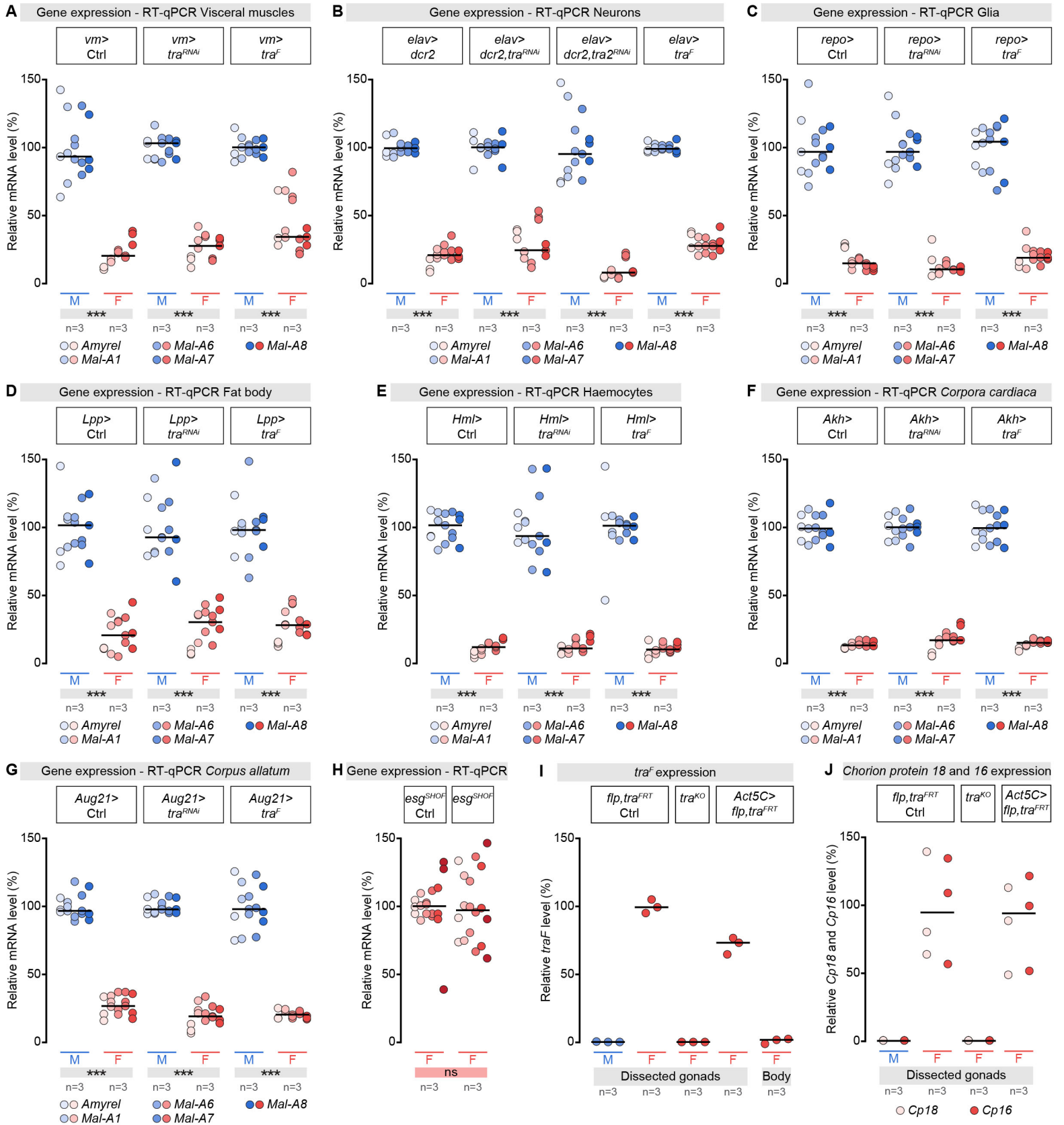
A
Gene expression - RT-qPCR Visceral muscles
vm> Ctrl
vm> traRNAi
vm> traF
B
Gene expression - RT-qPCR Neurons
elav> dcr2
elav> dcr2,traRNAi
elav> dcr2,tra2RNAi
elav> traF
C
Gene expression - RT-qPCR Glia
repo> Ctrl
repo> traRNAi
repo> traF
D
Gene expression - RT-qPCR Fat body
Lpp> Ctrl
Lpp> traRNAi
Lpp> traF
E
Gene expression - RT-qPCR Haemocytes
Hml> Ctrl
Hml> traRNAi
Hml> traF
F
Gene expression - RT-qPCR Corpora cardiaca
Akh> Ctrl
Akh> traRNAi
Akh> traF
G
Gene expression - RT-qPCR Corpus allatum
Aug21> Ctrl
Aug21> traRNAi
Aug21> traF
H
Gene expression - RT-qPCR
esgSHOF Ctrl
esgSHOF
ns
I
traF expression
flp,traFRT Ctrl
traKO
Act5C> flp,traFRT
Dissected gonads
Body
J
Chorion protein 18 and 16 expression
flp,traFRT Ctrl
traKO
Act5C> flp,traFRT
Dissected gonads
Relative mRNA level (%)
Relative traF level (%)
Relative Cp18 and Cp16 level (%)
M
F
***
n=3
Amyrel
Mal-A1
Mal-A6
Mal-A7
Mal-A8
Cp18
Cp16

Figure S4

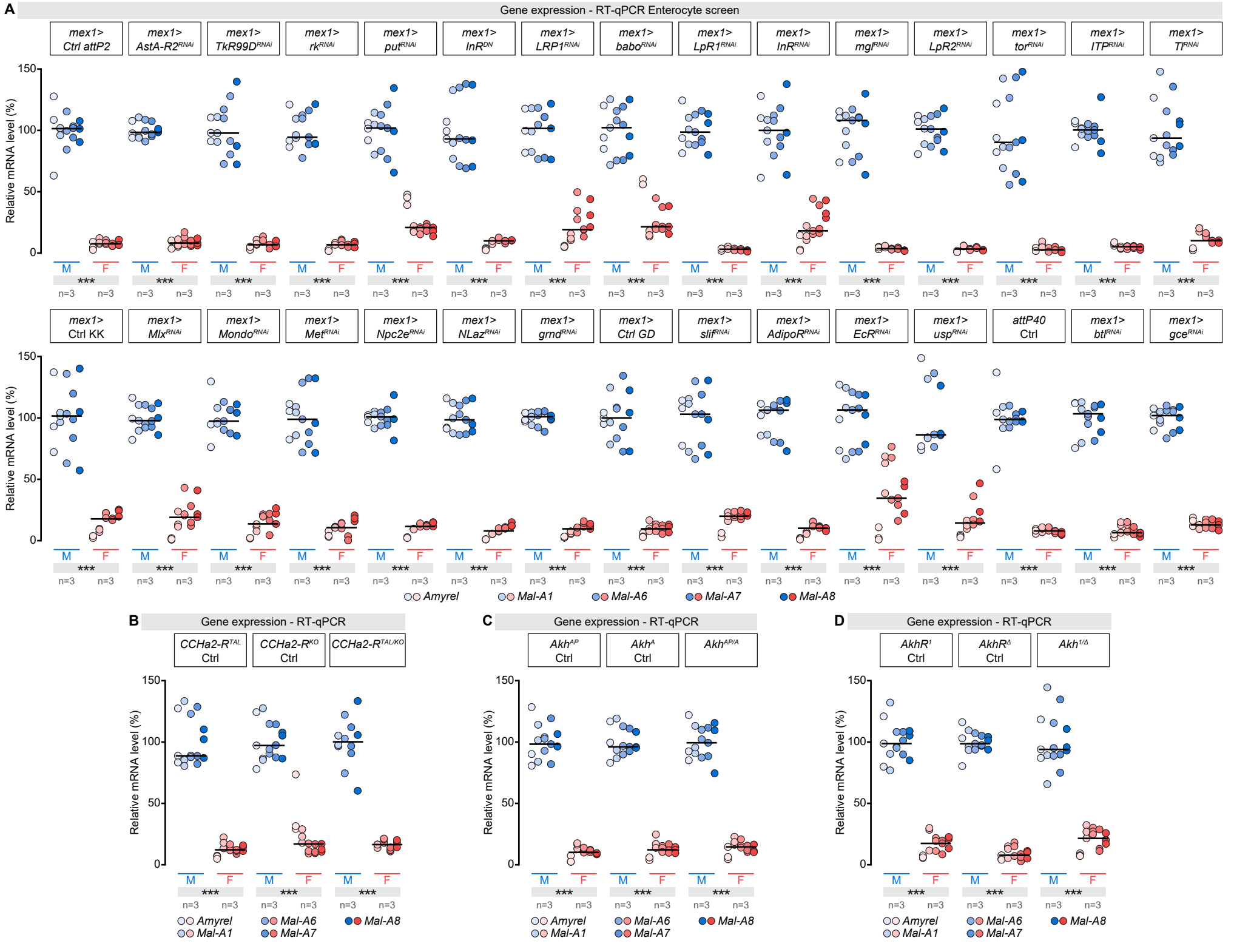
A
Gene expression - RT-qPCR Enterocyte screen
mex1> Ctrl attP2
mex1> AstA-R2RNAi
mex1> TkR99DRNAi
mex1> rkRNAi
mex1> putRNAi
mex1> InRDN
mex1> LRP1RNAi
mex1> baboRNAi
mex1> LpR1RNAi
mex1> InRRNAi
mex1> mglRNAi
mex1> LpR2RNAi
mex1> torRNAi
mex1> ITPRNAi
mex1> TlRNAi
mex1> Ctrl KK
mex1> MlxRNAi
mex1> MondoRNAi
mex1> MetRNAi
mex1> Npc2eRNAi
mex1> NLazRNAi
mex1> grndRNAi
mex1> Ctrl GD
mex1> slifRNAi
mex1> AdipoRRNAi
mex1> EcRRNAi
mex1> uspRNAi
attP40 Ctrl
mex1> btlRNAi
mex1> gceRNAi
Relative mRNA level (%)
150
100
50
0
M
F
***
n=3
Amyrel
Mal-A1
Mal-A6
Mal-A7
Mal-A8
B
Gene expression - RT-qPCR
CCHa2-RTAL Ctrl
CCHa2-RKO Ctrl
CCHa2-RTAL/KO
C
Gene expression - RT-qPCR
AkhAP Ctrl
AkhA Ctrl
AkhAP/A
D
Gene expression - RT-qPCR
AkhR1 Ctrl
AkhRΔ Ctrl
Akh1/Δ

Figure S5

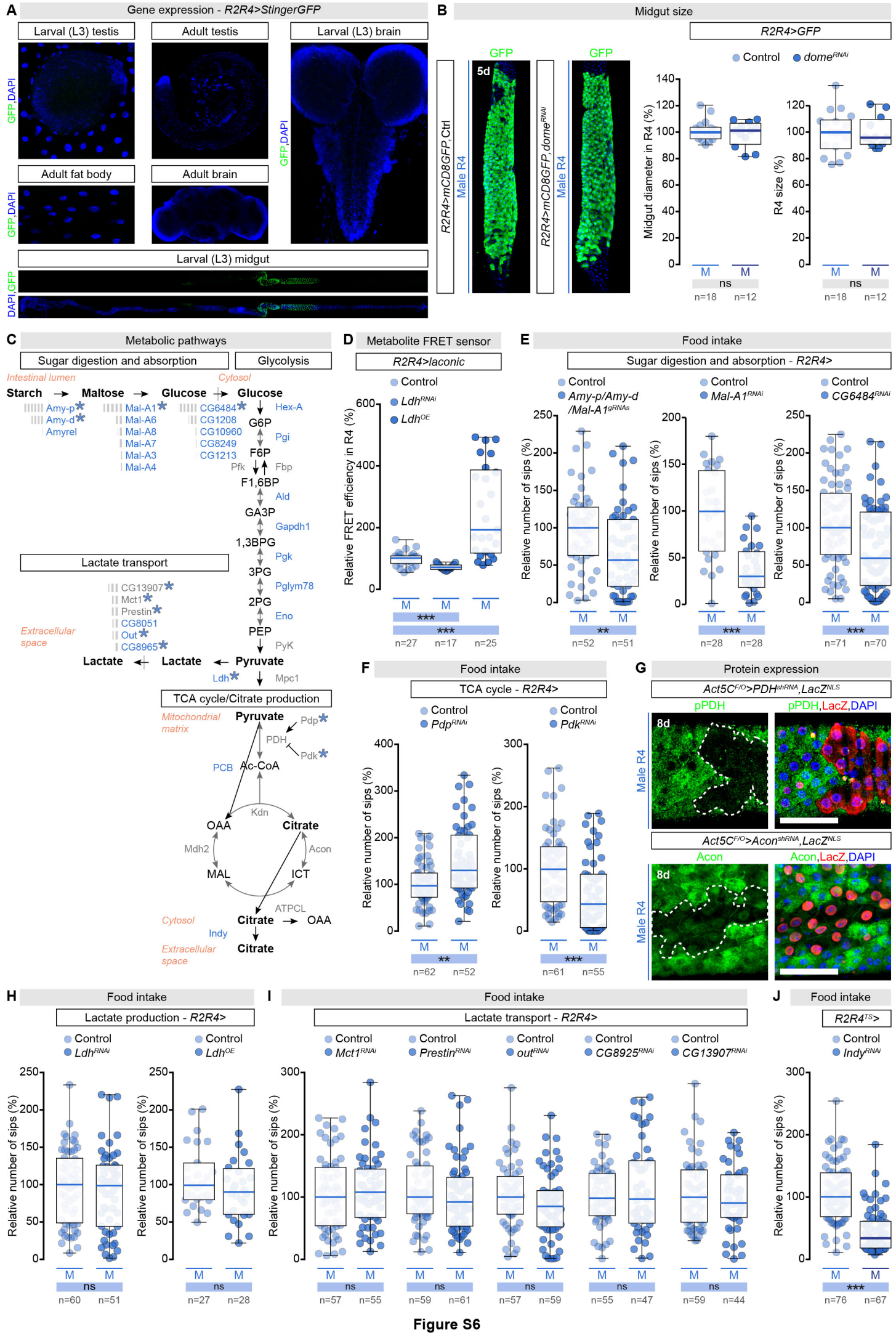
A
Gene expression - R2R4>StingerGFP
Larval (L3) testis
Adult testis
Larval (L3) brain
Adult fat body
Adult brain
Larval (L3) midgut
GFP,DAPI
DAPI,GFP
B
Midgut size
R2R4>GFP
Control
dome^RNAi
R2R4>mCD8GFP,Ctrl
R2R4>mCD8GFP,dome^RNAi
Male R4
GFP
5d
Midgut diameter in R4 (%)
R4 size (%)
ns
n=18
n=12
C
Metabolic pathways
Sugar digestion and absorption
Glycolysis
Intestinal lumen
Cytosol
Starch
Maltose
Glucose
Amy-p
Amy-d
Amyrel
Mal-A1
Mal-A6
Mal-A8
Mal-A7
Mal-A3
Mal-A4
CG6484
CG1208
CG10960
CG8249
CG1213
Hex-A
G6P
Pgi
F6P
Pfk
Fbp
F1,6BP
Ald
GA3P
Gapdh1
1,3BPG
Pgk
3PG
Pglym78
2PG
Eno
PEP
PyK
Lactate transport
CG13907
Mct1
Prestin
CG8051
Out
CG8965
Extracellular space
Lactate
Pyruvate
Ldh
Mpc1
TCA cycle/Citrate production
Mitochondrial matrix
PDH
Pdp
Pdk
PCB
Ac-CoA
Kdn
OAA
Citrate
Mdh2
Acon
MAL
ICT
ATPCL
Cytosol
Indy
D
Metabolite FRET sensor
R2R4>laconic
Control
Ldh^RNAi
Ldh^OE
Relative FRET efficiency in R4 (%)
***
n=27
n=17
n=25
E
Food intake
Sugar digestion and absorption - R2R4>
Amy-p/Amy-d /Mal-A1^gRNAs
Mal-A1^RNAi
CG6484^RNAi
Relative number of sips (%)
**
n=52
n=51
n=28
n=28
n=71
n=70
F
Food intake
TCA cycle - R2R4>
Pdp^RNAi
Pdk^RNAi
n=62
n=52
n=61
n=55
G
Protein expression
Act5C^F/O>PDH^shRNA,LacZ^NLS
pPDH
pPDH,LacZ,DAPI
8d
Male R4
Act5C^F/O>Acon^shRNA,LacZ^NLS
Acon
Acon,LacZ,DAPI
H
Food intake
Lactate production - R2R4>
Control
Ldh^RNAi
Ldh^OE
Relative number of sips (%)
ns
n=60
n=51
n=27
n=28
I
Food intake
Lactate transport - R2R4>
Mct1^RNAi
Prestin^RNAi
out^RNAi
CG8925^RNAi
CG13907^RNAi
n=57
n=55
n=59
n=61
n=57
n=59
n=55
n=47
n=59
n=44
J
Food intake
R2R4^TS>
Indy^RNAi
n=76
n=67

Figure S6

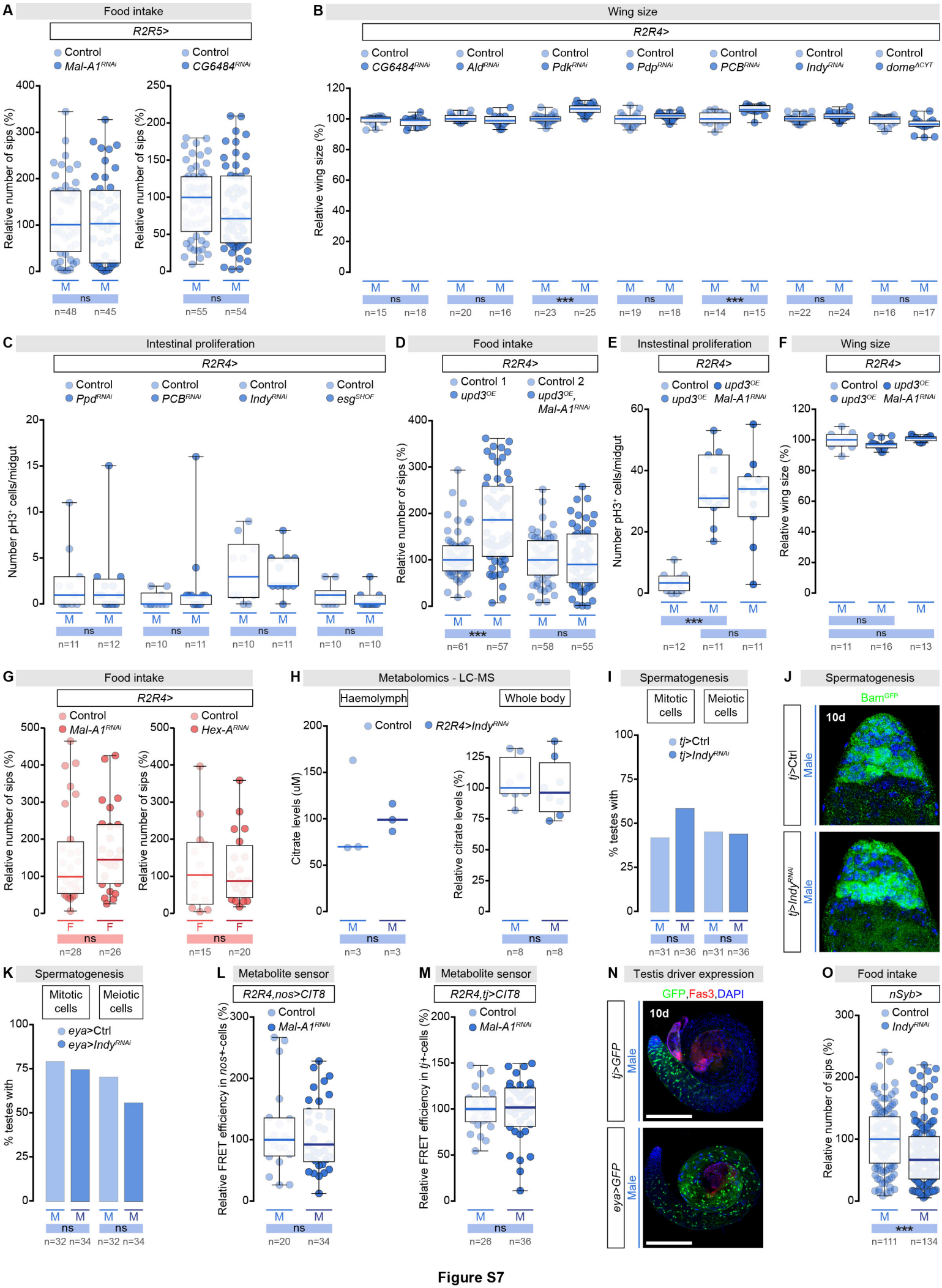
A
Food intake
R2R5>
Control
Mal-A1RNAi
Control
CG6484RNAi
Relative number of sips (%)
M M
ns
n=48 n=45
n=55 n=54
B
Wing size
R2R4>
Control
CG6484RNAi
Control
Ald RNAi
Control
Pdk RNAi
Control
Pdp RNAi
Control
PCB RNAi
Control
Indy RNAi
Control
domeΔCYT
Relative wing size (%)
ns
***
n=15 n=18
n=20 n=16
n=23 n=25
n=19 n=18
n=14 n=15
n=22 n=24
n=16 n=17
C
Intestinal proliferation
R2R4>
Control
Ppd RNAi
Control
PCB RNAi
Control
Indy RNAi
Control
esgSHOF
Number pH3+ cells/midgut
n=11 n=12
n=10 n=11
n=10 n=11
n=10 n=10
D
Food intake
R2R4>
Control 1
upd3OE
Control 2
upd3OE, Mal-A1RNAi
Relative number of sips (%)
***
ns
n=61 n=57
n=58 n=55
E
Instestinal proliferation
R2R4>
Control
upd3OE
upd3OE
Mal-A1RNAi
Number pH3+ cells/midgut
***
ns
n=12 n=11 n=11
F
Wing size
R2R4>
Control
upd3OE
upd3OE
Mal-A1RNAi
Relative wing size (%)
ns
n=11 n=16 n=13
G
Food intake
R2R4>
Control
Mal-A1RNAi
Control
Hex-ARNAi
Relative number of sips (%)
F F
ns
n=28 n=26
n=15 n=20
H
Metabolomics - LC-MS
Haemolymph
Whole body
Control
R2R4>IndyRNAi
Citrate levels (uM)
Relative citrate levels (%)
M M
ns
n=3 n=3
n=8 n=8
I
Spermatogenesis
Mitotic cells
Meiotic cells
tj>Ctrl
tj>IndyRNAi
% testes with
ns
n=31 n=36 n=31 n=36
J
Spermatogenesis
BamGFP
10d
tj>Ctrl
Male
tj>IndyRNAi
Male
K
Spermatogenesis
Mitotic cells
Meiotic cells
eya>Ctrl
eya>IndyRNAi
% testes with
ns
n=32 n=34 n=32 n=34
L
Metabolite sensor
R2R4,nos>CIT8
Control
Mal-A1RNAi
Relative FRET efficiency in nos+cells (%)
ns
n=20 n=34
M
Metabolite sensor
R2R4,tj>CIT8
Control
Mal-A1RNAi
Relative FRET efficiency in tj+cells (%)
ns
n=26 n=36
N
Testis driver expression
GFP,Fas3,DAPI
10d
tj>GFP
Male
eya>GFP
Male
O
Food intake
nSyb>
Control
IndyRNAi
Relative number of sips (%)
***
n=111 n=134

Figure S7